STUDY OF FLOW PATTERNS AND VOID FRACTION IN INCLINED TWO PHASE FLOW

By

ADEKUNLE LUKMAN OYEWOLE

Bachelor of Science in Mechanical Engineering

University of Ilorin

Ilorin, Nigeria

2009

Submitted to the Faculty of the
Graduate College of the
Oklahoma State University
in partial fulfillment of
the requirements for
the Degree of
MASTER OF SCIENCE
December, 2013

STUDY OF FLOW PATTERNS AND VOID

FRACTION IN INCLINED TWO PHASE FLOW

Thesis Approved:

Dr. Afshin J. Ghajar

Thesis Adviser

Dr. Khaled Sallam

Dr. A.J Johannes

ACKNOWLEDGEMENTS

My sincere gratitude goes to my advisor Dr. Afshin Ghajar for his guidance and support throughout the course of this study and my Master's degree. It has been an honor to know and work under him. I am thankful to Dr. Khaled Sallam and Dr. A.J Johannes for being members of my thesis committee.

I would like to thank all my colleagues that worked with me on this research, Edgar Lares, Srinaga Kalapatapu, Tabassum Hossainy and Swanand Bhagwat. Special appreciation goes to Swanand Bhagwat for his assistance, suggestions and brilliant ideas during this study.

This thesis is dedicated to my parents, Mr. & Mrs. Oyewole for their care, unwavering love, prayers and faith in me. I am also thankful to my cousins, Ghafar, Gladys and Shefiu Shittu for their support throughout my Master's program.

Finally, I want to express my gratitude to Kendrall Springs for her support and faith in me.

Acknowledgements reflect the views of the author and are not endorsed by committee members or Oklahoma State University.

Name: ADEKUNLE LUKMAN OYEWOLE.

Date of Degree: DECEMBER, 2013.

Title of Study: STUDY OF FLOW PATTERNS AND VOID FRACTION IN INCLINED TWO PHASE FLOW.

Major Field: MECHANICAL ENGINEERING.

Abstract: In the field of multiphase flow, much research has been done on flow patterns and void fraction in vertical upward, vertical downward and horizontal pipes with only very little investigation done in inclined pipes. Experimental investigation was conducted in present study over six pipe orientations ($+5^o$, $+10^o$, $+20^o$, -5^o, -10^o & -20^o) using air-water as fluid combination in a 12.7 mm diameter pipe. Flow visualization was conducted for flow pattern identification, flow pattern maps were developed showing effect of pipe orientation on flow pattern transition boundaries and 700 void fraction data points were measured and analyzed. Effect of pipe orientation on void fraction was also observed and reported. Fourteen void fraction correlations were selected for experimental data prediction based on previous works and the best performing void fraction correlation for upward inclined pipe, downward inclined pipe and near horizontal pipe orientation was determined. A unique phenomenon called flow reversal in co-current two phase flow was observed in upward inclined pipe orientation and investigated in present study. Flow reversal was investigated using Bernoulli's equation and dimensionless numbers (Froude, Reynolds & Weber number) which gave in-depth analysis of this phenomenon.

TABLE OF CONTENTS

LIST OF TABLES

Table Page

LIST OF FIGURES

Figure Page

NOMENCLATURE

A	Cross sectional area, m^2
C_o	Distribution parameter
D	Pipe diameter, m
f	Friction factor
Fr	Froude number
g	Acceleration due to gravity, m s^{-2}
G	Flux, kg s^{-1} m^{-2}
L	Length, m
La	Laplace number
$\dot{m}$	Mass flow rate, kg s^{-1}
P	Pressure, kg m^{-1} s^{-2}
Re	Reynolds number
S	Perimeter over which stress acts, m. Equation (4.1)
Sr	Slip ratio
U	Velocity, m s^{-1}
V	Volume, m^3
w	Uncertainty
We	Weber number
x	Thermodynamic quality

Greek symbols

α	Void fraction
α_H	Homogenous void fraction
β	Gas volumetric flow fraction
δ	Liquid film thickness, m
ϵ	Surface roughness
ε	Liquid holdup
γ	Liquid film height for flat stratified interface, m. Equation (4.5)
λ	Input liquid content
μ	Dynamic viscosity, kg m^{-1} s^{-1}
ν	Kinematic viscosity, m^2 s^{-1}
ρ	Density, kg m^{-3}
σ	Surface Tension, kg m^{-1} s^{-2}
τ	Shear stress, kg m^{-1} s^{-2}
θ	Inclination angle, ^{o}

Subscripts

cr	Critical
cs	Cross sectional
dy	Dynamic
h	Hydraulic
g	Gas
gm	Drift
i	Interfacial
l	Liquid
m	Mixture

s	Superficial
sg	Superficial gas
sl	Superficial liquid
sys	System
T	Trapped
tp	Two phase

Superscript

*	Dimensionless

CHAPTER I

INTRODUCTION

Two phase flow is the simplest form of multiphase flow and it involves the simultaneous movement of two distinct phases in a pipe. Two phase flow can exist in the form of gas-liquid flow like bubbly flow, gas-solid flow like pneumatic transport of particles and liquid-solid flow like slurry flow. Two phase flow can further be divided into two forms which are boiling and non-boiling two phase flow. Boiling two phase flow is attained when a single phase fluid evaporates due to heat transfer and the simultaneous flow of liquid and vapor of the same component in the pipe is termed single component two phase flow. Boiling two phase flow is observed in steam-water flow in power generating plants, flow of refrigerants in air conditioning systems. Non-boiling two phase flow involves two distinct components and is observed in oil production activities where there is flow of natural gas and crude oil through pipes. The application of two phase flow is found in major areas like the cooling of fuel rods in a nuclear reactor for power generation, enhancing mass transfer in the chemical industry, understanding and predicting wax deposition during crude oil and natural gas transportation in the oil and gas industry, condensate formation in natural gas transportation.

Two phase flow phenomenon has been studied since the 1930's in four major aspects which are flow patterns, void fraction, pressure drop and heat transfer. Due to the very broad nature of two phase flow, research in each major aspect is concentrated on certain pipe orientation, fluid combination or range of system pressure. For example, some researchers investigate flow patterns, void fraction or heat transfer in specific pipe orientation or develop correlations to predict heat transfer, void fraction or pressure drop for certain fluid combination. The present study is focused on flow patterns and void fraction studies in non-boiling air-water two phase flow in near horizontal pipes which covers both upward and downward inclined pipes

When liquid and gas flow through a pipe, interaction between the two phases occur due to difference in fluid properties, flow properties (this determines the dominant forces acting in the two phase flow) and pipe orientation. The two phase flow rearranges itself based on the above mentioned factors and the nature of the reorganization is termed flow pattern. Flow pattern plays an important role in void fraction, heat transfer and pressure drop analysis as they are largely influenced by changes in flow pattern. Thus, critical understanding of flow pattern is necessary for accurate modeling in two phase flow. Flow pattern maps have been investigated and developed over decades for the purpose of predicting change in flow pattern with respect to change in flow properties. However, there exist no universal flow pattern map independent of fluid combination and pipe orientation in two phase flow. Extensive research has been done on flow pattern in vertical and horizontal pipe orientations whereas very little work has been done in inclined systems especially near horizontal pipe orientations. For example, horizontal and directional drilling in oil wells has significantly increased in an attempt to efficiently reach and tap into oil reservoirs. Since oil wells are made of both vertical and near horizontal portions, flow pattern studies in near horizontal pipe orientation is necessary for accurate modeling of heat transfer and pressure drop in oil production activities. Hence, this justifies the need to conduct flow pattern studies in near horizontal pipe orientation.

Generally, void fraction refers to the fraction of gas to liquid and gas mixture flowing in a pipe. Void fraction has a direct dependence on flow pattern and it also serves as an input parameter needed for pressure drop and heat transfer models in two phase flow. For example, void fraction is needed to determine two phase density and viscosity of the system. Void fraction was measured in near horizontal orientation to determine the effect of pipe orientation on void fraction in present study. During the course of flow visualization and void fraction measurement, flow reversal was observed at different pipe orientations over certain liquid and gas flow rates, hence this phenomenon was further investigated in present study. The current work done on flow reversal in co-current non-boiling two phase flow serves as a framework for further investigation to develop a model for this phenomenon in near horizontal pipe orientation. Accurate modeling of flow reversal can be used to effectively design and fabricate back flow preventers applicable to two phase flow system which can be incorporated in oil wells and hence, significantly reduce pump work needed to get the two phase mixture to the surface in oil production activities.

Present study was conducted over six pipe orientations which are $+5^{o}$, $+10^{o}$, $+20^{o}$, -5^{o}, -10^{o} and -20^{o} in a 12.7 mm diameter pipe. The main objective of present study was to carry out extensive studies of flow pattern with the aid of photographic evidence and void fraction in these pipe orientations. These pictures helped to adequately understand and explain complex two phase flow physics resulting from the effects of buoyant, gravity and inertial forces in present study.

Present study is divided into four chapters. Literature search was conducted in chapter II to review previous works on flow patterns, flow maps and void fraction in inclined and near horizontal two phase flow. Fourteen void fraction correlations were selected based on previous analysis done by different researchers and these correlations were discussed in chapter II. Chapter III focuses on the experimental procedure which covers procedure for flow visualization and void fraction. Modification of lighting arrangement was done in present study to improve picture quality and clarity of the two phase flow mixture in the pipe during flow visualization. Validation

of measured void fraction with data from other sources and predictions of the top performing void fraction correlations was also discussed in chapter III. The results of present study were discussed in chapter IV. These results consist of the effect of pipe orientation on flow patterns, effect of pipe orientation on flow pattern transition boundaries in flow maps, effect of pipe orientation on void fraction and variation of void fraction with flow pattern at different pipe orientations. Chapter IV discusses the performance of selected void fraction correlations in various void fraction regions chosen for analysis in order to come up with the best performing correlation for near horizontal pipe orientation. The final part of chapter IV focuses on flow reversal which was extensively investigated and discussed. Chapter V draws conclusions from the results obtained in chapters III and IV and provides recommendations for future research in two phase flow.

CHAPTER II

LITERATURE REVIEW

Previous work done on two phase flow in inclined pipes was investigated and discussed in this chapter. For the purpose of literature search, this chapter is divided into three parts. The first part focuses on the various flow patterns observed in inclined two phase flow for near horizontal pipe orientation. Since flow patterns are dependent on experimental apparatus used for investigation, the various flow patterns observed by different investigators were briefly discussed with details of setup and method used for flow visualization. Based on various definitions given by different researchers, it was observed that the major flow patterns in near horizontal pipe orientation are in four distinct forms which are stratified flow, slug flow, bubbly flow and annular flow. Other flow patterns observed are a combination of the major flow patterns. A quick review of flow maps developed by different investigators was done for various orientations and the comparative study carried out to determine a universal mapping parameter to improve flow map accuracy was reported.

The third part of this literature review discusses the four models of void fraction correlation. Correlations are further categorized and discussed based on pipe orientation over which they are applicable in the order of; correlations developed for vertical orientation, correlations developed for horizontal orientation and void fraction correlations developed for multiple orientations and applicable to near horizontal orientation.

2.1 Flow Patterns

When liquid and gas flow simultaneously in a pipe, spatial arrangement of liquid and gas occur due to difference in fluid properties (density and viscosity), pipe orientation and other forces acting in the two phase flow. This spatial or geometric reorganization of the liquid and gas phase in the pipe is termed flow pattern. Researchers have conducted flow pattern studies over the years and various flow patterns have been reported by different investigators. However, it has been proved that flow patterns observed show more dependence on pipe orientation than pipe diameter or fluid combination.

Beggs and Brill (1973) conducted two phase flow studies in inclined pipe over the entire pipe orientation of $+90^{o}$ to -90^{o} in 25.4 and 38.1 mm diameter pipes. They categorized the observed flow patterns into regions which are segregated flow, intermittent flow and distributed flow. Segregated flow consists of stratified flow, wavy flow and annular flow. Intermittent flow is made of plug and slug flow while distributed flow consists of bubble flow and mist flow.

Spedding and Nguyen (1980) conducted extensive research on air-water two phase flow in a 4.55 cm internal diameter pipe from vertical downward to vertical upward flow. Flow visualization was done by observation in the transparent pipe, measuring pressure fluctuation at the wall and by photography using Xrays or fluorescent light. Similar flow patterns having slight differences in geometry were observed in various pipe orientations and the flow patterns were categorized into four major types. The flow patterns are stratified flow, bubble-slug flow, droplet flow and mixed flow. Stratified flow was sub divided into straight stratified, stratified plus ripple, stratified plus roll and stratified plus inertial wave. They explained that by keeping the liquid flow rate constant and increasing the gas phase flow rate in horizontal pipe orientation, straight stratified flow progressed into stratified plus ripple waves and then to stratified plus roll waves. Further increase in gas flow rate led to droplets being torn from the liquid interface, the straight stratified flow was

observed to completely vanish under these conditions and the flow pattern was termed stratified flow plus inertial waves. Limited straight stratified flow was observed in upward inclined pipe orientation. For upward inclined pipe orientation, bubble/slug flow was reported as the dominant flow pattern and was observed to be independent of liquid phase flow rate. In the downward inclined pipe orientation, straight stratified flow was observed to persist over a very wide range of liquid flow rates while bubble flow was difficult to achieve.

Weisman and Kang (1981) conducted flow pattern studies in upward inclined pipe using air-water and air-glycerol as fluid combination. Flow visualization was carried out in a 6.1 m long transparent pipe having diameters of 12.7 mm, 25.4 mm and 50.8 mm with maximum pipe inclination of 7^o from horizontal. Flow visualization was conducted over inclination angles of 0^o (horizontal), 0.5^o, 2^o and 7^o. They reported that flow patterns observed in slightly inclined pipe orientations are very similar to horizontal flow patterns. Elimination of stratified flow in upward inclined pipe from horizontal was the major change in the flow patterns between these pipe orientations. Stratified flow was replaced by plug flow at inclination angle as low as 0.5^o and wavy flow pattern was observed at higher liquid flow rates. The flow rates initially occupied by wavy flow in horizontal pipe were observed to be occupied by broken slug flow in inclined pipe. They described broken slug flow as slug flow in which liquid phase is not in contact with top pipe wall surface. The major flow patterns observed in this study are stratified flow, slug flow, plug flow, bubbly flow, wavy flow and annular flow.

Barnea et al. (1982) conducted experimental study of flow pattern in downward inclined two phase flow. The experimental apparatus used consist of two transparent plexi-glass 10 m long pipes with internal diameters of 2.55 and 5.1 cm. The apparatus has the capacity of variable inclination from horizontal to vertical. They carried out visual observation and also employed an oscilloscope display which uses electro conductivity probes to determine the flow patterns. Four major flow patterns which are stratified flow, slug flow, bubbly flow and annular flow were

observed. They categorized stratified flow into two types based on the nature of the interface, smooth stratified flow and wavy stratified flow. Smooth stratified flow was not observed for pipe inclinations above 5^o due to gravity induced waves generated at the stratified interface. Transition flow patterns having a combination of two or more major flow patterns were also observed which are intermittent and wavy/annular flow.

Barnea et al. (1985) conducted flow pattern transition studies for upward inclined flow from horizontal to vertical pipe orientation using air-water as fluid combination. Eight flow patterns were observed in the horizontal pipe and were categorized into four types. The four categories of flow patterns are stratified flow, intermittent flow, annular flow and dispersed bubble flow. Stratified flow was observed from horizontal orientation till upward inclination of $+10^o$ after which it disappeared. For upward inclinations from $+10^o$ to $+90^o$, the flow patterns observed are intermittent, annular and dispersed bubble flow.

Mukherjee and Brill (1985) conducted experimental two phase flow studies in a 5.08 cm pipe over various pipe orientations in both upward and downward inclinations. Four major flow patterns were observed which are slug flow, bubbly flow, stratified flow and annular flow. They observed a concentration gradient of discrete bubbles across the pipe cross section due to gravitational effects at lower angles of upward pipe orientation, and as pipe orientation increased bubbles were observed to distribute over a wider cross section of the pipe. In the downward pipe orientation, they observed that bubble rise velocity is always counter-current to the general flow direction which leads to shear of large bubbles into smaller bubbles. They described the formation of slug in upward inclined pipe as the process by which liquid flow rate is high enough to push the large wedge-shaped bubbles down the pipe while in the downward inclined pipe orientation, they described slugs as the process by which waves bridge pipe cross section. Stratified flow was observed in horizontal and downward inclined pipe orientation. They reported that a velocity gradient exist across the liquid film in downward inclined pipe orientation for

stratified flow, this velocity gradient was observed to increase with further shift in pipe orientation in the downward direction. Annular flow was observed in both upward and downward inclined pipe orientation which they described as the gas phase being continuous along the pipe core. They also described the nature of the continuous gas phase (either concentric or not) in annular flow as dependent on pipe orientation in both upward and downward flows.

Kokal and Stanislav (1989a) conducted two phase flow (air-oil) studies in a test section having 25 m long pipe with diameters 25.8 mm, 51.2 mm and 76.3 mm, with variable inclination of $\pm 10^{o}$ from horizontal. Flow patterns were determined using volume sensor traces. Flow patterns were categorized into 3 major regions which are gas dominated flows, liquid dominated flows and intermittent flow. The gas dominated flows are stratified flow, annular flow, intermittent flow, elongated bubble flow, elongated bubble with dispersed bubble flow and slug flow. The liquid dominated flows are dispersed bubble flow and dispersed froth flow. Intermittent flow they described as a combination of liquid slugs and large bubbles.

Dezhang and Ning (1992) conducted flow pattern and heat transfer studies of boiling two phase flow in upward and downward inclined pipes. Flow visualization was conducted at 0^{o}, $\pm 30^{o}$, $\pm 60^{o}$ and $\pm 90^{o}$. Various flow patterns were observed based on heat flux and pipe orientation. The major flow patterns observed are slug flow, annular flow, wavy flow and saturated bubble flow. Other flow patterns include slug/annular flow and bubble/slug flow.

Spedding et al. (1999) carried out co-current two phase flow studies in inclined pipe. Flow visualization was done in a 11.28 m long and 5.08 cm internal diameter pipe over pipe orientation of -5^{o} to $+5^{o}$ from horizontal and using air-water as fluid combination. The major flow patterns observed are stratified flow, annular flow, slug flow and bubble flow.

Tshuva et al. (1999) conducted two phase flow studies in parallel inclined pipes having internal diameters of 2.4 cm and variable inclination from 0^{o} to 90^{o}. Quick closing valves were used for

the measurement of void fraction and it also assesses the symmetry of flow in the pipe. Flow patterns were divided into symmetric and asymmetric flow. Studies were conducted over inclination angles of 5^o, 10^o, 20^o, 45^o, 70^o and 90^o. They observed that in the low liquid and gas flow rate region and low pipe inclinations, flow starts symmetric and progresses into asymmetric flow as pipe inclination increased.

Oddie et al. (2003) conducted experimental two phase flow studies in an 11 m long and 15 cm diameter pipe over inclination angles of vertical upward to 2^o below horizontal pipe orientation using different fluid combinations. Six flow patterns were observed in their experimental procedure over the range of pipe orientations which are bubble, churn, stratified, slug, elongated-bubble and stratified wavy flow. They observed bubble flow in vertical and 5^o deviation from vertical orientation. At 45^o, a combination of slug flow, churn flow and elongated–bubble flow was observed where churn flow was the dominant flow pattern. They reported that as pipe inclination shifted to 70^o and 88^o from vertical, slug and elongated-bubble flow were the only flow patterns observed and at 90^o and 92^o from vertical, stratified and stratified wavy flows were observed at constant flow rates.

Wongwises and Pipathattakul (2006) conducted two phase flow experimental studies in an 88 cm long inclined narrow annular channel of hydraulic diameter of 4.5 mm. Slug flow, plug flow, annular flow, bubbly flow and churn flow were observed. Transition flow patterns like annular/slug, bubbly/plug and slug/bubbly flow were also observed. Studies were conducted at inclination angles of 0^o, 30^o and 60^o. All the above named flow patterns were observed at 0^o (horizontal orientation) at various superficial liquid and gas velocities except slug/bubbly flow which was observed only in the inclined channel (30^o and 60^o).

Ghajar and Tang (2007) conducted two phase flow experimental studies in horizontal and slightly inclined pipe having a diameter of 27.9 mm. Flow visualization was carried out in the transparent

portion of the pipe over inclination angles of 0^o, 2^o, 5^o and 7^o. They reported that the flow patterns observed for horizontal pipe orientation (0^o) were somewhat different from those observed in the slightly inclined pipe orientations (2^o, 5^o and 7^o). The major flow patterns observed in this study are stratified flow, slug flow, plug flow, wavy flow and annular flow. Slug/wavy flow, slug/bubbly flow and wavy/annular flow were observed as transition flow patterns. They explained that stratified flow observed in 0^o was replaced by slug flow at small inclination angle of 2^o and there was an increase in wave height and splashing for each flow pattern as pipe orientation increased beyond 2^o through 5^o then to 7^o.

In sum, similar flow patterns were observed by different researchers in near horizontal pipe orientation. The major flow patterns are slug flow, bubble flow, stratified flow and annular flow. These major flow patterns were observed during flow visualization and reported in present study. Thus, this literature review on flow pattern serves as an introduction to this concept and further analysis of flow pattern is discussed in chapter IV.

2.2 Flow Maps

Flow maps have been investigated and developed over decades in order to present graphical representation of how flow patterns change with corresponding change in flow properties in a two phase system. The size of flow maps have been reported to vary with capacity of experimental setup used. For horizontal pipe orientation, Baker (1954) developed one of the first flow maps in two phase flow. A few of the previous works on horizontal and near horizontal flow maps include Mandhane et al. (1974), Weisman et al. (1979) and Spedding and Nguyen (1980). Flow map comparison has been done by investigators over the years to illustrate the similarities and differences in flow maps developed by different researchers.

Mandhane et al. (1974) conducted two phase flow studies on the effect of pipe diameter and fluid properties on flow patterns in horizontal pipe. Pipe diameters in the range of 1.2 to 5 cm were used for experimentation and visual observation was supplemented with analysis of pressure drop fluctuation for accurate determination of flow patterns. A flow pattern map was developed for horizontal pipe orientation which was believed to predict flow patterns accurately.

Spedding and Nguyen (1980) conducted comparison of regime maps for two phase flow over various pipe orientations. They reported that the main error from flow map comparison was due to inaccurate drawings of the transition lines between flow patterns and difference in flow parameter used to develop the flow maps to be compared. However, they observed that different flow maps still show similarities in certain flow regimes. For example, in horizontal flow, flow map by Baker (1954) show similarities with Schicht (1969) in stratified flow, slug flow, plug flow and bubble flow. Comparisons of flow maps in the vertical pipe orientation was also done and they reported that more discrepancies were observed in the vertical pipe orientation than the horizontal due to no formal description of the flow patterns by investigators. However, comparison between flow maps developed by Spedding and Nguyen (1980) and other researchers in vertical orientation gave better similarities than in the horizontal due to more definite transition and fewer flow patterns in the vertical pipe orientation. Upward and downward inclined flow maps were developed which illustrated the change in transition lines with pipe orientation.

Troniewski and Ulbrich (1984) analyzed flow regime maps of two phase flow in pipes. Based on theoretical considerations, a universal coordinate system was developed to analyze 31 flow maps in vertical pipe orientation and 21 regime maps in horizontal pipe orientation. The universal coordinate system was verified with experimental results measured and they reported that excellent agreements were observed.

Spedding and Spence (1993) investigated flow regimes in two phase gas liquid flow by conducting co-current experiments in a 93.5 mm internal diameter horizontal pipe. Visual observation was carried out and pressure fluctuation was measured to determine flow pattern in the two phase flow. Preexisting maps like the Baker (1954) map and Lin and Harranty (1987) were analyzed and compared with their investigation. They reported that the previous regime maps and theories did not satisfactorily predict their observation due to difference in flow parameters adopted.

In sum, there is no universal procedure for developing flow maps and investigators develop flow maps based on the experimental setup used, pipe orientation and choice of flow parameter for analysis. Hence, flow map comparison is a difficult task. Flow maps were developed for each pipe orientation and comparison between flow maps developed in present study and other studies to illustrate the shift in flow pattern transition boundaries are discussed in chapter IV.

2.3 Void Fraction Correlations

As reported by Woldesemayat and Ghajar (2007), the correlations developed to predict void fraction are in four major forms based on the analysis adopted for modeling of the two phase flow system. They are drift flux model correlations, slip ratio correlations, empirical correlations and homogenous void fraction correlation (α_H).

Drift flux model

Wallis (1969) defined the drift flux model as a separated flow model based on relative velocity between the phases rather than individual phase velocity. Drift flux model can be used to analyze both steady and unsteady two phase flow over a wide range of flow patterns such as slug flow, stratified flow, annular flow, bubble flow and mixed flow patterns. For gravity dominated flows,

Wallis (1969) explained that the drift flux model analyzes the flow regimes appropriately by balancing out the pressure gradient and the forces between the components. The one dimensional formulation of the drift flux model was first proposed by Zuber and Findlay (1965) in terms of

$$\alpha = \frac{U_{sg}}{C_o U_m \pm U_{gm}}$$

Where α is void fraction, U_{sg} is superficial velocity of gas phase, U_m is superficial velocity of the two phase mixture (U_{sg} + U_{sl}), C_o is distribution parameter, U_{gm} is the drift velocity. The drift velocity can either be positive or negative in value based on the direction the gas phase travels relative to the two phase mixture. Assuming that fluid properties do not change across pipe cross section, cross sectional flow averaging is applied to the drift flux model and is shown as

$$\langle \alpha \rangle = \frac{\langle U_{sg} \rangle}{C_o \langle U_m \rangle \pm U_{gm}}$$

By definition,

$$\langle b \rangle = \frac{1}{A} \int b dA$$

Where b is the variable being analyzed.

The distribution parameter is defined as the concentration of the gas phase across pipe cross section and as explained by Wallis (1969), it is also used as a correction to the one dimensional flow theory which does not account for concentration across pipe cross section. The mathematical representation of distribution parameter is given as

$$C_o = \frac{\langle \alpha U_m \rangle}{\langle \alpha \rangle \langle U_m \rangle}$$

As explained by Wallis (1969), the expression for distribution parameter which is the ratio of the average of the product of mixture superficial velocity and concentration to the product of the averages can be used to obtain near unity parameters in two component flows.

The drift velocity is defined as the ratio of the averaged product of concentration and difference between the component velocity and the mixture velocity to the cross sectional averaged concentration. The mathematical representation of drift velocity is given as

$$U_{gm} = \frac{\langle \alpha (U_g - U_m) \rangle}{\langle \alpha \rangle}$$

Bhagwat and Ghajar (2013) explained that drift velocity is flow pattern dependent and as two phase flow progresses into the annular region, the drift velocity becomes negligible. They also explained that void fraction analysis either by cross sectional relation or volumetric relation is valid for non-boiling two phase flow. Hence, no distinctions exist between volumetric and cross sectional void fraction as it can be expressed as $\langle \alpha \rangle = \alpha$, and analysis of the distribution parameter and drift velocity follows the same concept. The drift flux model can be expressed in the form of equation of a straight line $y = mx + c$ given as

$$\frac{U_{sg}}{\alpha} = U_g = C_o U_m \pm U_{gm}$$

where C_o represents the slope m and U_{gm} represents the intercept y. Drift flux model has been analyzed by many investigators and comprehensive performance analysis of drift flux model based void fraction correlations was carried out by Woldesemayat and Ghajar (2007), Godbole et al. (2011) and Bhagwat and Ghajar (2013). They all reported that the top performing correlations are based on drift flux model. Some drift flux models were developed to have constant drift velocity and distribution parameter in the two phase system over the entire flow combinations of superficial velocities of liquid and gas phase. For example, Morooka et al. (1989) calculated constant values of drift velocity and distribution parameter as 0.45 and 1.08, Greskovic and

Cooper (1975) developed a correlation by assigning a constant value of 1 to distribution parameter while drift velocity is dependent on constant values of pipe diameter and pipe orientation. Niklin et al. (1962) calculated 1.2 as constant distribution parameter and the drift velocity is a function of pipe diameter and acceleration due to gravity given as $0.35\sqrt{gD}$. Some correlations developed by other researchers have constant distribution parameter while the drift velocity varies with change in flow properties. Gomez et al. (2000) assigned a constant value of 1.15 to the distribution parameter while the drift velocity is a function of density difference, surface tension, pipe orientation, void fraction and other flow parameters. Bonnecaze et al. (1971) gave a constant value of 1.2 to distribution parameter and drift velocity varies with density ratio of the liquid and gas phase at various flow conditions. Similarly, other drift flux correlations were developed to have both distribution parameter and drift velocity vary with flow properties. Examples of these correlations are Woldesemayat and Ghajar (2007), Sun et al. (1981), Rouhani and Axelsson (1970) and Bhagwat and Ghajar (2013). Bhagwat and Ghajar (2013) explained that in order to accurately develop drift flux model based void fraction correlation, drift velocity and distribution parameter must be accurately analyzed and modeled. Since distribution parameter is a function of void fraction and void fraction varies with flow pattern, then the distribution parameter must change with void fraction or flow pattern accordingly. They reported that in the annular flow region in vertical pipes, distribution parameter approaches unity as void fraction profile is almost flat except near wall axis. For slug and bubbly flow, void fraction profile peaks at pipe center and distribution parameter was observed around 1.2. Distribution parameter is found to be less than 1 in the near horizontal downward inclined pipe orientation at low gas velocities due to higher residence time of gas phase in the pipe and thus higher void fraction is observed. Based on all the observations discussed above, they modeled the distribution parameter by considering pipe diameter, liquid and gas phase superficial velocities, densities, critical pressure of the system, void fraction, thermodynamic quality and liquid phase dynamic viscosity.

They modeled the drift velocity based on various fluid properties, pipe orientation (pipe orientation determines the balance between gravitational and drag forces on the gas phase), pipe diameter and void fraction. In sum, drift flux model void fraction correlation has been verified to predict void fraction with highest accuracy due to the simplicity, flexibility and ability to predict flow physics of a two phase system. However, it has its limitations to one dimensional flow modeling.

Slip ratio

By definition, slip ratio is the ratio of cross sectional averaged gas phase velocity to liquid phase velocity. Mathematically, slip ratio is given as

$$Sr = \frac{\langle U_g \rangle}{\langle U_l \rangle}$$

Where U_g and U_l are gas and liquid phase intrinsic velocities.

From the fundamental void-quality relation, slip ratio can be expressed in terms of thermodynamic quality, wetness fraction, void fraction and liquid and gas phase densities given as

$$\frac{\langle x \rangle}{1 - \langle x \rangle} = \frac{\rho_g}{\rho_l} Sr \frac{\langle \alpha \rangle}{1 - \langle \alpha \rangle}$$

Generally, slip ratio correlations are expressed in terms of the ratio between wetness fraction (*1 - x*), quality *x* and other two phase fluid properties. The performance of a few slip ratio correlations in predicting void fraction was analyzed in present study which are Smith (1969), Lockhart and Martinelli (1949) and Yashar et al. (2001).

Homogenous void fraction α_H

These correlations are a function of the homogenous void fraction term α_H. This term is also referred to as the volumetric flow quality β in Guzhov et al. (1967) given as

$$\beta = \frac{U_{sg}}{U_{sg} + U_{sl}}$$

A few correlations based on the α_H parameter as reported by Woldesemayat and Ghajar (2007) are Bankoff (1960), Hughmark (1962), Greskovic and Cooper (1975) and Czop et al. (1994).

Empirical

As explained by Woldesemayat and Ghajar (2007), empirical correlations are referred to as general void fraction correlations. They explained that these general correlations are a function of various physical parameters which are defined from basic fluid principles and experimental data. Some of the empirical correlations reported by Woldesemayat and Ghajar (2007) are Minami and Brill (1987), Kawaji et al. (1987), Hart et al. (1989) and Wallis (1969).

A plethora of correlations exist for calculating void fraction based on various flow conditions. Most void fraction correlations are developed based on pipe orientation at which experimental studies were conducted. Investigators are often faced with the problem of limited data from outside sources for appropriate modification of developed correlation to account for different flow conditions, pipe orientation and pipe diameters. The major pipe orientations at which void fraction correlations have been developed are vertical upward, vertical downward and horizontal pipe orientation. Beggs and Brill (1973) observed that void fraction reaches a minimum value at pipe inclination of approximately $+50^o$ and maximum value at -50^o from horizontal. They reported that void fraction at $+90^o$ and $+20^o$ are approximately equal, hence this explains why some correlations developed for vertical upward two phase flow predict void fraction accurately in the horizontal orientation. For the purpose of limiting the scope of this study (near horizontal

pipe orientation) and based on the comprehensive void fraction correlation comparison studies previously done by Woldesemayat and Ghajar (2007) for horizontal and upward inclined pipes and Godbole et al. (2011) for vertical upward pipe orientation, fourteen void fraction correlations were selected for analysis in presented study (analysis are discussed in chapter IV). These correlations are discussed in this chapter based on the pipe orientation over which they were developed. Specifically, void fraction correlations are discussed for vertical upward pipe orientation, horizontal pipe orientation and multiple pipe orientations including near horizontal orientation.

2.3.1 Void Fraction Correlations Developed for Vertical Pipe Orientation

The use of Nicklin et al. (1962) was reported by Woldesemayat and Ghajar (2007) and Godbole et al. (2011). Nicklin et al. (1962) conducted two phase flow studies in vertical tubes and developed a drift flux model based correlation which is given as

$$\alpha = \frac{U_{sg}}{(C_o U_m + U_{gm})}$$

Where

$U_{gm} = 0.35\sqrt{gD}$

$C_o = 1.2$

Rouhani and Axelsson (1970) studied two phase flow in subcooled and quality boiling regions. Void fraction correlation was developed based on calculated steam quality by using the derivations of Zuber and Findlay (1965). They reported that the correlation performed well over different geometries including small rectangular channel and large bundle rods for pressures from 19 to 138 bars. The Rouhani and Axelsson correlation as reported by Woldesemayat and Ghajar (2007) is given as

$$\alpha = \frac{U_{sg}}{(C_o U_m + U_{gm})}$$

Where

$$U_{gm} = 1.18\left(g\sigma\frac{\rho_l - \rho_g}{\rho_l^2}\right)^{0.25}$$

For correlation referred to as Rouhani and Axelsson – I,

$$C_o = 1 + 0.2(1 - x)$$

For correlation referred to as Rouhani and Axelsson – II,

$$C_o = 1 + 0.2(1 - x)\left(\frac{gD\rho_l^2}{G^2}\right)^{0.25}$$

In the study of Woldesemayat and Ghajar (2007), Rouhani and Axelsson – I performed better than Rouhani and Axelsson – II.

Sun et al. (1981) conducted studies on the prediction of two phase mixture level and hydro dynamically controlled dry out under low flow conditions and developed a model to predict void fraction in vertical pipe orientation based on conservation laws and loop momentum equations. The drift flux void fraction correlation developed by Sun et al. (1981) is given as

$$\alpha = \frac{U_{sg}}{\left(U_m\left[0.82 + 0.18(P_{sys}/P_{cr})\right]^{-1}\right) + 1.41\left(g\sigma\frac{\rho_l - \rho_g}{\rho_l^2}\right)^{0.25}}$$

Morooka et al. (1989) conducted void fraction studies on a vertical 4 x 4 rod bundle for steam-water two phase flow using advanced X-ray CT scanner. Two parameters were used to evaluate the void fraction data measured, these parameters are pressure, quality and mass flux. Based on the measured data, a drift flux model was developed to predict void fraction in vertical upward pipe which gave constant distribution parameter and drift flux velocity as given as

$$\alpha = \frac{U_{sg}}{1.08U_m + 0.45}$$

2.3.2 Void Fraction Correlations Developed for Horizontal Pipe Orientation

One of the first void fraction correlations developed for horizontal pipe orientation was proposed by Lockhart and Martinelli (1949). As reported by Woldesemayat and Ghajar (2007), the Lockhart and Martinelli (1949) void fraction correlation is given as

$$\alpha = [1 + 0.28\left(\frac{(1-x)}{x}\right)^{0.64}\left(\frac{\rho_g}{\rho_l}\right)^{0.36}(\frac{\mu_l}{\mu_g})^{0.07}]^{-1}$$

Yashar et al. (2001) conducted experimental studies to determine void fraction for condensation and evaporation processes in horizontal microfin tubes using refrigerants R134a and R410A. Tubes having diameters of 7.3 mm and 8.9 mm with the axial and 18 degree helix which are 1.2 m long were used for experimentation. Evaporation experiments were conducted in all four tubes while condensation was carried out in the 8.9 mm diameter tube. Quick closing valves were used for void fraction measurement and based on the experimental data a correlation was developed to predict void fraction which is given as

$$\alpha = \left[1 + \sqrt{\frac{(1-x)gD\rho_l^2}{G^2x^3} + \left(\frac{1-x}{x}\right)^{0.9}\left(\frac{\rho_g}{\rho_l}\right)^{0.5}\left(\frac{\mu_l}{\mu_g}\right)^{0.1}}\right]^{-0.321}$$

2.3.3 Void Fraction Correlations Developed for Multiple Pipe Orientations Including Near Horizontal

The use of Guzhov et al. (1967) correlation for predicting void fraction was reported by Woldesemayat and Ghajar (2007) which was developed for slug and stratified flow and pipe orientation in the range of ±9^o from horizontal. Guzhov et al. (1967) correlation is given as

$$\alpha = 0.81\beta(1 - \exp(-2.2\sqrt{Fr}\,)$$

Where β is volumetric flow quality and Fr is Froude number

$$\beta = \frac{U_{sg}}{U_{sg} + U_{sl}} \; and \; Fr = \frac{(U_{sg+}U_{sl})^2}{gD}$$

Smith (1969) developed a correlation which assumes two phase flow regime is annular flow. It is a slip ratio based correlation which adopts an equal velocity head model for the liquid phase and homogenous mixture to predict void fraction. Smith (1969) correlation can be applied over a range of inclined pipe orientation and is given as

$$\alpha = \left(1 + \frac{\rho_g}{\rho_l}\left(\frac{1-x}{x}\right)\left[0.4 + 0.6\left(\frac{\rho_l/\rho_g + 0.4(1/x-1)}{1 + 0.4(1/x-1)}\right)^{0.5}\right]\right)^{-1}$$

Bonnecaze et al. (1971) conducted experimental two phase flow in a 24.4 m long and 38 mm diameter pipe over pipe inclination from -10^o to +10^o. They developed drift flux model based void fraction correlation for slug flow in inclined pipes by analyzing the mass and momentum balance on the two phase flow. The void fraction for slug flow was related to translational velocity, no-slip velocity and volumetric flow fraction of the liquid phase. A constant value of 1.2 was assigned to the distribution parameter and the correlation is given as

$$\alpha = \frac{U_{sg}}{\left(1.2U_m + 0.35\sqrt{gD(1 - \frac{\rho_g}{\rho_l})}\right)}$$

Greskovic and Cooper (1975) conducted two phase flow studies in upward inclined pipes over pipe orientation from horizontal to +10^o using 2.54 cm and 7.94 cm diameter pipes using air-water as the fluid combination. They developed the correlation based on the technique proposed by Bonnecaze et al. (1971) and the void fraction is a function of Froude number and pipe inclination. They reported that the correlation predicted between ±5% for high void fraction values and ±10% for low void fraction. The correlation developed by Greskovic and Cooper (1975) is given as

$$\alpha = \frac{U_{sg}}{C_o U_m + U_{gm}}$$

Where

$$U_{gm} = 0.671\sqrt{gD}\,(sin\theta)^{0.263}, C_o = 1$$

Gomez et al. (2000) developed a correlation to predict liquid holdup for slug flow from horizontal pipe to vertical pipe orientation. A total of 283 data points were gathered from different sources for pipe diameters of 5.1 cm to 20.3 cm with fluid combinations of air-water, Freon-water, air-oil, and air-kerosene. They explained that void fraction is a function of pipe inclination which is minimum at vertical and maximum at horizontal orientation. They also reported that void fraction is a function of mixture velocity and viscosity of the liquid phase. The correlation developed by Gomez et al. (2000) is given as

$$\alpha = \frac{U_{sg}}{(C_o U_m + U_{gm})}$$

Where

$$U_{gm} = 1.53(\frac{g\sigma\Delta\rho}{{\rho_l}^2})^{0.25}\sqrt{1-\alpha}\,sin\theta, C_o = 1.15$$

Woldesemayat and Ghajar (2007) conducted void fraction correlation comparison for different flow patterns in horizontal and upward inclined pipes. 68 void fraction correlations were analyzed based on 2845 data points of void fraction gathered from various sources. The Dix (1971) drift flux model correlation was modified by Woldesemayat and Ghajar (2007) for improved predictive capacity based on their analysis of the 68 selected void fraction correlations for their study. The correlation developed by Woldesemayat and Ghajar (2007) was observed to perform better than all 68 correlations analyzed in the study, is independent of flow patterns and can be used over pipe orientations from horizontal to vertical upwards and is given as

$$\alpha = \frac{U_{sg}}{C_o U_m + U_{gm}}$$

Where

$$C_o = \frac{U_{sg}}{U_{sg} + U_{sl}}\left[1 + \left(\frac{U_{sl}}{U_{sg}}\right)^{(\rho_g/\rho_l)^{0.1}}\right]$$

$$U_{gm} = 2.9(1.22 + 1.22sin\theta)^{(P_{sys}/P_{atm})}\left[\frac{gD\sigma(1 + cos\theta)(\rho_l - \rho_g)}{\rho_l^2}\right]^{0.25}$$

The leading constant of 2.9 carries units of $m^{-0.25}$.

Cioncolini and Thome (2012) conducted two phase flow studies in annular flow and developed a correlation based on gathered data to predict void fraction. 2673 void fraction data points were collected from 29 sources and the data covers 8 different fluid combinations of air-water, nitrogen-water, argon-water, steam-water, R410a, air-kerosene, air-alcohol and water plus air-alcohol for pipe diameters in the range of 1.05 mm to 45.5 mm for both circular and non-circular geometry. They developed a correlation based on biochemical kinetics used in mathematical physiology which is a function of vapor quality and gas to liquid density ratio given as

$$\alpha = hx^n/(1 + (h - 1)x^n)$$

Where

$$h = -2.129 + 3.129(\rho_g/\rho_l)^{-0.2186}$$

$$n = 0.3487 + 0.6513(\rho_g/\rho_l)^{0.515}$$

Bhagwat and Ghajar (2013) conducted extensive research in two phase flow to develop a drift flux model based void fraction correlation that is independent of flow patterns (covers both the major flow patterns and transition flow patterns), pipe orientation ($-90^o \leq \theta \leq +90^o$) and pipe geometry (circular, annular and rectangular) over range of 0.5 to 305 mm. The void fraction correlation covers fluids within viscosity range of 0.0001 Pa-s to 0.6 Pa-s, system pressure range of 0.1 MPa to 18.1 MPa and Reynolds number range of 10 to $5x10^6$. This highly versatile correlation also has the capacity to predict void fraction in fluid combinations of air-water, argon-water, natural gas-water, air-kerosene, air-glycerin, argon-acetone, argon-ethanol, argon-alcohol,

refrigerants (R11, R12, R22, R134a, R114, R410A, R290 and R1234yf), steam-water and air-oil. The correlation was verified with 8255 data points collected from more than 60 sources and was determined to perform consistently accurate and satisfactorily over the collected data. The void fraction correlation developed by Bhagwat and Ghajar (2013) is given as

$$\alpha = \frac{U_{sg}}{C_o U_m + U_{gm}}$$

Where

$$C_o = \frac{2 - (\rho_g/\rho_l)^2}{1 + (Re_{tp}/1000)^2} + \frac{\left[\sqrt{(1 + (\rho_g/\rho_l)^2\, cos\theta)/(1 + cos\theta)}^{\,1-\alpha}\right]^{2/5} + C_{o,1}}{1 + (Re_{tp}/1000)^2}$$

$$C_{o,1} = \left(C_1 - C_1\sqrt{\rho_g/\rho_l}\right)\left((2.6 - \beta)^{0.15} - \sqrt{f_{tp}}\right)(1 - x)^{1.5}$$

$$U_{gm} = (0.35 sin\theta + 0.45 cos\theta)\sqrt{\frac{gD_h(\rho_l - \rho_g)}{\rho_l}}(1 - \alpha)^{0.5} C_2 C_3 C_4$$

$$C_1 = 0.2$$

$$C_2 = \begin{cases} \left(\frac{0.434}{log_{10}(\mu_l/0.001)}\right)^{0.15} & (\mu_l/0.001) > 10 \\ 1 & (\mu_l/0.001) \le 10 \end{cases}$$

$$C_3 = \begin{cases} (La/0.025)^{0.9} & La < 0.025 \\ 1 & La \ge 0.025 \end{cases}, La = \sqrt{\sigma/(g\Delta\rho)}/D_h$$

$C_4 = -1$ $\left(0° > \theta \ge -50°, Fr_{sg} \le 0.1\right)$, otherwise $C_4 = 1$

$$Re_{tp} = \frac{(U_{sl} + U_{sg})\rho_l D_h}{\mu_l}, \beta = \frac{U_{sg}}{U_{sg} + U_{sl}}$$

$$\frac{1}{\sqrt{f_{tp}}} = -4.0 log_{10}\left(\frac{\in/D_h}{3.7} + \frac{1.256}{Re_{tp}\sqrt{f_{tp}}}\right)$$

In sum, the fourteen void fraction correlations discussed in this literature review were used to predict measured void fraction in all six pipe orientations to determine the top performing correlation for the specified void fraction region. Analysis was further conducted based on upward pipe orientation, downward pipe orientation and the entire pipe orientation (near horizontal) as discussed in chapter IV.

CHAPTER III

EXPERIMENTAL SETUP

The experimental setup used in present study is discussed in this chapter with all the major components used alongside for its operation. The test section which encompasses void fraction, pressure drop, heat transfer and flow visualization section is briefly discussed. Flow visualization procedure for flow pattern identification is discussed and the technique for taking still-pictures developed by Cook (2008) was modified to improve picture quality by changing both the orientation and type of light source used. The procedure taken for experimentation and data acquisition process using LabVIEW are briefly discussed. Also, the effect of pipe orientation on void fraction calibration parameter was observed.

Validation of measurement technique (quick closing valve) was done by comparison with other void fraction measurement techniques existing in literature. Measured void fraction data was validated by comparison of experimental void fraction data measured in present study with data gathered from other sources and also by predictions of the four top performing correlations selected for analysis in present study (chapter IV). Experimental uncertainty for all six pipe orientations was calculated and presented to determine the accuracy of measured void fraction in present study.

3.1 Details of Experimental Setup

The experimental setup used in present study is situated at the Two Phase Flow Lab, Oklahoma State University and it was designed, fabricated, tested and validated by Cook (2008). The experimental setup has a robust capacity to measure data for the three major aspects of two phase flow which are void fraction, pressure drop and heat transfer in both smooth and rough pipe, with variable inclinations from vertical downward (-90^o) to vertical upward ($+90^o$). The test branches are supported by a platform made from aluminum sheet which measures 3.35 m (11 ft) in length and 0.61 m (2 ft) in width. The test platform is supported by the variable inclination frame which is made of a heavy outer frame and lighter inner rolling frame. The heavier outer frame measures 4.57 m (15 ft) in length, 0.84 m (33 in) in width and 3.66 m (12 ft) in height and made from rectangular steel tubing. The lighter inner rolling frame is made of steel angle and allows for adjustment of test platform inclination over 180 degrees from vertical downward to vertical upward.

The test section is divided into two branches, the flow visualization/ void fraction branch and the heated test branch. Smooth transparent pipe was used for the flow visualization/ void fraction branch for ease of identification of flow patterns through the pipe. Still-pictures of flow patterns were taken in this section to better assist investigator in flow pattern identification. The smooth pipe is made of polycarbonate material and the rough pipe is made of stainless steel both having internal diameter of 0.0127 m. The fluid combination used in present study is water and air and the schematic diagram of the experimental setup is shown as Figure 3.1

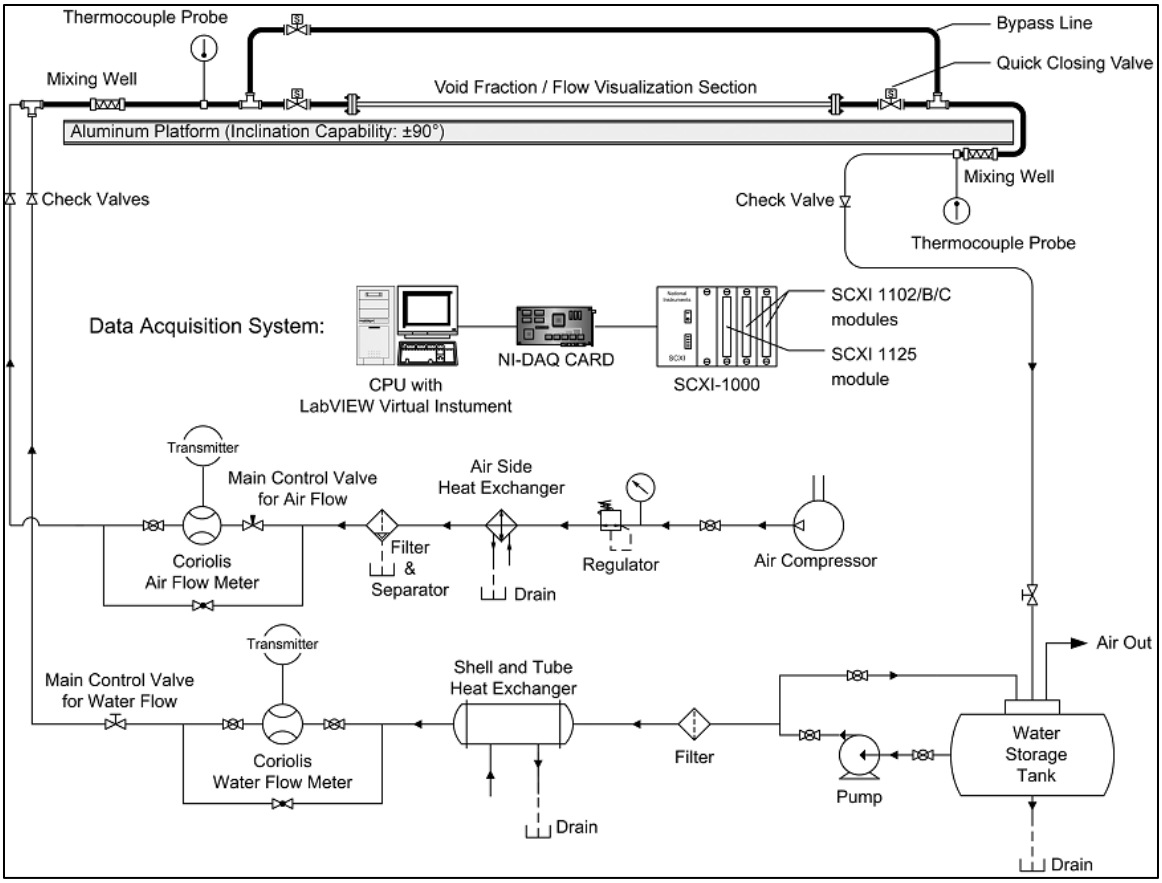

Figure 3.1 Schematic diagram of experimental setup adapted from Cook (2008)

The schematic diagram in Figure 3.1 shows the test section and the major components required for transporting the liquid and gas phases into the test branches. The liquid and gas phases have different flow circuits and are mixed at test section entrance to give the two phase mixture needed for experimentation.

Water flow circuit

Distilled water was used as working fluid for the setup which was stored in a 208.2 L (55 gallon) polyethylene cylindrical tank. A Bell and Gosset 1535 series Coupled Centrifugal Pump was used to pull water from the tank, the pump model number is 3545 D10. The pump can generate water flow rate up to 0.226 kg/s which was sufficient for both single phase and two phase flow

experimental purposes on this setup. An Aqua-Pure AP12T water purification system was installed right after the pump to prevent growth of organic matter and also trap foreign objects introduced in the water system. The maximum operating temperature of the water purification system is 38^{o} C (100^{o} F) and maximum pressure of 862 kPa (125 psi). After filtration, the water runs through a shell and tube heat exchanger (ITT Model BCF 4063) which was incorporated in the water transport system in order to maintain constant water temperature through the experimental setup. Cooling water was obtained from tap water, and the temperature varied based on outside temperature usually between the range of 18^{o} C (64.4^{o} F) and 26^{o} C (78.8^{o} F). The water goes through the Coriolis flow meter which controls the flow rate by a gate valve located just after the flow meter assembly. After water flow rate has been fixed by the flow meter as it runs through it, the water then mixes with air as it passes through the test section and then returns to the 208.2 L cylindrical tank.

Air flow circuit

Ingersoll-Rand T30 Model 2545 air compressor provides the air for the experimental process. The maximum air pressure attained by compressor is 862 kpa and maximum flow rate of 0.25 kg/min. The air passes through a filter-drier assembly/ regulator immediately after leaving the compressor in order to maintain constant air pressure, remove moisture from the air and trap unwanted objects. The air then passes through a simple copper coil heat exchanger submerged in running water. The heat exchanger was used to remove heat generated by the compressor and maintain close inlet water and air temperature. The air was further dried by passing through another filter-drier assembly and regulated by a Parker Model 24NS 82(A) – V8LN-SS needle valve. After air regulation, it then goes through either the high or low (Micro Motion Elite Series model CMF 025 or LMF 3M) flow meter before being mixed with purified water in the mixing section of the experimental setup. Figure 3.2 shows the schematic diagram of void fraction section, flow visualization section, mixing section and thermocouple array adapted from Cook (2008).

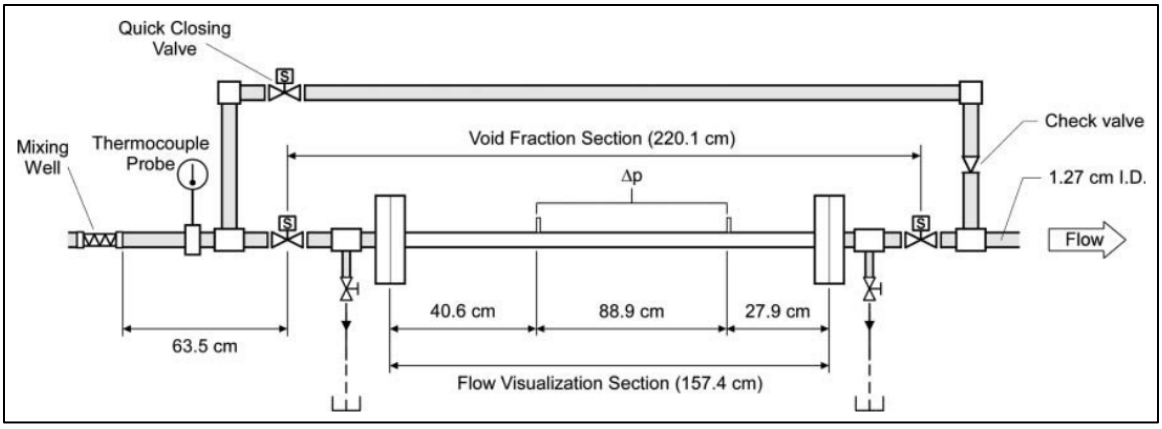

Figure 3.2 Flow visualization/ Void fraction branch adapted from Cook (2008)

Mixing section

Static mixers installed at the inlet and exit of test section are Koflo Model 3/8-40C-4-3V-2. The primary purpose of the two mixers was to ensure mixing of the two phases so that the inlet and exit thermocouples could sense the representative temperature of the two phase mixture entering and leaving the test section. The inlet mixer also served the purpose of eliminating the effect of inlet geometry on flow patterns observed in the test section.

Thermocouple probes

Thermocouple probes were installed at test section entry and exit. They serve the purpose of sensing the temperature of two phase mixture at inlet and exit of test section. The thermocouple probes were placed after the static mixers to sense the two phase mixture temperature immediately after mixing. They are Omega TMQSS-06U-6 models.

Void fraction branch

Three quick closing solenoid valves are used in this section. The solenoid valves are W.E. Anderson model ABV1DA101 pneumatically operated ball valves. Two of the valves are normally open and were installed in entry and exit of the test section while the third solenoid valve is a normally closed valve installed in the bypass line of the test section. When the switch controlling the valves is triggered, the normally open solenoid valves which have a shut time of 0.03 seconds closes to trap the two phase mixture in the test section while the normally closed solenoid valve opens to allow continuous flow of the two phases through the bypass line. Compressed air was used to ensure maximum removal of trapped liquid from the test section.

Flow visualization

This section is located in the central portion of the void fraction section. Optical clarity of this section is highly important in order to accurately observe flow patterns developed in the test section, hence two phase flow was observed inside transparent polycarbonate pipe during flow visualization. The arrangement of photography lighting also plays a key role in flow visualization because poor lighting, wrong proximity and orientation of light source and type of backdrop affect the quality of still-pictures taken. Arrangement for photography lighting for this experimental setup was developed by Cook (2008). However, the arrangement was modified and was observed to produce improved picture quality in present study. The schematic diagram for photography lighting developed by Cook (2008) and the modified arrangement are given in Figures 3.3 and 3.4.

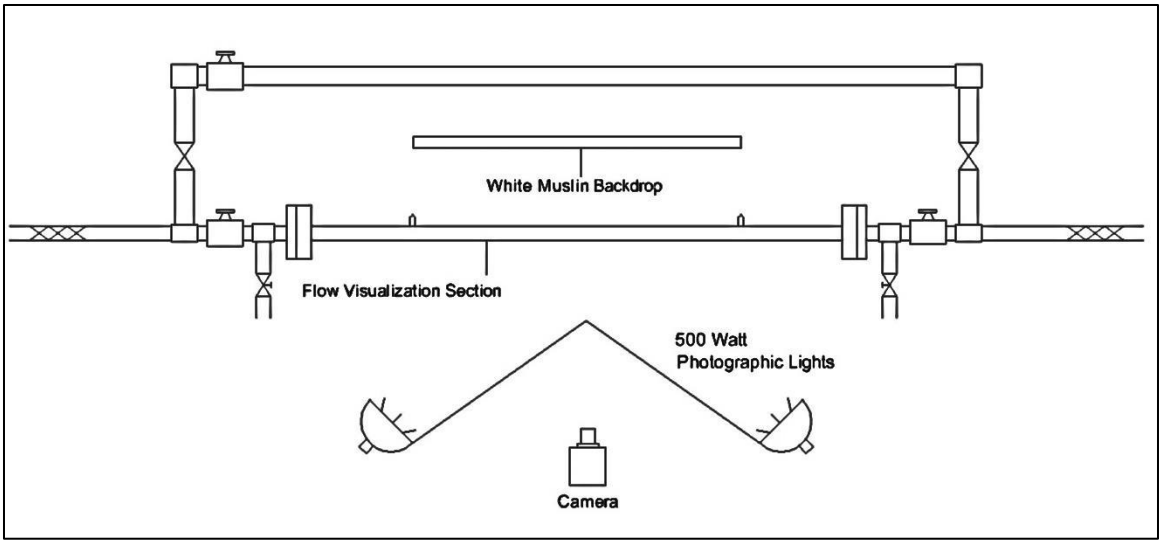

Figure 3.3 Photography lighting and backdrop arrangement adapted from Cook (2008)

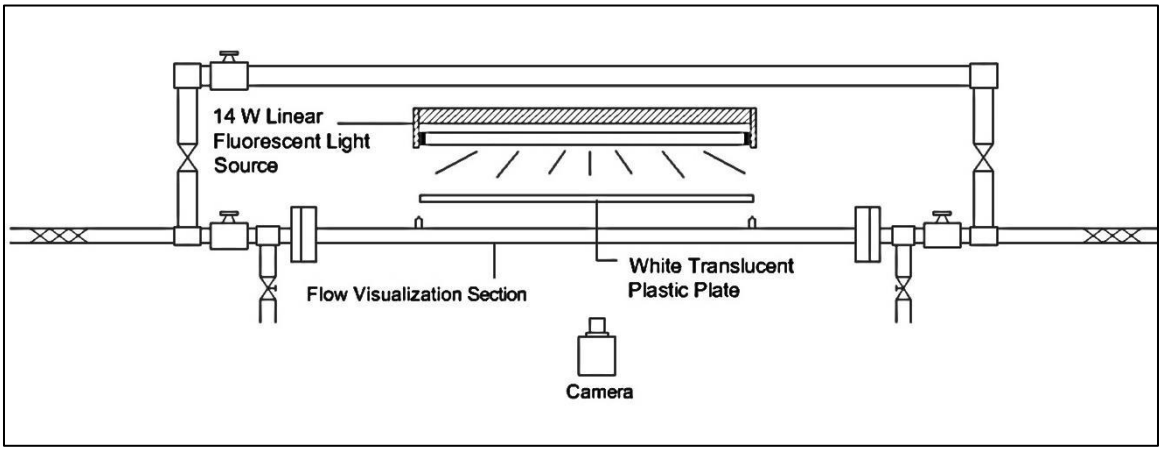

Figure 3.4 Modified lighting arrangement used in present study

In the modified arrangement shown as Figure 3.4, the light source was supplied using a 14 Watt linear fluorescent tube and placed behind the flow visualization section. This light source was easier to fit and maneuver due to portability and was placed about 50 mm from the flow visualization section unlike the previous method shown in Figure 3.3. This proximity of the light source to the flow visualization section helped to adequately concentrate the light to the portion of the transparent pipe needed for photography. White translucent plastic plate was placed in

between the 14 Watt fluorescent light source and the transparent pipe. This arrangement helped to filter the scattered light rays coming from the source and also create the adequate backdrop for the required background lighting. Crystal clear pictures were observed due to reduced reflection off the transparent pipe and clear distinction between the two phases in the pipe was observed.

3.2 Procedure for Flow Visualization

Flow visualization was conducted in a 154.7 cm long pipe portion of the void fraction section. Flow visualization was done several times to ensure repeatability and consistency with observed flow patterns. Observing the transition between flow patterns was the most challenging task because this determines the nature of the boundaries on the flow map and how they shift with respect to change in pipe orientation. Visual observations were supported with various definitions available in the literature and with the aid of high resolution 14 megapixels Nikon D3100 camera with shutter speed of $1/4000^{th}$ of a second. The use of the camera was necessary because at high liquid and gas mass flow rates, flow pattern identification with ordinary eyes became very difficult. Four major flow patterns were observed in the upward inclined pipe orientation and five major flow patterns were observed in the downward. Details of these flow patterns are fully discussed in chapter IV.

3.3 Procedure to Measure Void Fraction

The procedure for void fraction measurement was followed as developed by Cook (2008). This is a four step procedure which includes pre-operation checks, system warm up, data collection and shut down. The calculated volume of test section is 277.5 cc and can hold 276.9 g of water. As reported by Cook (2008), liquid phase gets trapped in the fittings of the solenoid valves and

pressure taps in the test section. Calibration of void fraction section was necessary to prevent inaccurate void fraction measurements due to the trapped liquid mass. Single phase liquid is run through the test section, trapped, drained into a 9.8L tank and then weighed. Trapped mass was calculated with the relation, $m_T = 276.9 - m_{liq}$. This process was repeated at least 3 times and the average value was taken as the actual trapped mass for the pipe orientation. Calibration for every pipe orientation was necessary because trapped mass was observed to change with pipe orientation. The calculated trapped mass for each pipe orientation is given as Table 3.1

Table 3.1 Calculated trapped mass for each pipe orientation

Pipe Orientation (θ)	Trapped Mass (g)
$+20^o$	14.9
$+10^o$	13.9
$+5^o$	13.1
-5^o	14.4
-10^o	15.4
-20^o	14.9

Void fraction was measured by fixing the flow rates of the liquid and gas phase followed by trapping the mixture in the void fraction/ flow visualization section. The trapped liquid was then drained and weighed. This was repeated four times for very small variation in drained liquid for the same flow combination, or repeated 6 times when very high variation was observed in liquid drained from the test section i.e., non-uniform slug flow pattern region. The average of the recorded drained liquid was taken as the actual mass of the liquid phase at the given flow rates. Hence, this gave a better representative value of the mass of the liquid phase drained from the void fraction section. The measured void fraction for the given flow rates for all six pipe

orientations was calculated by the expression, $\alpha = 1 - \frac{m_{liq}+m_T}{m_{tot}}$, where m_{liq}, m_T and m_{tot} are the mass of liquid drained from the test section at the given flow rates, trapped mass for the pipe orientation and total mass of liquid the test section can hold. m_{tot} was taken constant for 276.9 g for all six pipe orientations.

Data acquisition system

The components of the data acquisition system were products of National Instruments. The data acquisition system consisted of three major parts: chassis, modules and terminal blocks. The chassis with model number SCXI 1000 serves as a housing of the components. Two 32 channel analog modules of model number SCXI 1102 and 8 channel analog modules with model number SCXI 1125 were connected to the chassis for signal processing. The terminal blocks were connected to the end of the modules. The terminal blocks model numbers were SCXI 1303 for the 32 modules and SCXI 13138 for the 8 modules. LabVIEW was developed as a graphical interface between the user and the program for the data acquisition process. The program was developed by Jae-Yong Kim, a former PhD student and modifications were made by Clement Tang, another former PhD student and former member of two phase flow research team.

3.4 Uncertainty Analysis of Void Fraction Data

Uncertainty analysis of measured void fraction was calculated to evaluate the accuracy of measured void fraction and performance of experimental setup. The uncertainty associated with void fraction was calculated using the relation,

$w_\alpha = \sqrt{\left(\frac{w_{liq}}{m_{tot}}\right)^2 + \left(\frac{m_{liq}}{m_{tot}^2} w_{m_{tot}}\right)^2}$, where m_{liq} represents the mass of liquid trapped in the test section and m_{tot} is the total mass that can be trapped in the test section (276.9 g). Considering the worst case scenario, the value of m_{tot} had an estimated uncertainty of ±2.0 g and m_{liq} had an

estimated uncertainty of ±3.0 g. Readers should kindly refer to Cook (2008) for more information about these uncertainties.

Hence, uncertainty calculated with this equation is dependent on liquid flow rate and it was observed that uncertainty increased for decrease in void fraction. Uncertainty was calculated for all measured void fraction data in six pipe orientations. The minimum and maximum uncertainty for each pipe orientation is given in Table 3.2.

Table 3.2 Void fraction uncertainty for six pipe orientations

Pipe Orientation	Uncertainty (Min)	Uncertainty (Max)	Liquid flow rate Max (kg/min)	Gas flow rate (kg/min)	Void fraction
$+20^o$	±1.3%	±42%	12.3	0.0015	0.03
$+10^o$	±1.3%	±13.8%	11.4	0.0015	0.09
$+5^o$	±1.3%	±16.5%	11.4	0.0015	0.08
-5^o	±1.3%	±14.3%	11.4	0.0015	0.13
-10^o	±1.3%	±12.7%	11.4	0.0015	0.1
-20^o	±1.3%	±10.1%	11.4	0.0015	0.09

As shown in Table 3.2, minimum uncertainty of ±1.3% was calculated at the lowest liquid mass flow rate of 1.36 kg/min and high gas mass flow rate of 0.2 kg/min for all pipe orientations in present study. Percentage uncertainty is calculated based on the ratio of calculated uncertainty to measured void fraction and low values of void fraction give very high percentage uncertainty. As developed by Cook (2008),

$$Percentage\ Uncertainty = \frac{w_a}{\alpha}\ X\ 100$$

Where w_a is the calculated uncertainty associated with measured void fraction α. As stated above, calculated uncertainty is dependent on liquid flow rate and for high liquid flow rate of 12.3

kg/min at $+20^{o}$ pipe orientation, the measured void fraction is 0.03 and calculated uncertainty of 0.013 thereby giving percentage uncertainty of ±42% as shown in Table 3.2. It should be noted that maximum uncertainty was ±16.5% or less in present study for void fraction void fraction values ≥ 0.08. Similarly, the percentage uncertainty for $+5^{o}$ pipe orientation of ±16.5% is greater than ±13.8% of $+10^{o}$ at the same liquid and gas flow rates. This increase in percentage uncertainty was due to lower value of void fraction in $+5^{o}$ and thus percentage uncertainty is higher.

3.5 Accuracy of Void Fraction Data

Quick closing valve method of void fraction measurement was compared with other existing methods in literature. This was done to eliminate the dependency of measured void fraction on technique adopted. Kawanishi et al. (1990) conducted experimental study on co-current and counter-current steam-water two phase flow by using 102.3 mm and 10.9 mm diameter pipes. They compared measured void fraction data by using quick closing valves and electrical conductivity probe, they observed that the comparisons were within ±15% error bands. They reported that void fraction measured using quick closing valves also helped in developing drift flux parameters needed for two phase flow modeling. Yijun and Rezkallah (1993) carried out comparison on measured void fraction by using quick closing valves and Gamma densitometer. They observed that both methods gave void fraction values within ±10% error bands. Figures 3.5 and 3.6 give the graphical representation of measurement technique comparison developed by Kawanishi et al. (1990) and Yijun and Rezkallah (1993).

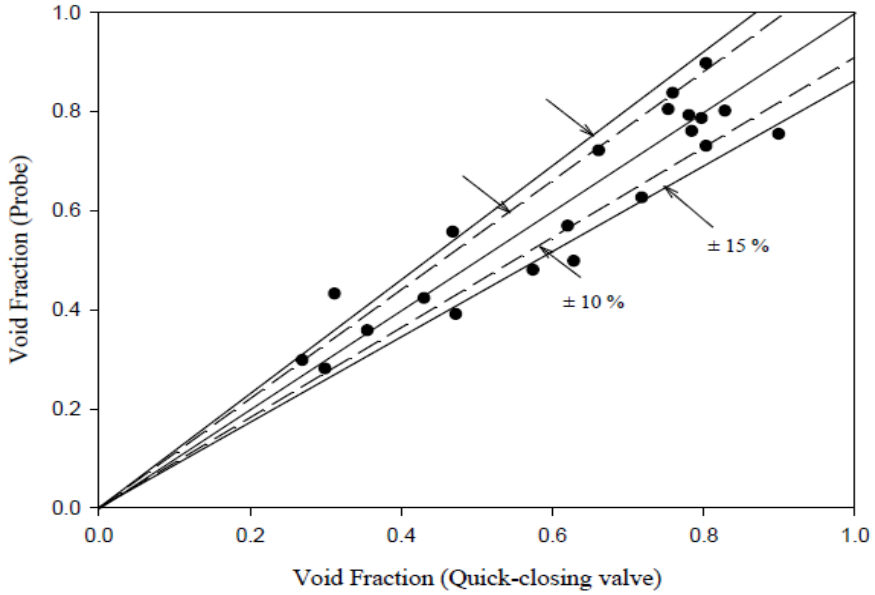

Figure 3.5 Comparison of void fraction measurement techniques adapted from Kawanishi et al. (1990)

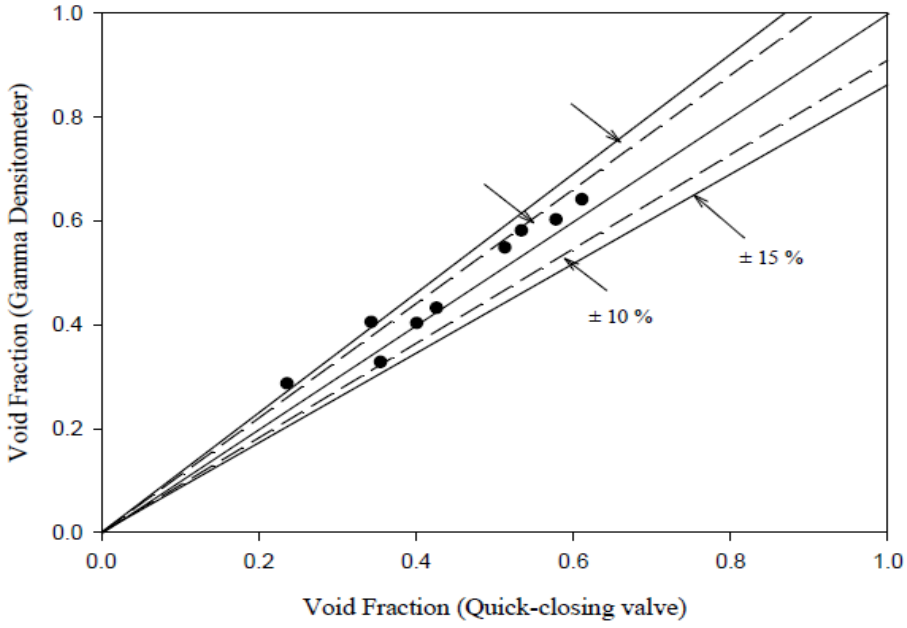

Figure 3.6 Comparison of void fraction measurement techniques adapted from Yijun and Rezkallah (1993)

Accuracy of measured void fraction was validated based on void fraction correlation predictions and direct comparison with void fraction data gathered from other investigators. From the void fraction correlation analysis done in chapter IV, four top performing correlations based on lowest percent RMS error for 700 measured void fraction data for all six pipe orientations in present study were selected for experimental validation. The selected void fraction correlations are Bhagwat and Ghajar (2013), Gomez et al. (2000), Guzhov et al. (1967) and Smith (1969) having 14.2%, 13.4%, 12.4% and 12.2% RMS error. Validation of measured void fraction data by using these correlations was divided into two void fraction regions which are $0 < \alpha < 0.5$ and $0.5 \leq \alpha < 0.1$. The selected void fraction correlations predicted measured void fraction data within ±15% error for $0 < \alpha < 0.5$ region and ±7.5% error for $0.5 \leq \alpha < 0.1$ as shown in Figures 3.7 and 3.8.

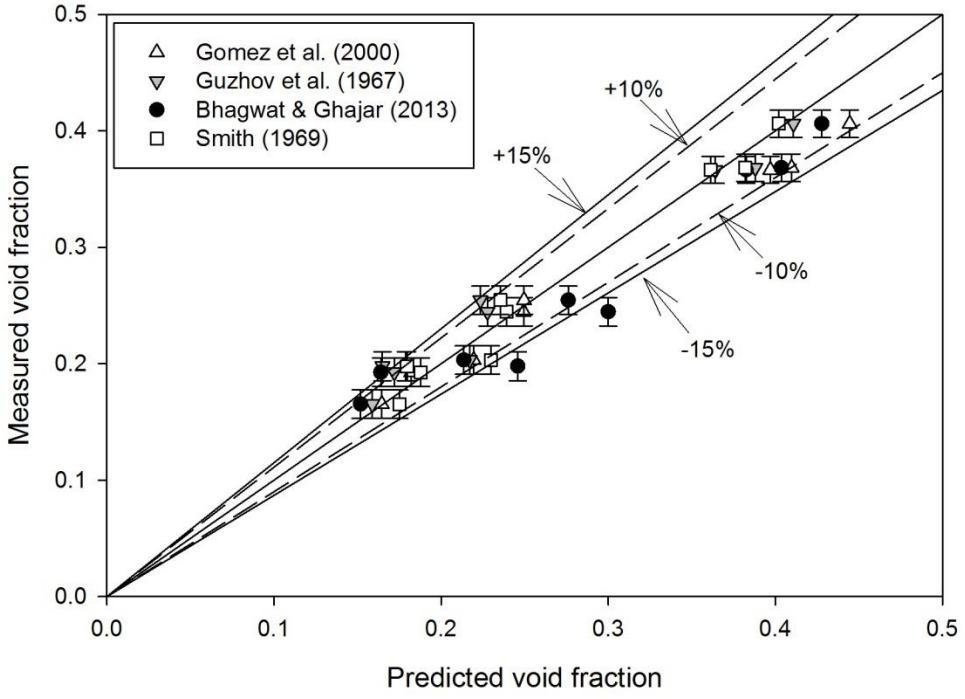

Figure 3.7 Comparison of measured void fraction with four top performing correlations (0 < α < 0.5 region)

High percentage error in the $0 < \alpha < 0.5$ region shown in Figure 3.7 was observed due to low values of void fraction and more explanation on prediction performance of void fraction correlations for different regions is provided in chapter IV. Validation of measured void fraction in the $0.5 \leq \alpha < 0.1$ region is shown as Figure 3.8.

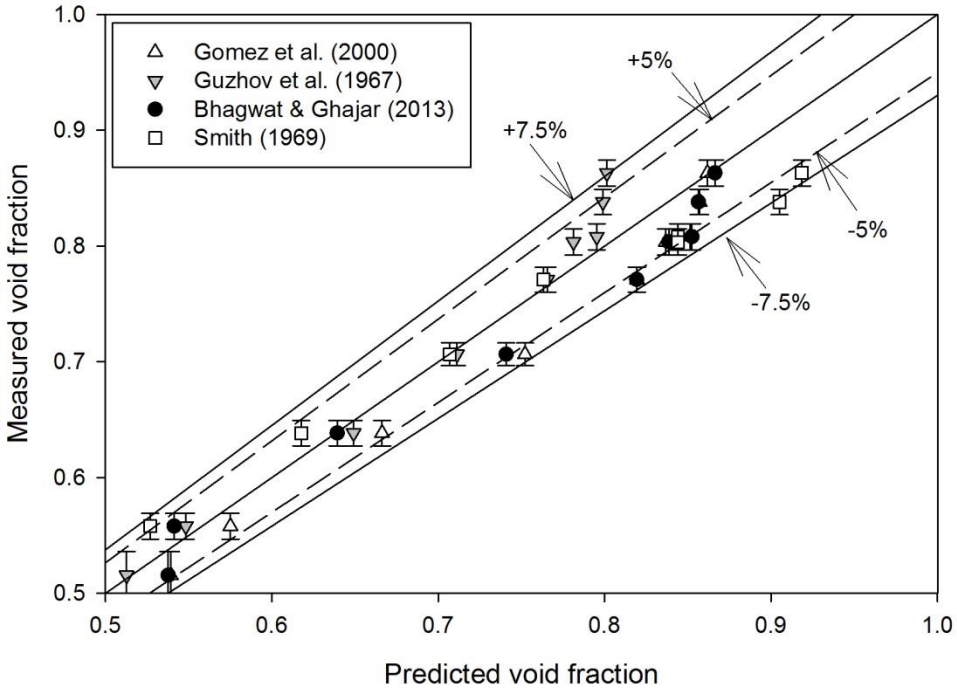

Figure 3.8 Comparison of measured void fraction with four top performing correlations ($0.5 \leq \alpha < 0.1$)

Void fraction data was selected in the range of $0 < \alpha \leq 0.25$, $0.25 < \alpha \leq 0.75$ and $0.75 < \alpha < 1$ (based on analysis done in chapter IV) for all 6 pipe orientations making a total of 18 void fraction data points to be predicted by each of the top performing correlations. Selected void fraction data points from all six pipe orientations cover values from 0.1 to 0.87 and the uncertainty associated with each data point is illustrated with the vertical error bars on the plots as shown in Figures 3.7 and 3.8. It can be observed that all four correlations predicted the measured void fraction data satisfactorily. Hence, this validates the accuracy of measured void fraction data

in present study. Further validation of measured void fraction was done by direct comparison with data gathered from other sources. These sources include Beggs (1972) and Mukherjee (1979). Beggs (1972) conducted void fraction measurements using 25.4 and 38.1 mm diameter pipes, Mukherjee (1979) conducted measurements in a 38.1 mm diameter pipe while a 12.7 mm diameter pipe was used in present study. For the purpose of direct comparison of data from other sources with present study, dependence of void fraction on pipe diameter must be eliminated. Mass flow rate is the parameter used for experimentation in present study and mass flow rate is a function of cross sectional area. However, mass flux eliminates dependence on pipe diameter as it depends only on superficial velocity and density of the fluid. Thus, the mass fluxes of these sources are identical to present study and comparison was done. Comparison was sub divided into upward pipe orientation and downward pipe orientation. Comparison of data in the upward pipe orientation was observed to be within ±10% error as shown in Figure 3.9.

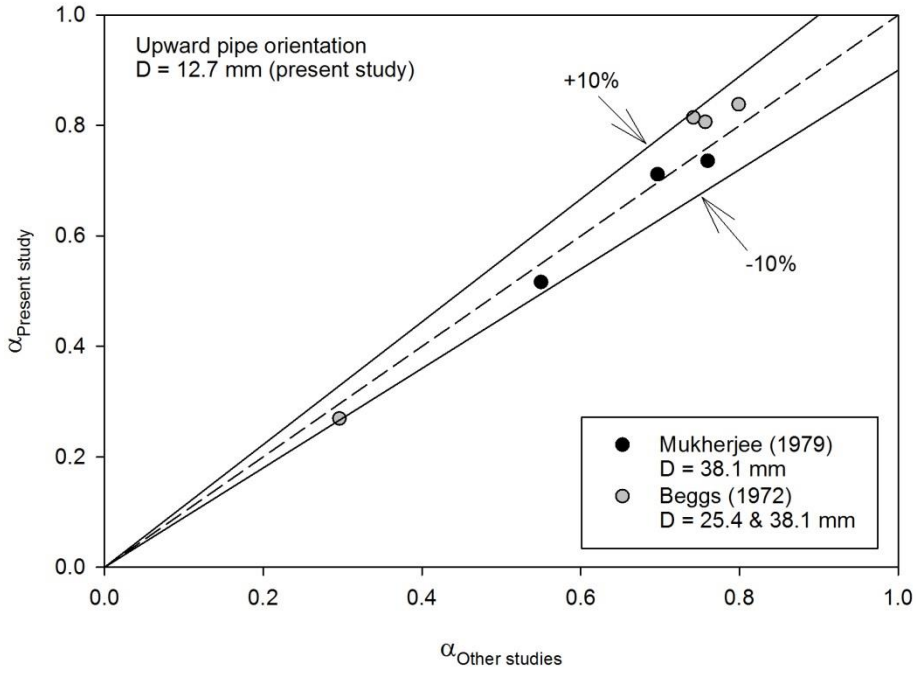

Figure 3.9 Comparison of measured void fraction with other studies (upward pipe orientation)

It should be noted that exact values of mass fluxes in present study and other sources was not observed as measurements were done at different flow rates or parameters. However, identical mass fluxes of the gas phase were observed and compared as shown in Figure 3.9. Details of void fraction comparison between present study and other sources showing their corresponding gas flux for upward pipe orientation is shown as Table 3.3.

Table 3.3 Void fraction comparison for upward pipe orientation

Present study			Other study		
Pipe orientation	Gas flux (kg/m^2s)	Void fraction	Investigator	Gas flux (kg/m^2s)	Void fraction
$+5^o$	18.6	0.81	Beggs (1972)	18.04	0.76
	19.9	0.84	Beggs (1972)	18.32	0.80
$+10^o$	1.31	0.27	Beggs (1972)	2.42	0.30
$+20^o$	19.69	0.81	Beggs (1972)	18.23	0.742
	4.00	0.52	Mukherjee (1979)	5.04	0.55
	9.84	0.71	Mukherjee (1979)	10.68	0.70
	13.39	0.74	Mukherjee (1979)	13.90	0.76

Table 3.3 gives the number of void fraction data points compared for each pipe orientation and the name of investigator whose data is used for comparison. Slight variation in the gas mass flux for the compared void fraction data points can be seen in Table 3.3. Similar analysis was done for downward pipe orientation and is shown as Figure 3.10 and Table 3.4.

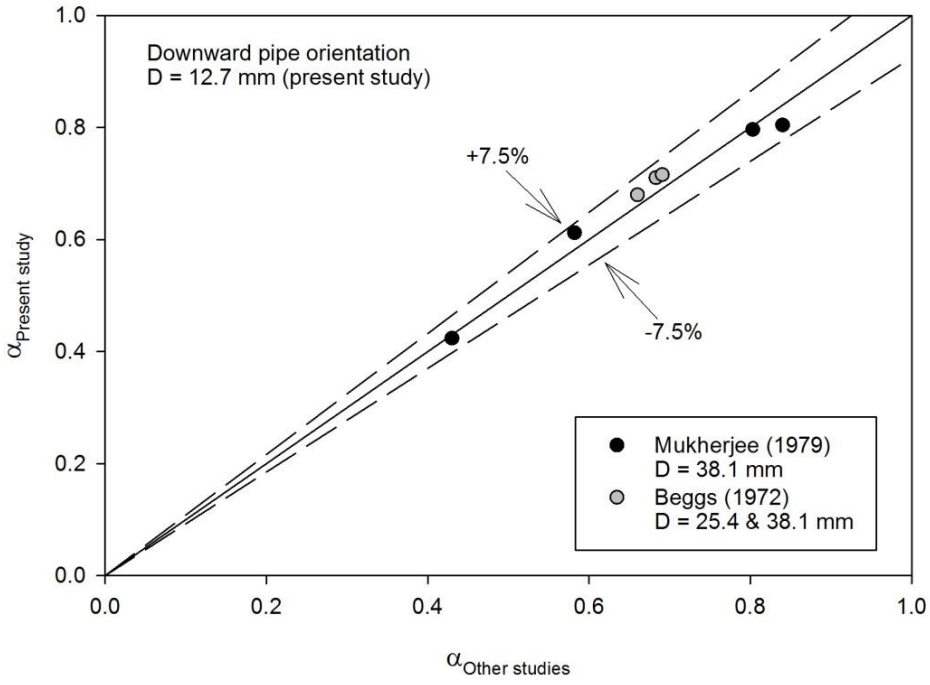

Figure 3.10 Comparison of measured void fraction with other studies (downward pipe orientation)

Table 3.4 Void fraction comparison for downward pipe orientation

Present study			Other study		
Pipe orientation	Gas flux (kg/m^2s)	Void fraction	Investigator	Gas flux (kg/m^2s)	Void fraction
-5^o	9.84	0.80	Mukherjee (1979)	8.59	0.80
	6.69	0.61	Mukherjee (1979)	7.76	0.58
-10^o	6.69	0.68	Beggs (1972)	6.79	0.66
	9.97	0.71	Beggs (1972)	8.64	0.68
-20^o	9.97	0.72	Beggs (1972)	8.69	0.69
	4.07	0.42	Mukherjee (1979)	4.36	0.43
	16.40	0.80	Mukherjee (1979)	16.11	0.84

Direct comparison of measured void fraction data with other sources are within ±7.5% error for downward pipe orientation as shown in Figure 3.10 and the details of the compared void fraction data are shown in Table 3.4. Worthy of note, the compared void fraction data between present study and other sources do not have exactly the same values of gas mass flux and hence comparison is not 100% accurate, but this is an acceptable form of analysis to compare data between different investigators and is sufficient to support and validate the experimental void fraction data measured in present study.

CHAPTER IV

RESULTS AND DISCUSSION

Experimental results discussed in this chapter cover six different pipe orientations ($+5^o$, $+10^o$, $+20^o$, -5^o, -10^o and -20^o) referred to as near horizontal pipe orientation. For ease of comparison and analysis, these pipe orientations were further categorized as upward inclined pipe orientation ($+5^o$, $+10^o$ and $+20^o$) and downward inclined pipe orientation (-5^o, -10^o and -20^o). Flow patterns were identified and flow maps were developed for all six pipe orientations. Comparison between upward and downward inclined flow patterns and flow maps was conducted due to distinctions that exist in these orientations. These distinctions are due to the simultaneous effects of gravitational, buoyant, inertial and surface tension forces acting on the two phase flow. A shift in transition boundaries of flow patterns was observed with change in pipe orientation.

Void fraction measurement was conducted for all six pipe orientations and analyzed. A total of 700 void fraction data points were measured, with upward and downward inclined orientations having 350 data points apiece. Variation of void fraction with flow pattern at different pipe orientations was observed and the effect of pipe orientation on void fraction was analyzed and discussed. Fourteen void fraction correlations were selected from literature and the best performing correlation based on specific void fraction range and pipe orientation (upward or downward inclined) was determined. A unique phenomenon called flow reversal was observed in upward inclined pipe orientation and discussed extensively in this chapter.

4.1 Flow Patterns and Flow Maps

Flow patterns are described as geometric distribution or arrangement of liquid and gas phase in a two phase flow system. Flow patterns have been investigated over decades and several flow patterns exist in literature yet there is not a universal procedure for identification of flow patterns. The simplest and most popular method of flow pattern identification is by flow visualization where the investigator observes the two phase flow in a transparent pipe. Video recordings and still-pictures of flow are taken to better assist in the identification. Hence, it is a highly subjective procedure which is based exclusively on the discretion of the investigator. Major two phase flow parameters such as void fraction, pressure drop and heat transfer are highly influenced by flow patterns and in order to accurately model two phase flow system, a thorough understanding of the flow patterns is of great importance. Flow visualization was conducted in this study using a 12.7 mm pipe and flow pattern map showing transition from one flow pattern to the other was developed for six pipe orientations ($+5^o$, $+10^o$, $+20^o$ -5^o, -10^o & -20^o). As reported by Brennen (2005), flow pattern boundaries in flow maps are not distinctive lines but a transition zone in which flow is unstable due to change in flow properties of either one or both phases and the growth of this instability leads to a change in flow pattern.

4.1.1 Flow Patterns in Upward and Downward Inclined Pipe Orientations

There are four distinct flow patterns in the upward inclined pipe orientation in present study which are slug flow, bubbly flow, wavy flow and annular flow while there are 5 distinct flow patterns in the downward inclined pipe orientation which are stratified flow, slug flow, bubbly flow, wavy flow and annular flow. The other flow patterns observed in present study are a combination of two or more of the distinct flow patterns named above. These flow patterns result from transition from one major flow pattern to the other and they occupy a wide range of flow

combination which justifies their documentation on the map. For example, slug-wavy flow is a combination of slug flow and wavy flow which serves as a transition flow pattern from ideal slug flow to fully established wavy flow. This change in flow pattern is achieved by keeping the liquid mass flow rate constant and gradually increasing the flow rate of the gas phase and vice versa. The pictures of the distinct flow patterns observed in present study for $+5^{o}$ are given as Figure 4.1

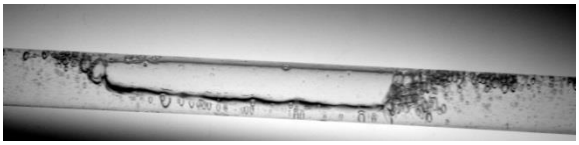

(A) Slug flow

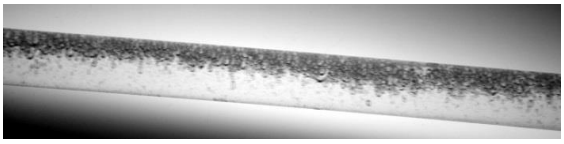

(B) Bubbly flow

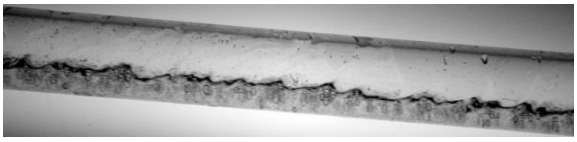

(C) Wavy flow

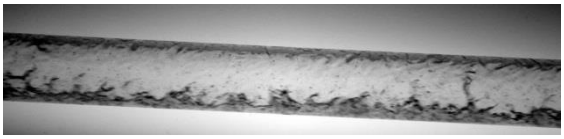

(D) Annular flow

Slug flow: $\dot{m}_l$ = 4.6 kg/min & $\dot{m}_g$ = 0.006 kg/min, Bubbly flow: $\dot{m}_l$ = 10.3 kg/min & $\dot{m}_g$ = 0.006 kg/min, Wavy flow: $\dot{m}_l$ = 4.6 kg/min & $\dot{m}_g$ = 0.075 kg/min, Annular flow: $\dot{m}_l$ = 3.4 kg/min & $\dot{m}_g$ = 0.2 kg/min.

Figure 4.1 Representative pictures of the four major flow patterns for $+5^{o}$ (Slug, Bubbly, Wavy and Annular flows)

Slug flow

Slug flow is characterized by the gas phase existing as long cylindrical bubble with a hemispherical nose. Taitel and Dukler (1976) described slug flow as agitation in a two phase system causing the liquid column to rise and touch the top pipe wall surface thereby leading to a break in gas phase column. Simmons and Harantty (2001) described the formation of slug in

horizontal two phase flow as the process by which waves grow intermittently on a stratified interface causing the liquid phase to fill the pipe cross section. In present study, slug flow was observed at very low liquid and gas flow rates. Slug length is directly influenced by flow rate of the gas phase, where increase in gas flow rate increases slug length at constant liquid flow rate and slug length was observed to vary between 4 – 20 inches during flow visualization. Slug flow occupies 0.14 – 0.58 void fraction range in present study and non-uniform slug length was observed for the high void fraction slug flow. However, in horizontal and near horizontal pipe orientations, the nose of the slug appears not completely hemispherical. This is due to gravitational force which keeps the liquid phase at the bottom pipe wall and buoyant force which keeps the gas phase in contact with the top pipe wall surface thereby giving a rather flat nose as shown in Figure 4.1 (A). Slug flow with hemispherical nose is observed in vertical upward orientation and a representative picture taken from Godbole (2009) is shown as Figure 4.2.

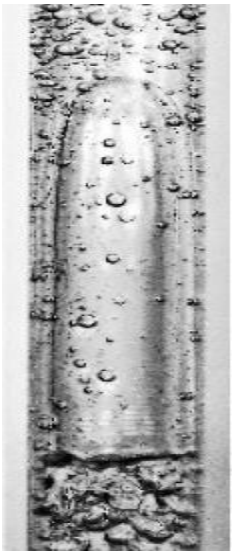

Figure 4.2 Representative picture of an ideal slug flow in vertical upward orientation by Godbole (2009)

Bubbly flow

Bubbly flow is characterized by the gas phase existing as bubbles while the liquid phase is continuous in the pipe. Bubbly flow is observed at high liquid flow rates and moderate gas flow rates. Bubbly flow exist in two forms, bubbly and dispersed bubbly flow. For horizontal and near horizontal pipe orientations, the bubbles were observed to be in contact with top pipe wall surface due to effects of buoyant force acting on the gas phase as shown in Figure 4.1 (B). Dispersed bubbly flow was attained at higher liquid flow rates where increase in flow rate increases the inertial force of the liquid phase. This leads to increase in shear force on the gas phase which reduces large bubbles into tiny bubbles and they are forced towards the pipe axis. In vertical upward and downward pipe orientations, bubbles were observed to be distributed throughout the pipe cross section due to uniform gravitational force acting on both phases. Bhagwat (2011) reported that in downward bubbly flow, the bubbles follow the path of least resistance in a zigzag spiraling motion due to dominant buoyant force as flow progresses downward in the pipe. It was observed that the bubbles are concentrated around the pipe axis and the liquid phase was observed continuous near the pipe wall. Oshinowo (1971) called this phenomenon coring bubbly flow. Models exist in literature for prediction of transition from slug and intermittent flow to bubbly flow. Taitel and Dukler (1976) reported that for horizontal and near horizontal pipe orientations, transition from intermittent to dispersed bubbly flow occurs at high liquid flow rates when the turbulent oscillations are strong enough to overcome the buoyant force acting on the gas phase. A transition criterion was developed for this theory and given as Equation (4.1)

$$U_l \geq \left[\frac{4A_g}{S_i}\,\frac{gcos\theta}{f_l}\,\left(1-\frac{\rho_l}{\rho_g}\right)\right]^{0.5} \tag{4.1}$$

Kokal and Stanislav (1989a) adopted a slightly different approach from Taitel and Dukler (1976) for modeling of transition from intermittent to dispersed bubbly flow where they assumed that a

balance must exist between the turbulence and buoyant force in order for transition to occur. Given as Equation (4.2) is the transition criterion developed by Kokal and Stanislav (1989a)

$$U_{sl} = 0.8\,[\frac{\rho_l - \rho_g}{\rho_l}\,\frac{cos\theta}{f_i} D^{0.8} {U_{sg}}^{0.4}]^{0.5} \quad (4.2)$$

In present study bubbly flow was observed to occupy void fraction range of 0.08 – 0.4, the higher limit of void fraction range (0.4) was observed in $+20^{o}$ pipe orientation where gravitational forces acting on the liquid phase become dominant and shear gas slugs to large bubbles at high void fraction.

Stratified flow

Stratified flow is characterized by complete separation of the liquid phase and gas phase in the pipe where the liquid phase is at the bottom pipe surface and gas phase at the top. Stratified flow can also be categorized into smooth stratified and wavy-stratified flow. Smooth stratified flow occurs at very low gas flow rates. However, high gas flow rates generate waves at the two phase interface as the gas phase tries to accelerate the liquid phase and hence, wavy-stratified flow. This phenomenon is referred to as the Kelvin-Helmholtz instability which describes the occurrence of shear at wavy interface of concurrent fluids due to difference in phase density and phase velocity. The magnitude and frequency of waves increase with increase in gas phase flow rate and waves begin to touch pipe wall top surface thereby partly eliminating the stratification. Wavy-stratified flow can also be referred to as wavy flow in present study and this flow pattern was observed in negative pipe orientations. Extensive research has been done on stratified flow over decades due to simplicity of flow geometry. There exist a plethora of models for calculating interfacial friction factor between the two phases, pressure drop, void fraction and other two phase parameters in

stratified flow. However, modeling of wavy-stratified flow has been reported to be very complex due to presence of waves at the interface.

Taitel and Dukler (1976) explained that waves are generated in stratified flow when viscous dissipation in waves are overcome by shear work and pressure, a criterion for transition from smooth to wavy stratified flow was developed and given as Equation (4.3)

$$U_g \geq \left[\frac{4\,\nu_l(\rho_l-\rho_l)g\,cos\,\theta}{s\,\rho_g U_l}\right]^{0.5} \tag{4.3}$$

Asante (2002) conducted experimental studies for air-water two phase flows in steel pipe diameters ranging from 1 – 3 inches and developed a correlation for interfacial friction factor with liquid and gas Reynolds number, liquid holdup (liquid holdup = 1 – void fraction) and liquid film thickness based on geometry of stratification (either flat or curved stratified flow). He reported that the transition from homogenous flow to stratified flow was observed at liquid holdup greater than 0.005, curved stratification was observed at liquid holdup less than 0.06 and flat interface at liquid holdup higher than 0.06. The interfacial friction factor developed for smooth and curved stratified flows by Asante (2002) are given as Equations (4.4) and (4.5).

For curved interface,

$$f_i = 303\left[{Re_l}^{0.37}\varepsilon^{0.34}{Re_g}^{-0.97}\delta^{0.31}\right] + 0.0077 \tag{4.4}$$

For flat interface,

$$f_i = 0.061\left[{Re_l}^{0.60}\varepsilon^{0.35}{Re_g}^{-0.52}\gamma^{0.61}\right] + 0.032 \tag{4.5}$$

Wavy flow

Also referred to as wavy-stratified flow, wavy flow pattern is formed at high flow rates of gas phase and moderate or low flow rates of liquid phase. In upward inclined pipe orientation, this

flow pattern was identified as wavy flow because of complete elimination of stratified flow. Wavy flow pattern shown in Figure 4.1 (C) represents the onset of instability as flow is in transition to turbulent flow as illustrated in Kelvin Helmholtz instability theory. The representative picture of wavy flow in Figure 4.1 (C) occupies superficial liquid and gas Reynolds number of 8200 and 6800.

Annular flow

In Annular flow, the liquid phase exist as a thin continuous film in contact with the entire pipe wall and the gas phase exist as a core. This can be compared to concentric tubes where the inner tube is the gas phase and the outer is the liquid phase. Annular flow was observed at very high gas flow rates and at low and moderate liquid phase flow rates. During flow visualization, annular flow pattern was observed to give a fuzzy two phase flow picture because of the continuous liquid film being sheared at the gas-liquid interface due to very high gas flow rates as shown in Figure 4.1 (D). High gas flow rates induce high interfacial shear which necessitates the modeling of annular flow in two phase systems. The relatively distinct flow regime (radial separation of the two phases) makes it possible to develop separated flow models in annular flow and a great deal of research in form of experimental and modeling work has been done in this area over the years.

Kokal and Stanislav (1989a) developed an equation to predict transition from intermittent to annular flow which is given as Equation (4.6).

$$U_{sg} = 10.36U_{sl} + C_1, \text{ where } C_1 = 2.98[\frac{gD(\rho_l - \rho_g)}{\rho_l}]^{0.5} \quad (4.6)$$

The four major flow patterns in $+5^o$ were also observed as the major flow patterns in $+10^o$ and $+20^o$, representative pictures of flow patterns for $+10^o$ and $+20^o$ are shown as Figures 4.3 and 4.4.

(A) Slug flow

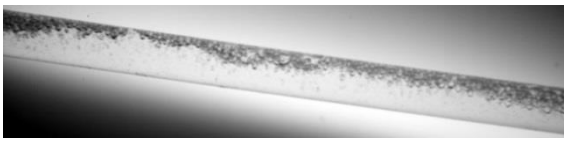

(B) Bubbly flow

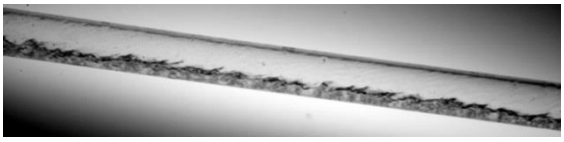

(C) Wavy flow

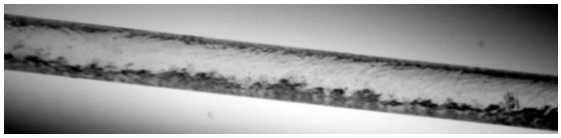

(D) Annular flow

Slug flow: $\dot{m}_l$ = 2.3 kg/min & $\dot{m}_g$ = 0.003 kg/min, Bubbly flow: $\dot{m}_l$ = 8 kg/min & $\dot{m}_g$ = 0.0045 kg/min, Wavy flow: $\dot{m}_l$ = 4.6 kg/min & $\dot{m}_g$ = 0.075 kg/min, Annular flow: $\dot{m}_l$ = 4.6 kg/min & $\dot{m}_g$ = 0.132 kg/min.

Figure 4.3 Representative pictures of the four major flow patterns +10^o (Slug, Bubbly, Wavy and Annular flows)

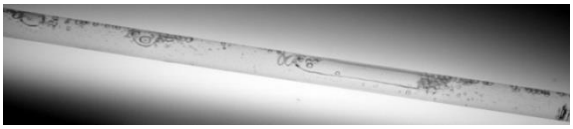

(A) Slug flow

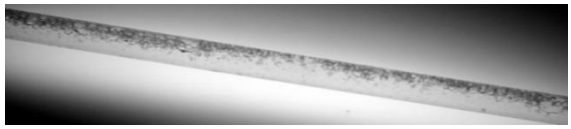

(B) Bubbly flow

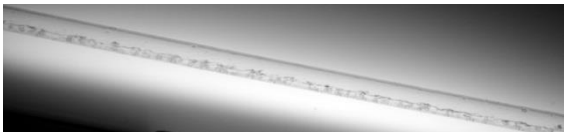

(C) Wavy flow

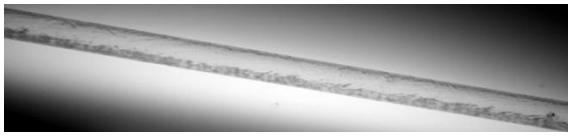

(D) Annular flow

Slug flow: $\dot{m}_l$ = 5.7 kg/min & $\dot{m}_g$ = 0.003 kg/min, Bubbly flow: $\dot{m}_l$ = 9 kg/min & $\dot{m}_g$ = 0.0045 kg/min, Wavy flow: $\dot{m}_l$ = 2.3 kg/min & $\dot{m}_g$ = 0.05 kg/min, Annular flow: $\dot{m}_l$ = 2.3 kg/min & $\dot{m}_g$ = 0.115 kg/min.

Figure 4.4 Representative pictures of the four major flow patterns +20^o (Slug, Bubbly, Wavy and Annular flows)

As shown in Figures 4.1, 4.3 and 4.4, the major flow patterns observed for all three upward inclined pipe orientations remain the same as inclination had no significant effect in changing the distribution of both phases in the major flow patterns.

4.1.2 Flow Maps

Flow pattern maps are graphical representations of flow patterns and are plotted based on different flow parameters. For example, most flow maps available in literature were developed based on mass flow rate, superficial velocity or Reynolds number. One of the first flow maps developed in two phase flow was proposed by Baker (1954) for horizontal pipe where the flow parameter used is the volumetric flow rate of the two phases. Due to dependence of flow map on experimental setup utilized, Taitel and Dukler (1976) reported that various data with different fluid combination and pipe diameters can be collapsed on the same region on a map and compared by simply choosing a suitable dimensionless parameter on the coordinate axis. In order to eliminate dependence of flow parameter on fluid properties, mass flow rate was adopted for the coordinate axis of flow maps developed for all six pipe orientations. As earlier mentioned, flow visualization is highly subjective but considerable effort was made in present study to develop flow maps based on flow pattern identification procedure and definitions given by previous researchers who worked in the same group and used the same experimental setup. This served as the basis for developing flow maps for different pipe orientations from previous studies. Hence, it amounts to a buildup of research on previous works done by the same group. Ghajar and Tang (2007) conducted investigation on flow visualization and flow pattern maps in horizontal and slightly inclined pipes with pipe diameter of 25.4 mm and superficial Reynolds number of each phase as coordinate axis. Their flow map for horizontal pipe is shown as Figure 4.5.

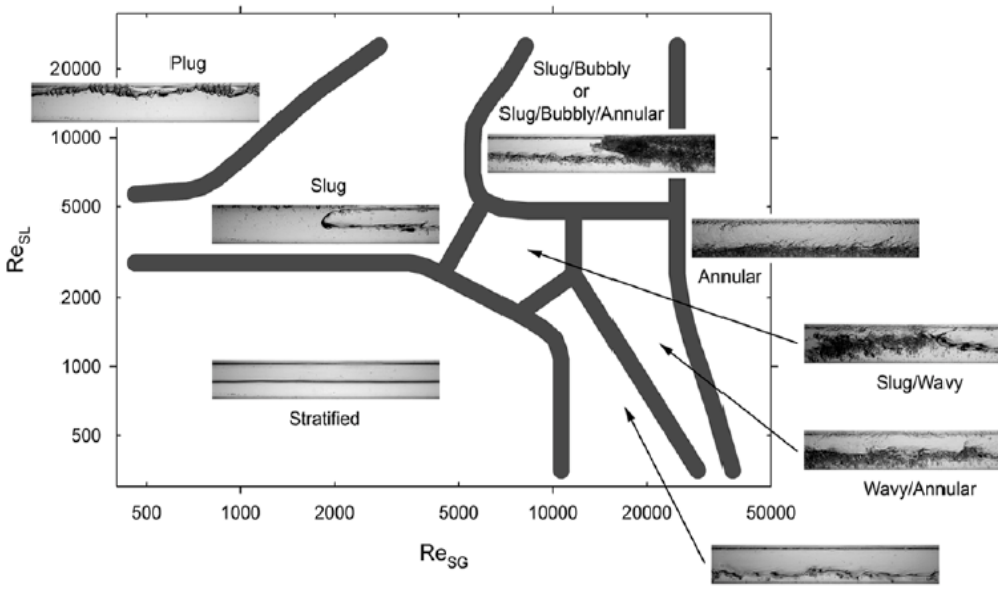

Figure 4.5 Horizontal flow pattern map by Ghajar and Tang (2007).

Flow map showing similar trend in transition boundary was developed by Ghajar and Bhagwat (2013) using mass flow rate as coordinate axis and 12.7 mm diameter pipe, the flow map is shown as Figure 4.6

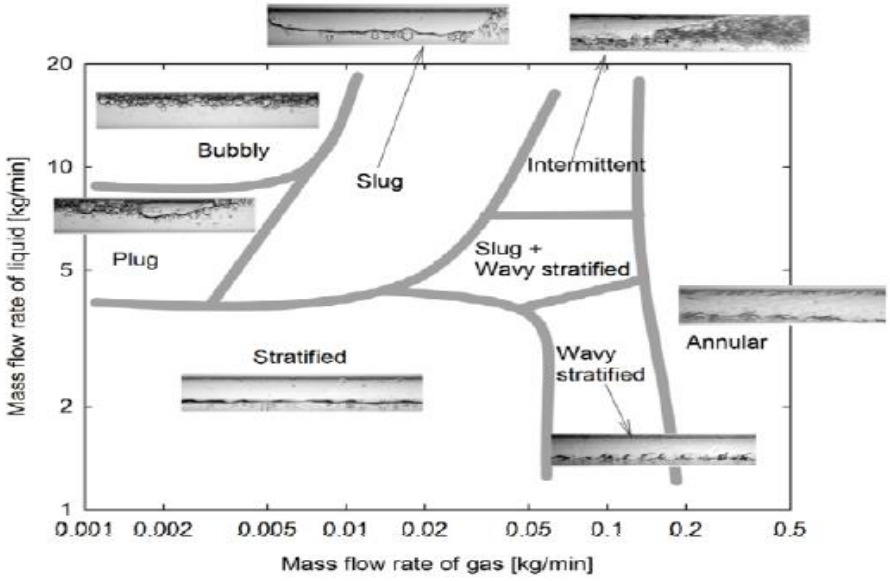

Figure 4.6 Horizontal flow pattern map Ghajar and Bhagwat (2013) mass flow rate coordinate axis.

Upward Inclined Flow Map (+5^o, +10^o & + 20^o)

At +5^o pipe orientation, stratified flow was not observed during flow visualization and similar observations have been reported by various investigators. Taitel and Dukler (1976) observed transition from stratified flow to intermittent flow at inclination angle of 0.1^o for low flow rates combination of liquid and gas phase. Perez (2008) conducted a study on gas-liquid (air-water) two phase flow in inclined pipes with an experimental setup of 6.5 m long test pipe with diameters of 37 mm and 67 mm having variable inclination angles from -20^o to +90^o. At low liquid superficial velocity of 0.2 m/s and gas velocity of 0.15 m/s, stratified flow was observed for horizontal flow (0^o inclination) and noticed to change into slug flow at inclination angle less than 5^o. Kokal and Stanislav (1989a) conducted experimental studies of two phase flow in slightly inclined pipes. They reported that very limited stratified flow was observed in uphill flow and inclination angles as low as 0.03^o from horizontal considerably affected the transition from stratified to intermittent flow.

Ghajar and Tang (2007) reported that the flow pattern transition boundaries for horizontal flow were found to be slightly different from that of inclined flow pattern boundaries. And at small inclination angle of 2^o, stratified flow observed in horizontal orientation was replaced by slug and slug-wavy flow. They also observed that as pipe orientation shifted from +2^o through +5^o to +7^o, the transition boundaries between distinct flow patterns on the map shifted accordingly. Figure 4.7 shows the flow map for slightly inclined two phase flow developed by Ghajar and Tang (2007).

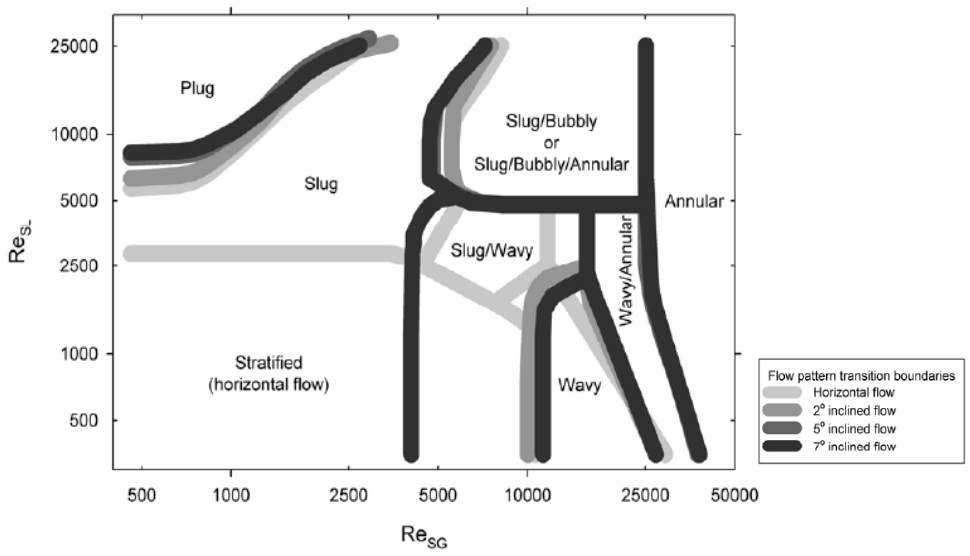

Figure 4.7 Change of flow pattern transition boundaries as pipe inclined upward from horizontal position by Ghajar and Tang (2007).

Having established the basis for flow visualization, flow pattern identification and flow map coordinate axis in the above discussion, the flow map for +5^{o} pipe orientation was developed as shown in Figure 4.8. Letters L and G on +5^{o} flow map represent mass flow rates in kg/min of liquid and gas phase for the corresponding flow pattern picture displayed therein.

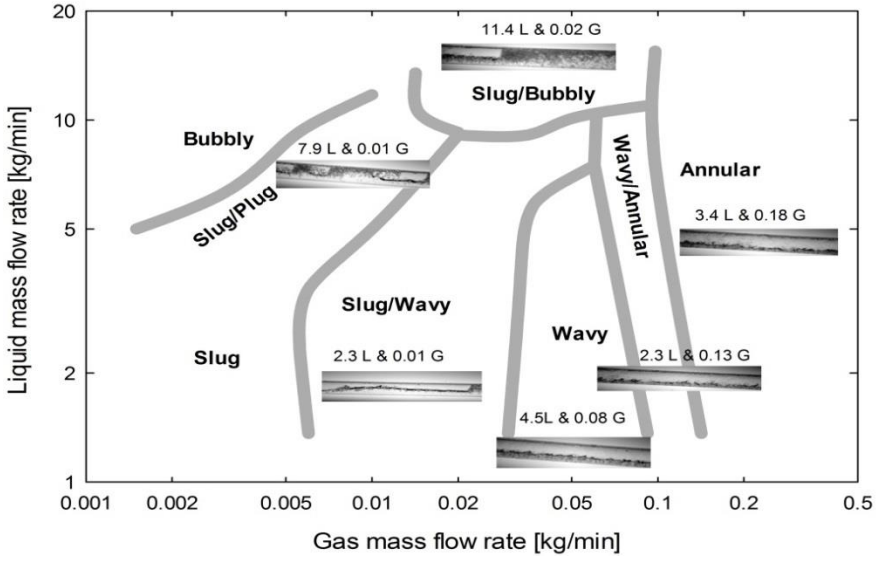

Figure 4.8 Flow map for +5^{o} pipe orientation.

The flow map shown in Figure 4.8 for +5^{o} was compared with the horizontal flow pattern map (Figure 4.6) developed by Ghajar and Bhagwat (2013). The flow maps were superimposed to observe the distinctions in flow pattern transition boundaries as shown in Figure 4.9.

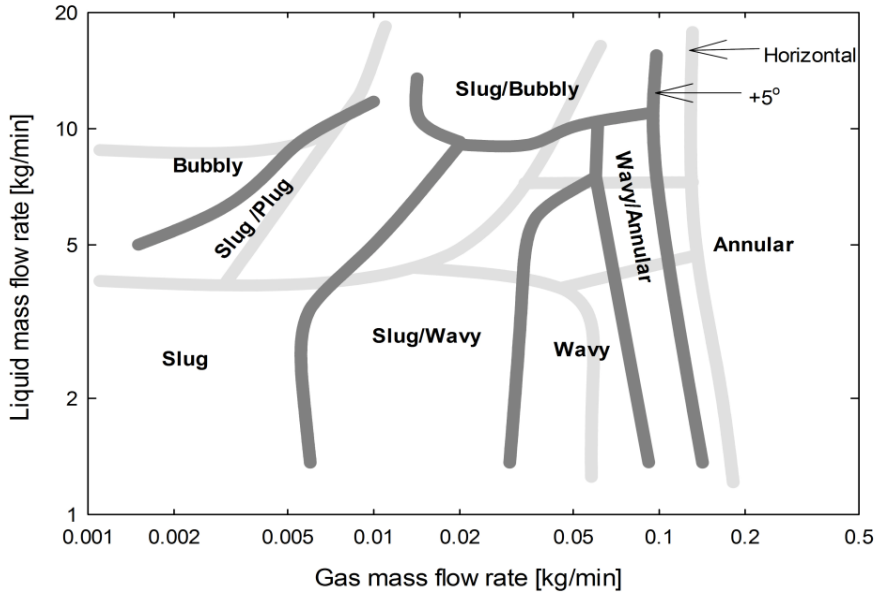

Figure 4.9 Flow map showing comparison between +5^{o} and horizontal developed by Ghajar and Bhagwat (2013).

Stratified flow was observed in the horizontal flow map and gets completely eliminated in the +5^{o}. Also, intermittent flow characterized by combination of slug flow and bubbly flow, observed at high flow rates of liquid and gas phase in horizontal flow map was termed slug/bubbly flow in +5^{o} map. As discussed above, annular flow pattern involves radial separation of the two phases in the pipe where the liquid phase exists in a continuous film surrounding the gas phase. The shift in transition boundary of annular flow to lower gas flow rate is attributed to decrease in inertial force needed for the gas phase to generate and maintain a core in the pipe. Since inertial force is a function of velocity and velocity is a function of mass flow rate, the mass flow rate needed by the gas phase for transition to annular flow region is reduced and hence the boundary shifts to the left. It was also observed from Figures 4.3 to 4.7 that annular flow region transition boundary is a

vertical line indicating that the flow regime is independent of the liquid phase flow rate (flow pattern was observed at both high and low liquid flow rates) and occurs only at high gas flow rate. Flow maps were developed for $+10^{o}$ and $+20^{o}$ pipe orientations in present study and superimposed on the $+5^{o}$ flow map to show how the transition boundaries shift with respect to pipe inclination as shown in Figure 4.10.

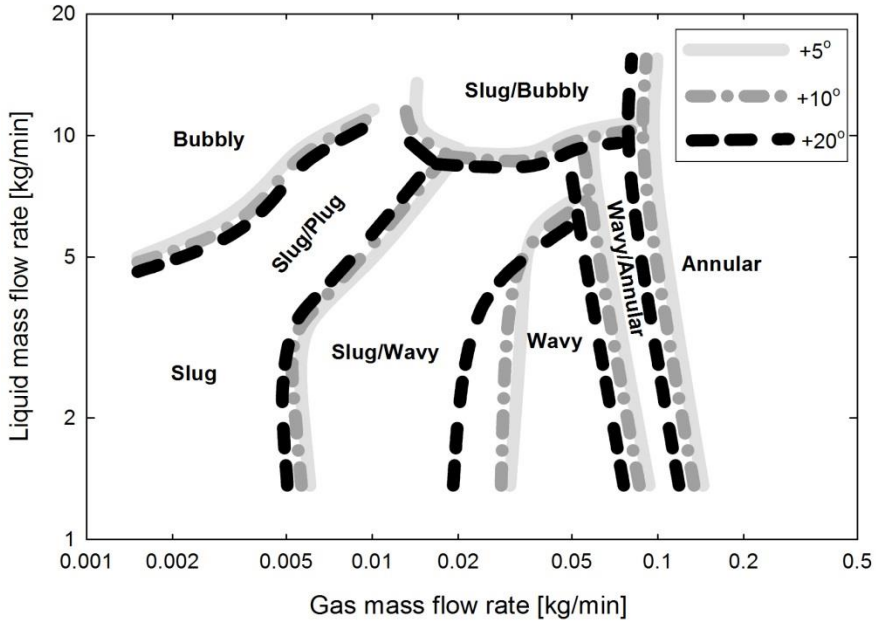

Figure 4.10 Flow map showing effect of upward inclined pipe orientation on transition boundaries

The transition boundaries shift to lower liquid flow rates (for bubbly flow, slug-bubbly flow and wavy flow patterns) and to lower gas flow rates (for annular, wavy-annular and slug-wavy flows) as pipe inclination progresses from $+5^{o}$ through $+10^{o}$ all the way to $+20^{o}$. There is a major shift in transition boundaries for all major flow patterns from $+10^{o}$ to $+20^{o}$ when compared with shift in transition boundaries from $+5^{o}$ to $+10^{o}$ as indicated in Figure 4.10. This is attributed to the significant rise in gravitational force acting on the liquid phase as inclination angle increases i.e., $sin20^{o}$ is approximately twice the value of $sin10^{o}$, hence the magnitude of the gravitational force in $+20^{o}$ is twice of $+10^{o}$. This increase in gravitational force reduces the liquid phase velocity as

the gas phase rises in the pipe. Interfacial shear plays an important role in flow pattern transition which is increased by increasing the inertial force of the two phases (mass flow rates). Since interfacial shear is a function of relative velocity of the phases, the decrease in liquid phase velocity (slippage) due to gravity increases the magnitude of the relative velocity of the two phase flow. This increase in relative velocity increases the interfacial shear which in turn decreases the inertial force (mass flow rate) required for transition between the above mentioned flow patterns and hence, the boundaries shift downward.

Oddie et al. (2003) conducted an experimental study on two and three phase flows in large diameter inclined pipes, having a test section that is 11 m long, 150 mm diameter transparent pipe and inclination angles from -2^{o} to $+90^{o}$. Major flow patterns were observed and it was reported that some of the flow patterns in this study have distinctions when compared to small diameter pipes. For example, elongated-bubble flow was reported to appear more like churn-slug flow as opposed to large bubbles. The representative pictures of the flow patterns observed by Oddie et al. (2003) are given in Figure 4.11.

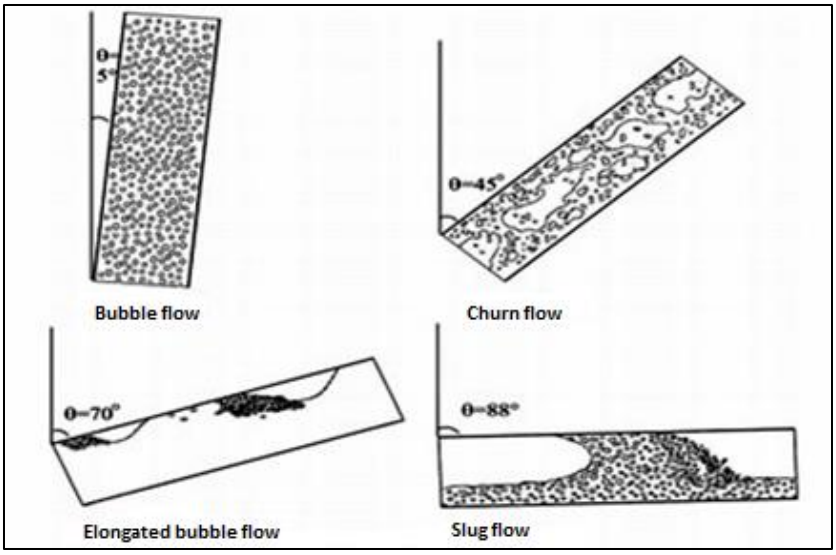

Figure 4.11 Flow patterns observed at variable inclination measured from horizontal by Oddie et al. (2003).

The flow maps developed by Oddie et al. (2003) showing effect of inclination angle on flow patterns observed are also given as Figure 4.12.

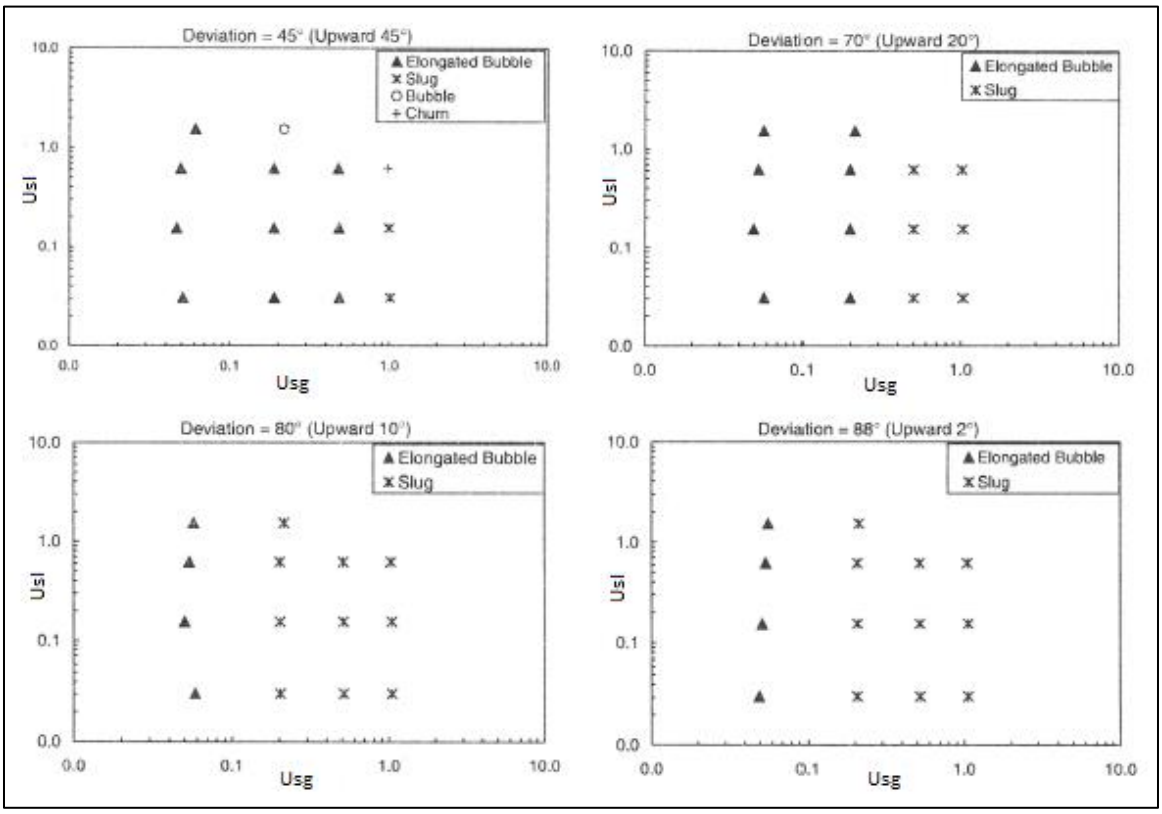

Figure 4.12 Flow map for air-water two phase flow by Oddie et al. (2003)

By analysis of Figure 4.12, similar trends were observed in the flow maps therein by Oddie et al. (2003) and present study. The upward 20^o flow map in Figure 4.12 showed that elongated bubble flow is the dominant flow pattern and slug flow being the less dominant of the two flow patterns (refer to elongated bubble and slug flow in Figure 4.11) at constant superficial velocities of liquid and gas phase. As inclination angle decreased to upward 10^o, slug flow dominated elongated bubble flow in the flow map presented (Figure 4.12). This reveals that for the same flow rates combination of liquid and gas phase, increase in pipe inclination shifts the transition boundary from slug flow to elongated bubble flow downwards as observed in present study slug to bubbly flow transition boundary.

Wongwises and Pipathattkul (2006) conducted two phase studies in a narrow annular channel with hydraulic diameter of 4.5 mm, they reported that the onset of transition from slug flow region to plug flow region and plug flow region to bubbly flow region shift to lower values of superficial air velocity when pipe inclination was increased.

Perez (2008) also reported that for constant superficial velocity of liquid and gas phase of 0.2 m/s and 0.15 m/s, 38 mm pipe diameter and $+5^o$ pipe orientation, slug was found to be discretized into bubbles as pipe inclination increased and fully established bubbly flow was observed at $+80^o$.

Simmons and Harantty (2001) conducted experimental two phase flow studies in an inclined pipe with test section of 76.3 mm diameter and length of 23 m over inclination angles of 0.05^o, 0.2^o, 0.4^o and 1.2^o. A critical superficial velocity was determined below which stratified flow disappeared due to instability generated by Kelvin Helmholtz theory for concurrent flow. They observed transition from stratified to slug flow at pipe inclination above 0.2^o from horizontal. All these observations reported by investigators over the years validate the claim that regardless of pipe diameter and flow parameter adopted for developing of flow maps, increase in pipe inclination angle at constant flow combination of liquid and gas phases shift transition boundaries between flow patterns to lower values of adopted flow parameter as observed in present study.

Downward Inclined Flow Map (-5^o, -10^o and -20^o)

The only distinct flow pattern seen in the downward pipe orientation and not observed in the upward pipe orientation was stratified flow. Stratified and wavy-stratified flow patterns were observed in the downward pipe orientation and were found to occupy larger area on flow map as pipe inclination increased from -5^o through -10^o to -20^o. Extensive studies have been carried out on flow map in horizontal, vertical upward, vertical downward and upward inclined two phase flow but very little work has been done on downward inclined pipe orientation. This justifies the

need to investigate the effect of inclination angle on flow map in downward inclined two phase flow. Barnea (1987) carried out flow pattern studies in downward inclined two phase flow with a setup having 10 m long transparent pipe and 25.5 mm and 51 mm diameter pipes. Barnea (1987) expressed that smooth stratified flow was not observed in the study as the stratified flow was always ripply for inclination angle above 1^o for 25.5 mm pipe and 5^o for 51 mm pipe.

Tzotzi et al. (2011) conducted experimental studies of two phase flow using a 2 mm diameter pipe and reported that smooth stratified flow disappeared in the downward orientation at pipe inclination as low as -1^o due to gravity-driven instabilities independent of interfacial shear. This theory was supported by calculations developed for a critical Reynolds number which determines the stability of inclined liquid films and an estimated value of 48 was taken for the critical Reynolds number. Above this value of Re_{cr}, liquid film was observed to be unstable for pipe inclination of -1^o and smooth stratified flow disappeared even at very low liquid phase flow rates. Similar observation was made in the downward inclined pipe orientation in present study where the stratified flow is full of ripples and twists as flow progressed downstream in the test section. However, the twists observed at the stratified flow interface in these orientations are largely due to the amplified effect of two phase mixer at test section entrance by increased gravitational force. A representative picture of ripply stratified flow for -5^o is given in Figure 4.13.

$\dot{m}_l$ = 1.4 kg/min & $\dot{m}_g$ = 0.0016 kg/min

Figure 4.13 Representative picture of ripply stratified flow -5^o

Based on the procedure for flow map analysis discussed in upward inclined pipe orientation, the -5^o flow map was developed and superimposed on the horizontal flow map developed by Ghajar

and Bhagwat (2013) to illustrate the shift in transition boundaries between horizontal and -5^{o} pipe orientation as shown in Figure 4.14.

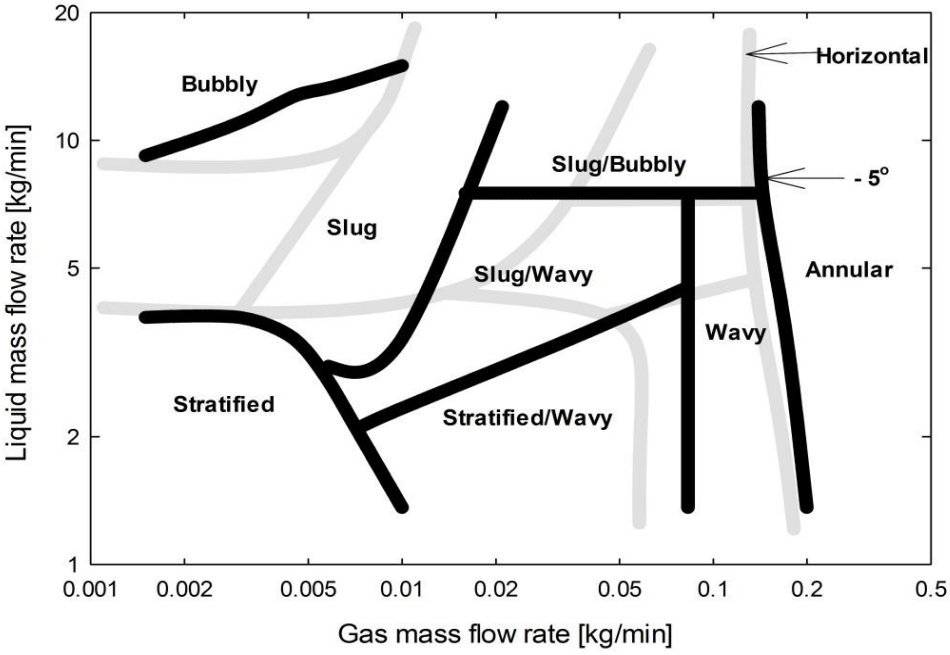

Figure 4.14 Comparison of -5^{o} flow map with horizontal developed by Ghajar and Bhagwat (2013)

Stratified flow for -5^{o} pipe orientation progresses into wavy-stratified flow by maintaining low liquid flow rates and increasing the gas flow rate. The change in flow pattern was attributed to generation of waves at the interface which grows to touch top pipe wall surface due to increase in gas flow rate. Between the ranges of 0.005 – 0.01 kg/min of gas phase flow rates and at low liquid flow rates, three different flow patterns were observed (stratified, stratified-wavy and slug-wavy flows). This observation was attributed to the role of buoyant force between superficial gas Reynolds number of 530 - 1040 and superficial liquid Reynolds number between 4100 – 6100. Buoyant force becomes more dominant within this range and opposes flow of gas phase in the downward direction. This behavior acts as a resistance to flow of liquid phase leading to buildup of liquid column in the pipe causing discontinuity in gas phase and hence slug flow is observed.

Further increase of gas flow rate increases the interfacial shear which leads to generation of waves on the stratification and hence wavy-stratified flow. Flow progresses into annular region with further increase in gas flow rate and it was observed that the annular flow transition boundary shifted to higher values of gas flow rate from horizontal. This was due to increased inertial force needed by the gas phase to overcome gravitational pull on the liquid to generate an annulus in the pipe. Barnea (1987) reported that the liquid phase in stratified flow moves more rapidly in the downward inclined orientation than horizontal and has a reduced liquid film thickness in the pipe cross section for same fluid combination due to gravitational force acting in the direction of flow. Hence, higher liquid and gas flow rates are required to induce transition from stratified flow. These flow rates also increase as angle of inclination increases downwards thereby leading to the expansion of the flow map as transition boundaries shifts to higher values of liquid and gas flow rate as shown in Figure 4.14. By adopting the same identification techniques discussed in upward inclinewd pipe orientation, the flow maps for -10^o and -20^o were developed and superimposed on the -5^o as shown in Figure 4.15.

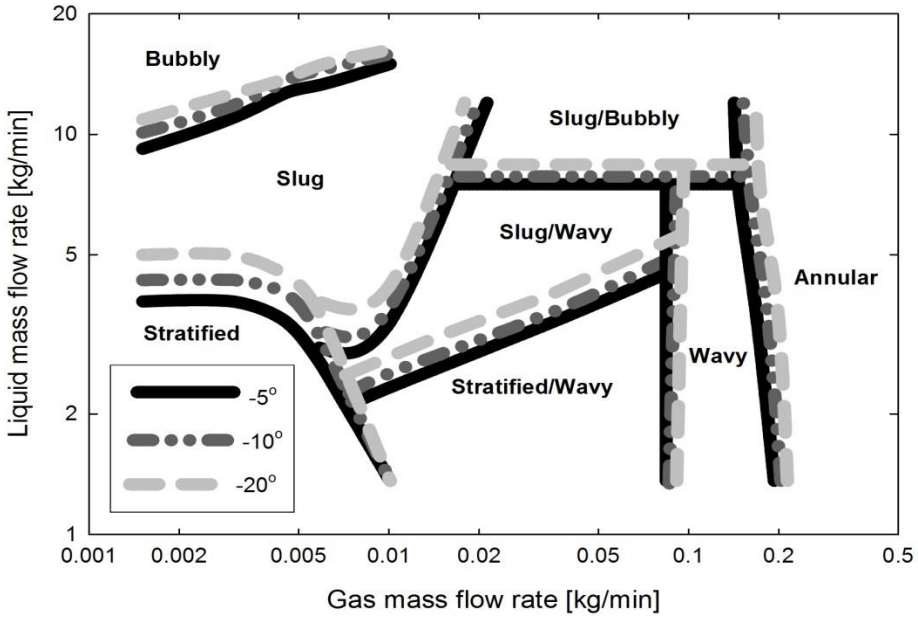

Figure 4.15 Downward flow map showing -5^o, -10^o & -20^o flow pattern transition boundaries

The stratified to slug flow transition boundary was observed to shift to higher liquid flow rate and likewise the transition boundary from slug to bubbly flow. Annular and wavy flow pattern transition boundaries were observed to shift to higher gas phase flow rate, therefore the map expands as pipe inclination goes from -5^{o} to -20^{o}.

Similar observation was made by Tzotzi et al. (2011) in the downward pipe orientation where transition line of stratified flow shift upwards as pipe inclination angle is changed from -0.25^{o} to -1^{o}, this was due to reduced height of liquid film and increased liquid phase velocity attributed to gravitational force acting in flow direction. The effect of pipe orientation on flow map developed by Tzotzi et al. (2011) is given as Figure 4.16.

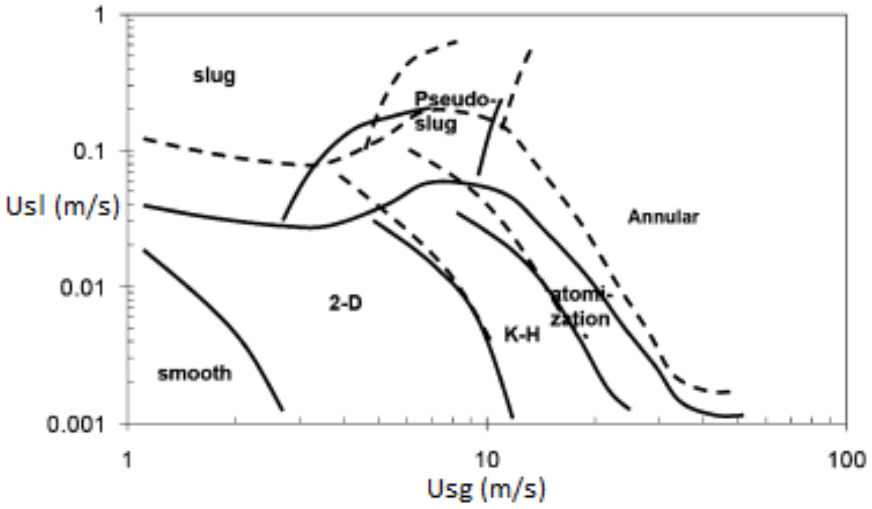

K-H = Kelvin Helmholtz instability waves and 2-D = Two dimensional waves

Figure 4.16 Effect of pipe orientation on flow pattern lines adapted from Tzotzi et al. (2011), Θ = 0.25^{o} for continuous line, Θ = 1^{o} for dashed line.

4.1.3 Effects of Pipe Orientation on Flow Pattern and Flow Maps

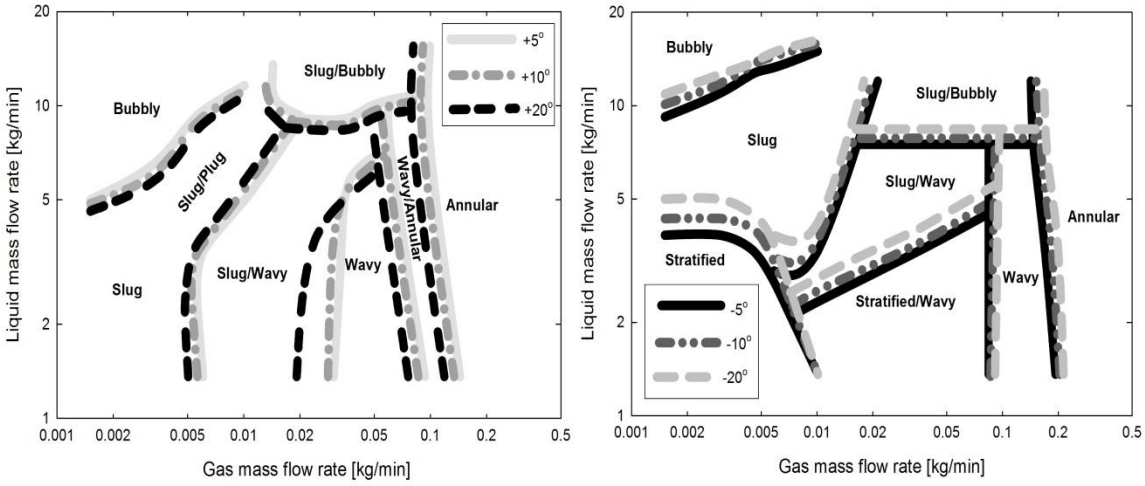

Figure 4.17 Comparisons between upward and downward inclined flow maps

The flow map developed for upward inclined pipe orientation contracts while that of the downward expands as shown in Figure 4.17. The liquid phase is more dominant in flow pattern formation than the gas phase because of very high liquid density when compared to gas density and the effects of gravitational force on the liquid phase plays an important role in both the type of flow pattern observed and the transition between distinct flow patterns.

For the upward inclined flow, gravitational force acts in opposite direction of liquid phase flow, this eliminates stratified flow and also increases the shear on the gas phase depending on the magnitude of the gravitational force due to pipe inclination. At lower angles of inclination, the gravitational pull is low but increases as pipe orientation increases upwards. The increase in gravitational force reduces the inertial force needed to transform the flow patterns and hence the transition boundaries shift to lower liquid and gas flow rates and the map contracts.

In the downward inclined flow, the gravitational force acts in the same direction as the liquid phase thereby increasing the inertial force (mass flow rate) needed to transform the flow patterns

and hence the transition boundaries shift to higher liquid and gas flow rate and the map expands as pipe orientation shifts further downwards.

Physical structure of the flow patterns remain the same for both upward and downward inclined flow except the slug flow that showed distinct properties in the downward inclined pipe orientation. Generally, slug flow is characterized by the gas phase existing in long cylindrical bullet shaped bubble with a hemispherical nose and a flat tail. Given in Figure 4.18 are representative pictures of slug flow in $+20^o$ and -20^o pipe orientations.

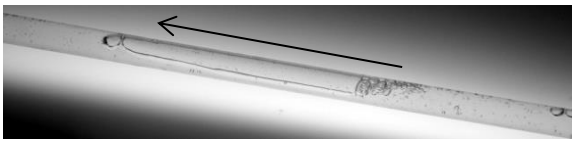

(A) Slug flow $+20^o$

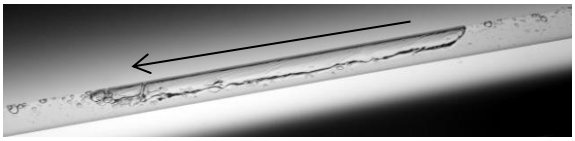

(B) Slug flow -20^o

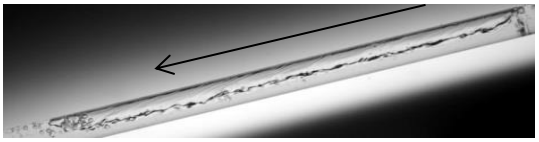

(C) Slug flow -20^o

(A) $\dot{m}_l$ = 2.3 kg/min & $\dot{m}_g$ = 0.003 kg/min, (B) $\dot{m}_l$ = 6.8 kg/min & $\dot{m}_g$ = 0.003 kg/min, (C) $\dot{m}_l$ = 6.8 kg/min & $\dot{m}_g$ = 0.003kg/min.

Figure 4.18 Representative pictures of slug flow pattern for $+20^o$ and -20^o pipe orientations.

The arrows in Figure 4.18 specify the flow direction for each pipe orientation as flow moves from right to left. Distinct characteristics can be observed in the slug flow pattern due to simultaneous effects of gravitational and buoyant forces acting in the two phase flow. For the upward inclined pipe orientation, the buoyant force acts in the flow direction while gravitational force opposes it.

This effect tends to pull the liquid phase downwards as the gas phase accelerates upwards resulting in slug flow pattern as shown in Figure 4.18 (A). While in the downward inclined pipe orientation, the gravitational force acts in flow direction which accelerates the liquid phase downwards while buoyant force acting on the gas phase opposes the flow. This effect slows down the velocity of the gas phase and generates laterally inverted slug which has the nose pointing in opposite flow direction as shown in Figure 4.18 (B) and (C).

4.2 Void Fraction

Void fraction is a critical parameter in two phase flow modeling as heat transfer and pressure drop calculations require two phase density and velocity which can only be determined by void fraction. As stated by Thome (2006), void fraction is defined based on method adopted for measurement. For example, chordal void fraction is defined as

$\alpha_{chordal} = \frac{L_g}{L_g+L_l}$ where L_g and L_l are the lengths of liquid and gas phase in the two phase system

Cross sectional void fraction is defined as

$\alpha_{cs} = \frac{A_g}{A_g+A_l}$ where A_l and A_g are the cross sectional areas occupied by liquid and gas phase

Volumetric void fraction is defined as

$\alpha_{vol} = \frac{V_g}{V_g+V_l}$ where V_l and V_g are the volumes of the liquid and gas phases

Void fraction calculation method employed in present study is the volumetric void fraction where quick closing valves are used to trap liquid and gas phase mixture in the test section.

4.2.1 Variation of Void Fraction with Flow Pattern

Void fraction is flow pattern dependent as bubbly flow was observed to occupy the lower void fraction range and wavy and annular flows observed in the higher void fraction range. The variation of void fraction with flow patterns is a logarithmic growth as void fraction notably increases with increase in gas phase flow rate in the low void fraction section (bubbly and slug flow). A relatively horizontal line showing small difference in values of void fraction with increase in gas flow rate was observed in the high void fraction region (wavy and annular flows). This indicates that void fraction is sensitive to increase in flow rates in the low gas flow region and has low sensitivity to increase in gas flow rate in the high gas flow region. Similar observation was made by Bhagwat (2011) and Godbole et al. (2011). Void fraction was plotted against the gas mass flow rate at constant liquid flow rates to observe the void fraction trends with increasing gas flow rates as shown in the Figure 4.19. Note that mass flow rate was used in the plot as opposed to Reynolds number or superficial velocity because Reynolds number depends on viscosity which changes with temperature while superficial velocity depends on pipe diameter and system pressure. However mass flow rate is a function of two independent properties (mass and time) which can easily be fixed on the flow meter regardless of change in temperature, pressure and pipe diameter. Variation of void fraction with flow pattern was plotted for each pipe orientation and they were observed to follow the same trend as shown in Figures 4.19 to 4.24. The range of void fraction for the distinct flow patterns are shown in Tables 4.1 to 4.6. The upward inclined pipe orientation plots for variation of void fraction with flow pattern are first discussed and given as Figures 4.19 to 4.21. Likewise Tables 4.1 to 4.3 give the range of void fraction for the distinct flow patterns for upward inclined pipe orientation.

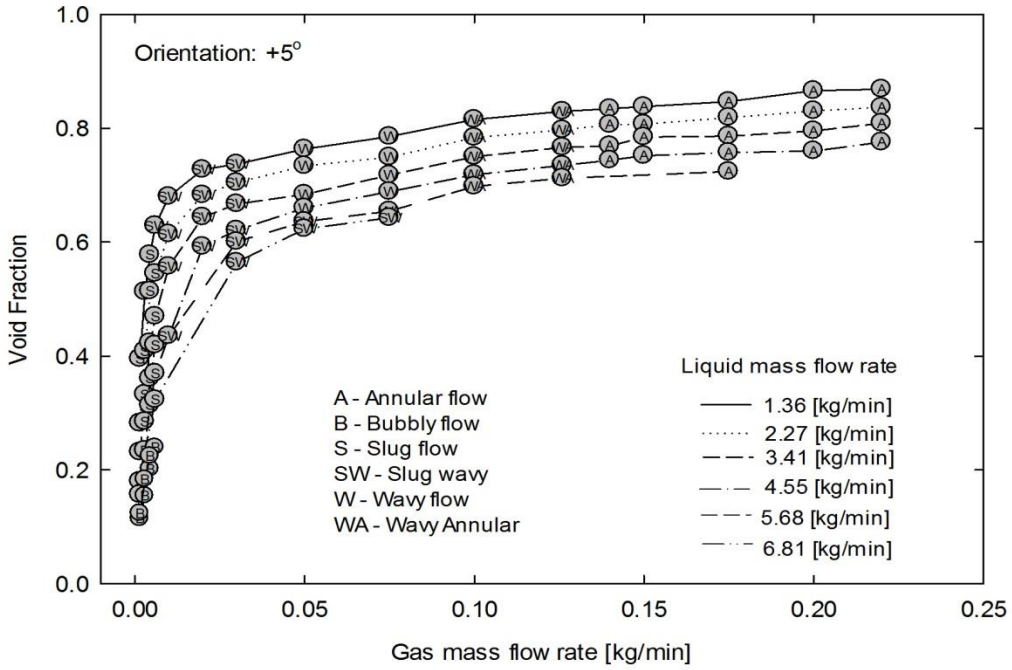

Figure 4.19 Variation of void fraction with flow pattern +5°

Table 4.1 Range of void fraction for distinct flow patterns observed in present study for +5°

Flow Pattern	Range of Void Fraction
Bubbly	0.08 – 0.24
Slug	0.23 – 0.58
Wavy	0.66 – 0.79
Annular	0.72– 0.87

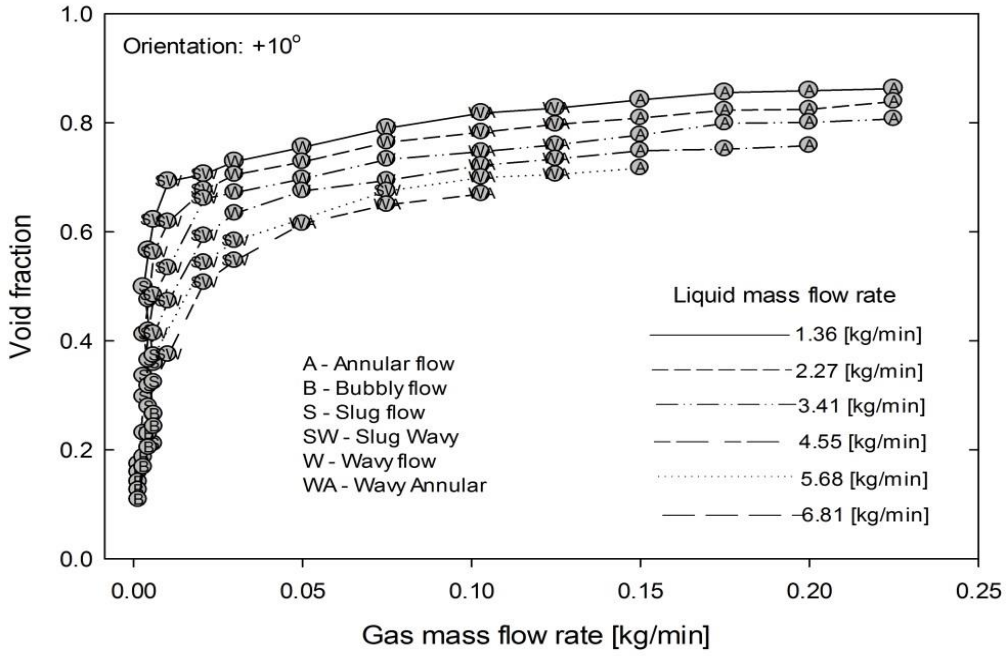

Figure 4.20 Variation of void fraction with flow pattern +10°

Table 4.2 Range of void fraction for distinct flow patterns observed in present study for +10°

Flow Pattern	Range of Void Fraction
Bubbly	0.09 – 0.27
Slug	0.17 – 0.57
Wavy	0.64 – 0.79
Annular	0.72 – 0.86

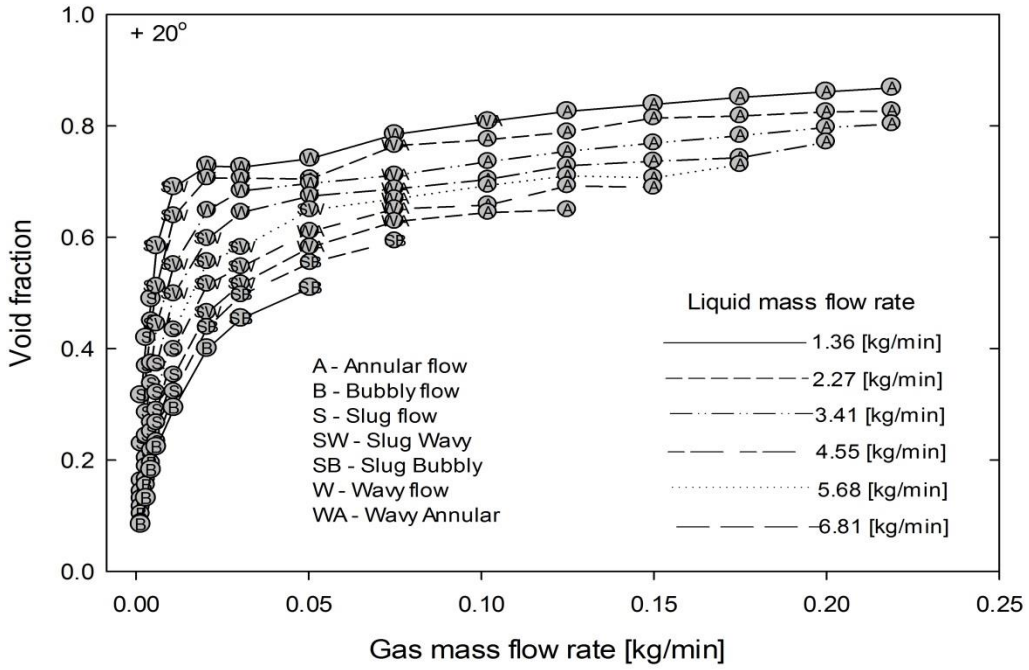

Figure 4.21 Variation of void fraction with flow pattern +20°

Table 4.3 Range of void fraction for distinct flow patterns observed in present study for +20°

Flow Pattern	Range of Void Fraction
Bubbly	0.08 – 0.40
Slug	0.14 – 0.45
Wavy	0.65 – 0.79
Annular	0.66 – 0.87

Figures 4.19 to 4.21 show the various void fraction sections the major flow patterns occupy in present study. This was achieved by maintaining constant liquid phase flow rate and increasing

the flow rate of the gas phase. For the bubbly flow section in Tables 4.1 to 4.3, the upper limits of void fraction can be seen to change with increase in inclination angle (0.24, 0.27, and 0.4 with uncertainty of ±5.1%, ±4.7% and ±2.9% for $+5^o$, $+10^o$ and $+20^o$). The accuracy of measured void fraction is determined by calculated experimental uncertainty based on flow properties. Refer to Chapter III for more information on experimental uncertainty. The upper limits of void fraction for bubbly flow for $+5^o$ and $+10^o$ are within experimental uncertainty, whereas the upper limit of $+20^o$ is not. This validates the claim in the upward inclined flow map in Figure 4.10 which showed downward shift in transition boundary (lower liquid flow rate) from slug to bubbly flow. Hence, bubbly flow was observed at higher void fraction when pipe inclination was increased. The lower limit of slug flow was observed to decrease with increase in inclination angle. The void fraction data for the lower limit of slug flow were measured at the lowest mass flow rates combination of $\dot{m}_l$= 1.36 kg/min & $\dot{m}_g$= 0.0015 kg/min. This reduction in void fraction is attributed to increase in gravitational force with inclination angle which increases slippage of liquid phase thereby reducing void fraction for the slug flow (0.23, 0.17 and 0.14 with experimental uncertainty of ±5.3%, ±7.5% and ±8.7% for $+5^o$, $+10^o$ and $+20^o$). The lower limits of void fraction for slug flow are not within experimental uncertainty, hence this confirms the claim that slug flow was observed at lower void fraction values with increase in pipe inclination. Due to mixing and disturbance waves observed in wavy flow, the void fraction did not follow a constant trend for lower and upper limits from $+5^o$ through $+20^o$. For instance, the lower limits of void fraction for wavy flow are 0.66, 0.63 and 0.65 with experimental uncertainty of ±1.7%, ±1.8% and ±1.7% for $+5^o$, $+10^o$ and $+20^o$. Since these values of void fraction for wavy flow are not within experimental uncertainty, void fraction of wavy flow was observed to increase from $+5^o$ to $+10^o$ then decreased at $+20^o$. The upper limit of void fraction of wavy flow was observed to be constant at approximately 0.79 with experimental uncertainty of ±1.4% for all three orientations. For annular flow, the lower limits of void fraction were measured as 0.72, 0.72 and 0.65 with uncertainty of ±1.5%, ±1.5% and ±1.7% for $+5^o$, $+10^o$ and $+20^o$. This also corroborates

the observation in the upward inclined flow map shown in Figure 4.10 that annular flow transition boundary shifts to the left (lower gas flow rate) as pipe inclination changed to $+20^{o}$. The downward void fraction plots are given as Figures 4.22 to 4.24. Range of void fraction covered by distinct flow patterns in downward inclined pipe orientation are given as Tables 4.4 to 4.6.

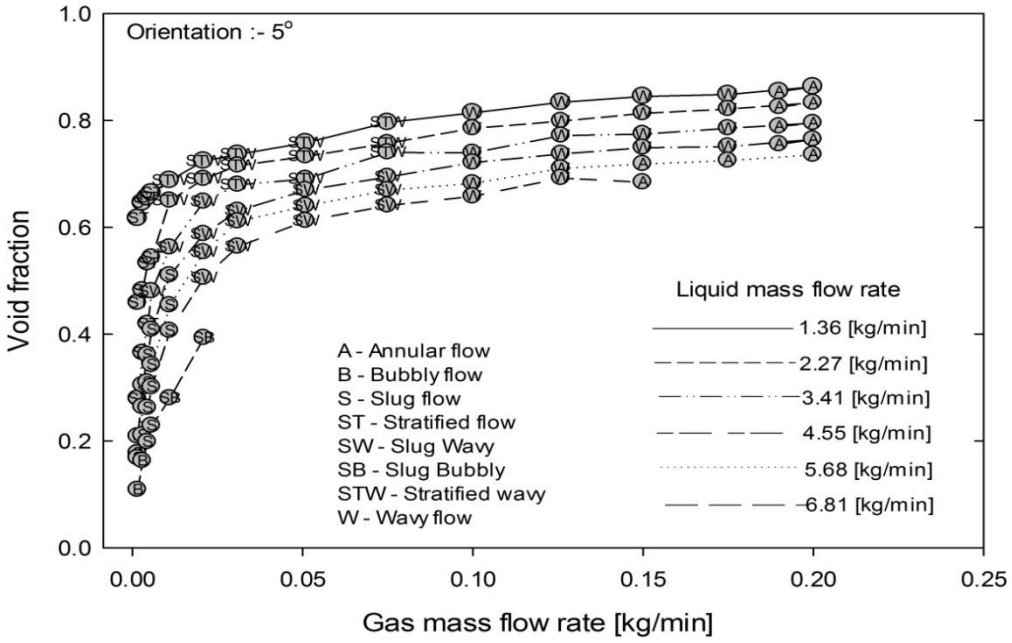

Figure 4.22 Variation of void fraction with flow pattern -5^{o}

Table 4.4 Range of void fraction for distinct flow patterns observed in present study for -5^{o}

Flow Pattern	Range of Void Fraction
Bubbly	0.11 – 0.16
Slug	0.17 – 0.51
Stratified	0.28 – 0.67
Wavy	0.66 – 0.85
Annular	0.68 – 0.86

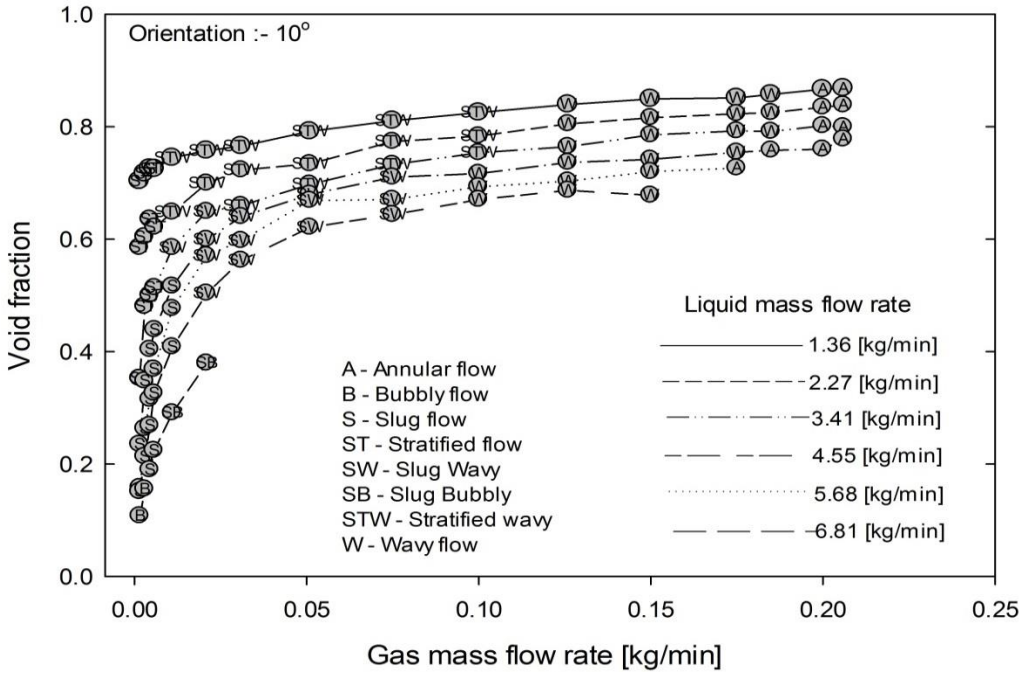

Figure 4.23 Variation of void fraction with flow pattern -10°

Table 4.5 Range of void fraction for distinct flow patterns observed in present study for -10°

Flow Pattern	Range of Void Fraction
Bubbly	0.11 – 0.16
Slug	0.15 – 0.52
Stratified	0.35 – 0.73
Wavy	0.67 – 0.84
Annular	0.73 – 0.87

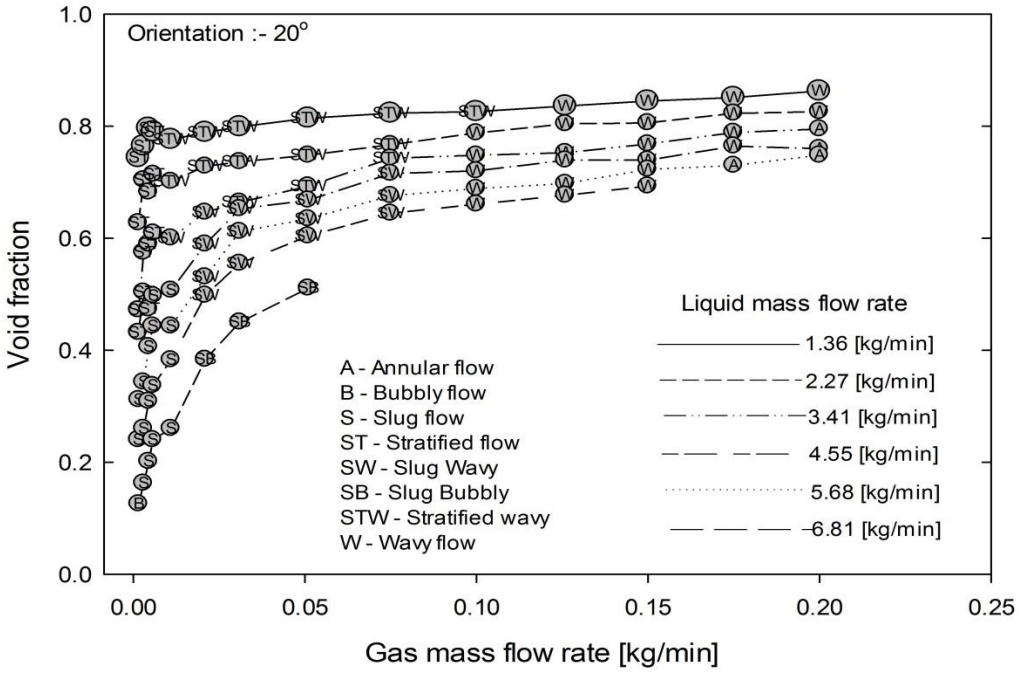

Figure 4.24 Variation of void fraction with flow pattern -20°

Table 4.6 Range of void fraction for distinct flow pattern observed in present study for -20°

Flow Pattern	Range of Void Fraction
Bubbly	≤ 0.12
Slug	0.14 – 0.54
Stratified	0.43 – 0.79
Wavy	0.66 – 0.86
Annular	≥ 0.74

As stated earlier, five distinct flow patterns were observed in the downward inclined pipe orientation (-5^o, -10^o & -20^o) as listed in Tables 4.4, 4.5 and 4.6. The upper limits of void fraction range for stratified flow are 0.67, 0.73, and 0.79 with experimental uncertainty of ±1.7%, ±1.5% and ±1.4% for -5^o, -10^o and -20^o. Hence, void fraction values are not within experimental uncertainty. The increase in upper void fraction limit for stratified flow was due to increase in liquid phase velocity and decrease in liquid film height. Hence, this increases void fraction. This effect was indicated in the downward flow map (Figure 4.15) which showed upward shift in transition boundary of stratified to slug flow. Unlike the upward inclined pipe orientation, the lower limit of void fraction in annular region for the downward inclined pipe orientation was observed as 0.68, 0.73, and 0.74 with uncertainty of ±1.6%, ±1.5% and ±1.5% for -5^o, -10^o and -20^o. Since lower void fraction limits of 0.68 and 0.73 for -5^o and -10^o are not within experimental uncertainty, the claim that annular flow was observed at higher flow rates from -5^o to -10^o was verified. Hence, transition boundary shifts to higher gas flow rates and flow map expands as indicated in Figure 4.15.

4.2.2 Performance Analyses of Void Fraction Correlations

A total of 700 void fraction data points were measured in present study with 350 points in the upward inclined pipe orientation and 350 points in the downward inclined pipe orientation. These data points were used to evaluate the prediction performance of selected void fraction correlations mentioned in the literature. Comprehensive analyses to come up with the best performing correlation in the upward, downward and all six pipe orientations was conducted. As reported by Godbole et al. (2011), the statistical parameter adopted for correlation performance comparison is based on the discretion of investigator due to ease of calculation and analyses. Different statistical parameters exist in literature which includes fractional deviation, logarithmic ratios, relative

performance factor and many more. Dukler et al. (1964) carried out the first void fraction correlation comparison for horizontal pipe orientation with different pipe diameters and the parameter employed for correlation analysis were standard deviation and arithmetic mean deviation. Palmer (1975) conducted inclined pipe comparison with a 51 mm diameter pipe for $+4.2^{o}$, $+7.1^{o}$ & $+7.5^{o}$ in the upward pipe orientation and -3.8^{o}, -4.3^{o} & -6.3^{o} in the downward pipe orientation, percentage error and standard deviation were the parameters used for comparison. The comparison parameter adopted in present study has been used by previous investigators in the same research group, hence this same type of analysis is deemed satisfactory for void fraction correlation performance. The performance of individual correlation was determined by percentage error (±10% & ±20%) and Root Mean Square error expressed as

$$RMS\ error = \sqrt{\frac{1}{N-1}\sum_{i=1}^{N}\left[\frac{(\alpha_{calc})_i-(\alpha_{meas})_i}{(\alpha_{calc})_i}\right]^2}\ \text{X } 100\%$$

Each of the six pipe orientations ($+5^{o}$, $+10^{o}$, $+20^{o}$ -5^{o}, -10^{o} & -20^{o}) was analyzed individually followed by their categorization as upward and downward inclined pipe orientations as done previously in this chapter for flow maps and variation of void fraction with flow pattern. This was followed by analysis of the total data set to determine the best performing correlation. In this study, the void fraction data was divided into three regions of $0 < \alpha \leq 0.25$, $0.25 < \alpha \leq 0.75$ and $0.75 < \alpha < 1$. This division was based on sensitivity of void fraction to gas flow rates and the specific flow patterns that occupy these particular regions. For example, bubbly and slug flow were observed to occupy the low void fraction region. Slug-bubbly, slug-wavy, wavy and wavy-annular flows were observed in the mid void fraction region while annular flow occupies the high void fraction region. Division of entire void fraction data into specific regions eliminates partial interpretation analysis based on the entire data set by revealing the specific regions of void fraction where correlations perform with higher accuracy. This ultimately helps in coming up

with detailed and appropriate conclusions for performance of each correlation. Fourteen correlations were chosen for analysis based on the following criteria.

1. Flow pattern and pipe orientation independent correlations: Different flow patterns and combination of two or more flow patterns were observed in present study. Flow pattern dependent correlation would ultimately fail in predicting void fraction in the transition flow pattern regions because of change in two phase structure in pipe cross section. Also pipe orientation independent correlation would ensure continuity in use of correlation for analyses of all six pipe orientations in present study.
2. Drift flux model correlations: As reported in the literature, drift flux model based void fraction correlations are the top performing correlations due to their ability to predict most accurately the flow physics of two phase flow. Woldesemayat and Ghajar (2007) conducted comparison of void fraction correlations for horizontal and upward inclined pipes. 68 correlations were selected for comparison and 6 correlations performed best, 5 out of the 6 correlations were based on drift flux model. Godbole et al. (2011) also conducted void fraction correlations comparison for vertical upward flow, 52 void fraction correlations were analyzed and only 8 correlations performed satisfactorily, all of which are drift flux models.
3. Empirical correlations: Some empirical correlations have been reported in the literature to perform satisfactorily for horizontal and near horizontal pipe orientations e.g., Guzhov et al. correlation (1967).
4. Separated flow model or slip ratio correlations: Separated flows were observed in present study (stratified and annular flows) and some correlations have been reported to perform better than other correlations in the separated region. Bhagwat and Ghajar (2013) conducted correlation comparison for 4227 air-water data points and reported a few top

performing separated flow model correlations. Woldesemayat and Ghajar (2007) also reported the top performing correlations in horizontal and upward inclined pipes.

Based on the above listed criteria, the following fourteen correlations were selected for prediction and analysis of experimental void fraction data in present study.

1. Bhagwat and Ghajar (2013)
2. Bonnecaze et al. (1971)
3. Cioncolini and Thome (2012)
4. Gomez et al. (2000)
5. Greskovic and Cooper (1975)
6. Guzhov et al. (1967)
7. Lockhart and Martinelli (1949)
8. Morooka et al. (1989)
9. Nicklin et al. (1962)
10. Rouhani and Axelsson (1970)
11. Smith (1969)
12. Sun et al. (1981)
13. Woldesemayat and Ghajar (2007)
14. Yashar et al. (2001)

The mathematical representations of the fourteen correlations are presented in Table 4.7.

Table 4.7 Void fraction correlations selected for present study

Author/Source	Void Fraction Correlation
	$Drift\ flux\ model: \alpha = \dfrac{U_{Sg}}{C_o(U_{Sg}+U_{sl})+U_{gm}}$
1. Bhagwat and Ghajar (2013)[D]	$C_o = \dfrac{2-(\rho_g/\rho_l)^2}{1+(Re_{tp}/1000)^2} + \dfrac{\left[\sqrt{(1+(\rho_g/\rho_l)^2\,cos\theta)/(1+cos\theta)}^{\,1-\alpha}\right]^{2/5}}{1+(Re_{tp}/1000)^2} + C_{o,1}$ $C_{o,1} = \left(C_1 - C_1\sqrt{\rho_g/\rho_l}\right)\left((2.6-\beta)^{0.15} - \sqrt{f_{tp}}\right)(1-x)^{1.5}$ $U_{gm} = (0.35sin\theta + 0.45cos\theta)\sqrt{\dfrac{gD_h(\rho_l-\rho_g)}{\rho_l}}(1-\alpha)^{0.5}C_2C_3C_4$ $C_1 = 0.2,\ C_2 = \begin{cases}\left(\frac{0.434}{log_{10}(\mu_l/0.001)}\right)^{0.15} & (\mu_l/0.001) > 10\\ 1 & (\mu_l/0.001) \le 10\end{cases}$ $C_3 = \begin{cases}(La/0.025)^{0.9} & La < 0.025\\ 1 & La \ge 0.025\end{cases},\ La = \sqrt{\sigma/(g\Delta\rho)}/D_h$ $C_4 = -1\ (0° > \theta \ge -50°, Fr_{sg} \le 0.1)$, otherwise $C_4 = 1$ $Re_{tp} = \frac{(U_{sl}+U_{sg})\rho_l D_h}{\mu_l},\ \beta = \frac{U_{sg}}{U_{sg}+U_{sl}},\ \frac{1}{\sqrt{f_{tp}}} = -4.0log_{10}\left(\frac{\epsilon/D_h}{3.7} + \frac{1.256}{Re_{tp}\sqrt{f_{tp}}}\right)$
2. Bonnecaze et al. (1971)[D]	$\alpha = U_{sg}\Big/\left(1.2U_m + 0.35\sqrt{gD(1-\dfrac{\rho_g}{\rho_l})}\right)$
3. Cioncolini and Thome (2012)[B]	$\alpha = hx^n/(1+(h-1)x^n)$ $h = -2.129 + 3.129(\rho_g/\rho_l)^{-0.2186}$ $n = 0.3487 + 0.6513(\rho_g/\rho_l)^{0.515}$
4. Gomez et al. (2000)[D]	$U_{gm} = 1.53(\dfrac{g\sigma\Delta\rho}{{\rho_l}^2})^{0.25}\sqrt{1-\alpha}\ sin\theta, C_o = 1.15$
5. Greskovic and Cooper (1975)[D]	$U_{gm} = 0.671\sqrt{gD}\ (sin\theta)^{0.263}, C_o = 1$
6. Guzhov et al. (1967)	$\alpha = 0.81\beta(1-\exp(-2.2\sqrt{Fr}),\ \beta = \frac{U_{sg}}{U_{sg}+U_{sl}}\ and\ Fr = \frac{(U_{sg}+U_{sl})^2}{gD}$
7. Lockhart and Martinelli (1949)[S]	$\alpha = [1+0.28(1-x/x)^{0.64}(\rho_g/\rho_l)^{0.36}(\mu_l/\mu_g)^{0.07}]^{-1}$
8. Morooka et al (1989)[D]	$\alpha = U_{sg}/(1.08U_m + 0.45)$
9. Nicklin et al. (1962)[D]	$\alpha = U_{sg}/(1.2U_m + 0.35\sqrt{gD})$
10. Rouhani and Axelsson (1970)[D]	$C_o = 1 + 0.2(1-x)\left(\frac{gD\rho_l^2}{G^2}\right)^{0.25},\ U_{gm} = 1.18\left(g\sigma\frac{\rho_l-\rho_g}{\rho_l^2}\right)^{0.25}$

11. Smith (1969)[S]	$\alpha = \left(1 + \frac{\rho_g}{\rho_l}\left(\frac{1-x}{x}\right)\left[0.4 + 0.6\left(\frac{\rho_l/\rho_g + 0.4(1/x-1)}{1+0.4(1/x-1)}\right)^{0.5}\right]\right)^{-1}$
12. Sun et al. (1981)[D]	$C_o = \left[0.82 + 0.18(P_{sys}/P_{cr})\right]^{-1}, U_{gm} = 1.41\left(g\sigma\frac{\rho_l-\rho_g}{\rho_l^2}\right)^{0.25}$
13. Woldesemayat and Ghajar (2007)[D]	$C_o = \frac{U_{sg}}{U_{sg}+U_{sl}}\left[1 + \left(\frac{U_{sl}}{U_{sg}}\right)^{(\rho_g/\rho_l)^{0.1}}\right]$ $U_{gm} = 2.9(1.22 + 1.22sin\theta)^{(P_{sys}/P_{atm})}\left[\frac{gD\sigma(1+cos\theta)(\rho_l-\rho_g)}{\rho_l^2}\right]^{0.25}$
14. Yashar et al. (2001)[S]	$\alpha = \left[1 + \sqrt{\frac{(1-x)gD\rho_l^2}{G^2x^3} + \left(\frac{1-x}{x}\right)^{0.9}\left(\frac{\rho_g}{\rho_l}\right)^{0.5}\left(\frac{\mu_l}{\mu_g}\right)^{0.1}}\right]^{-0.321}$

S = Slip ratio correlation, D = Drift flux correlation, B = Biochemical kinematics mathematical function.

Scatter plots used in analyses help to easily identify the trends and outliers of predicted data, the ±10% and ±20% error bands on the plots assist to visually recognize the range within which correlation is more accurate in predicting experimental data. Scatter plots for all fourteen correlations are presented as Figures 4.25 to 4.27 for +5° pipe orientation.

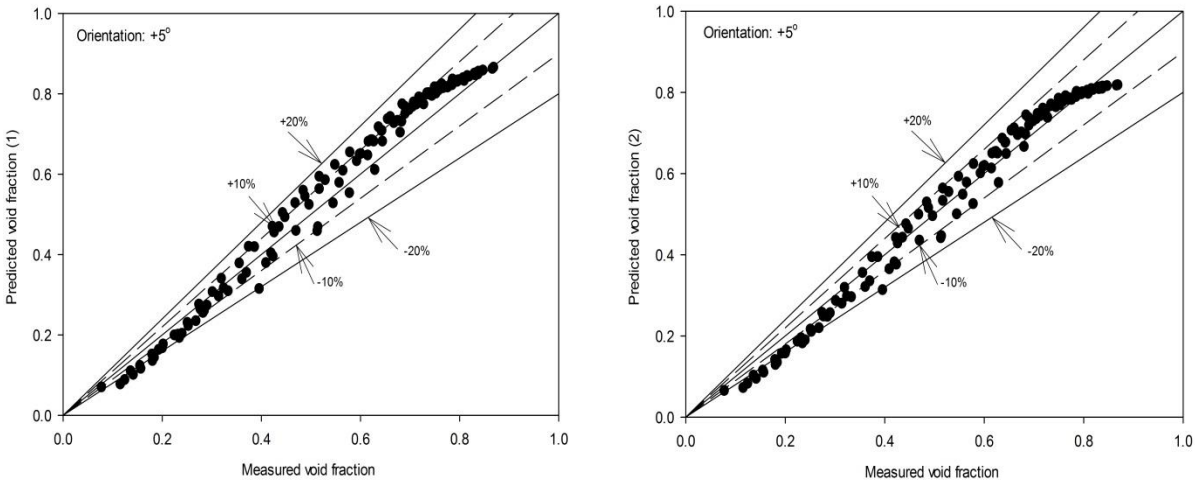

Figure 4.25 Void fraction data prediction for (1) Bhagwat and Ghajar (2013) and (2) Bonnecaze et al. (1971).

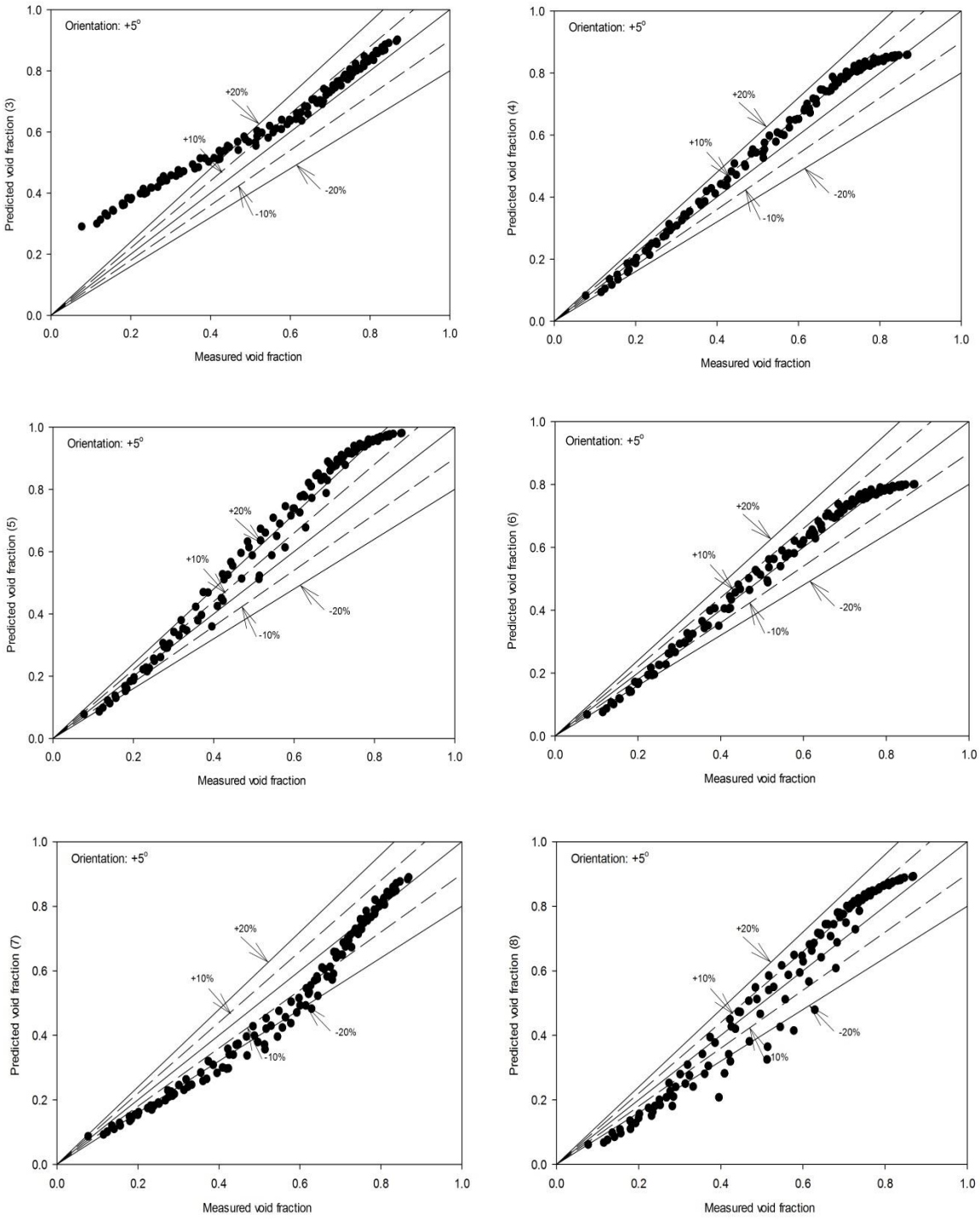

Figure 4.26 Void fraction data prediction for (3) Cioncolini and Thome (2012), (4) Gomez et al. (2000), (5) Greskovic and Cooper (1975), (6) Guzhov et al. (1967), (7) Lockhart and Martinelli (1949), and (8) Morooka et al. (1989)

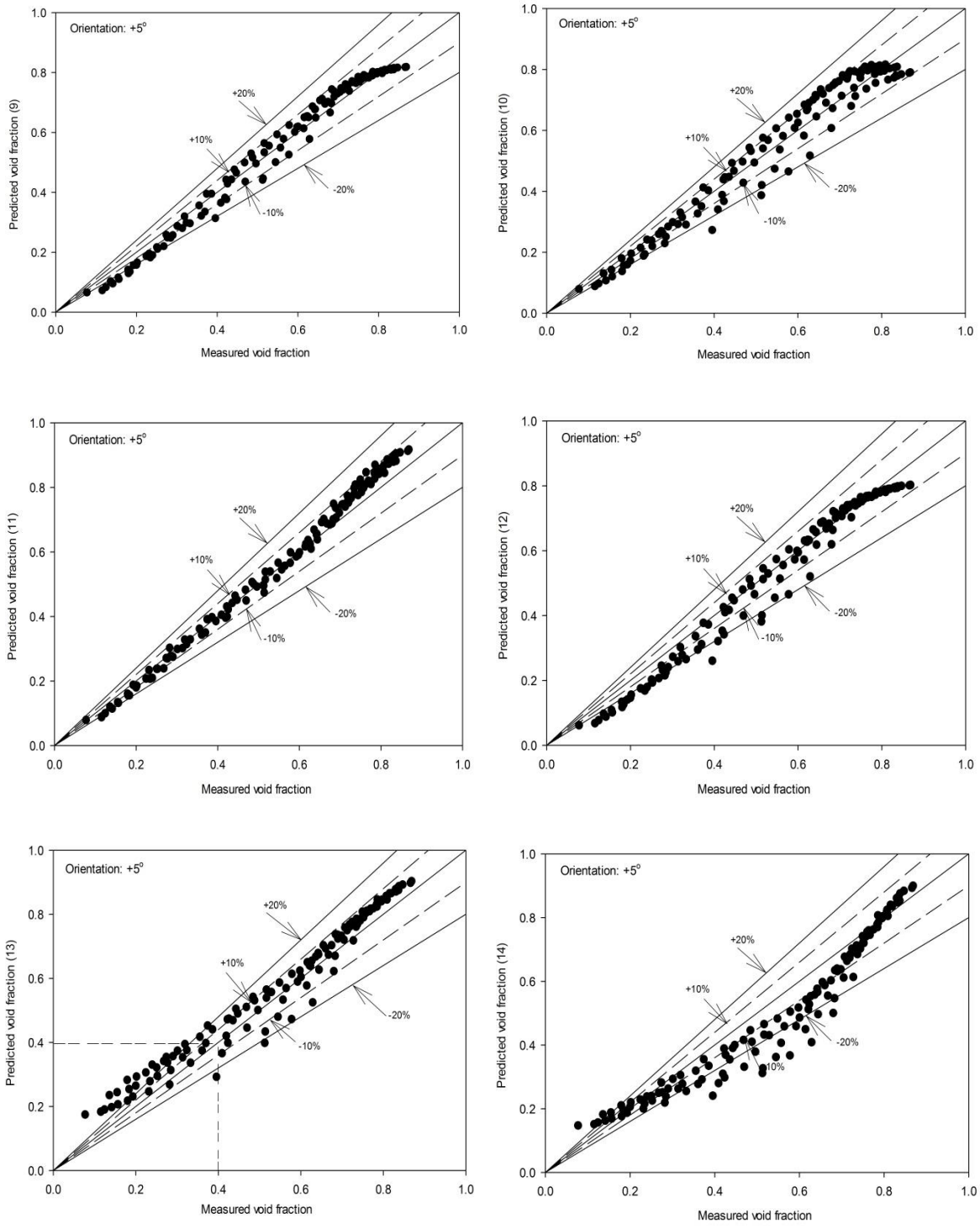

Figure 4.27 Void fraction data prediction for (9) Nicklin et al. (1962), (10) Rouhani and Axelsson (1970), (11) Smith (1969), (12) Sun et al. (1981), (13) Woldesemayat and Ghajar (2007) and (14) Yashar et al. (2001).

123 void fraction data points were analyzed for $+5^{o}$ pipe orientation, 105 data points were analyzed for $+10^{o}$ and 122 data points for $+20^{o}$. The scatter plots for $+10^{o}$ and $+20^{o}$ follow similar trend as Figures 4.25 to 4.27 for the selected correlations, therefore their presentation in present study was not necessary. A more detailed analysis of performance of each correlation is given in Tables 4.8 to 4.11. The highlighted (bolded and underlined) values in Tables 4.8 through 4.11 represent the percentage accuracies of top performing correlations within the corresponding void fraction region and error bands. Each Table has a total of 9 columns of prediction for each correlation and the first 2 columns show predictions for the entire void fraction data measured for the given pipe orientation in ±10% and ±20% error bands. Percent RMS error was calculated for each pipe orientation in column 3 which is based on the total void fraction data points analyzed in columns 1 and 2. Further analyses based on prediction of void fraction correlations for the given void fraction region ($0 < \alpha \leq 0.25$, $0.25 < \alpha \leq 0.75$ and $0.75 < \alpha < 1$) are shown in columns 4 to 9.

The error bands for $0.75 < \alpha < 1$ void fraction region was reduced to ±5% and ±7.5% from ±10% and ±20% due to high accuracy of void fraction correlations in predicting experimental data. The results for upward inclined pipe orientation are shown in Tables 4.8 to 4.11.

Table 4.8 Void fraction correlation comparison for 123 data points for +5°

Pipe Orientation: +5°									
123 Data Points			RMS Error	0 < α ≤ 0.25 (17 points)		0.25 < α ≤ 0.75 (79 points)		0.75 < α < 1 (27 points)	
Correlation	±10% Error	±20% Error	%	±10% Error	±20% Error	±10% Error	±20% Error	±5% Error	±7.5% Error
Bhagwat and Ghajar (2013)	65	94	**10.8**	6	65	66	99	59	93
Bonnecaze et al. (1971)	75	89	**11.1**	0	29	84	99	93	100
Cioncolini and Thome (2012)	55	63	51.9	0	0	53	63	52	93
Gomez et al. (2000)	50	97	10.8	24	76	41	100	48	70
Greskovic and Cooper (1975)	26	48	19.8	**59**	82	28	39	0	0
Guzhov et al. (1967)	**85**	94	**9.1**	6	53	**96**	100	85	93
Lockhart and Martinelli (1949)	39	70	16.6	0	47	27	66	**100**	100
Morooka et al. (1989)	43	75	17.8	0	6	39	80	11	41
Nicklin et al. (1962)	75	89	**11.1**	0	29	82	99	93	100
Rouhani and Axelsson (1970)	52	90	12.8	0	35	46	98	56	93
Smith (1969)	**87**	99	**6.9**	**35**	94	**99**	100	11	67
Sun et al. (1981)	68	75	14.4	0	0	71	89	85	96
Woldesemayat and Ghajar (2007)	65	85	18.4	6	24	65	91	15	96
Yashar et al. (2001)	51	80	17.6	**53**	71	34	75	**100**	100

Table 4.9 Void fraction correlation comparison for 105 data points for +10°

Pipe Orientation: +10°									
105 Data Points			RMS Error	$0 < \alpha \leq 0.25$ (16 points)		$0.25 < \alpha \leq 0.75$ (68 points)		$0.75 < \alpha < 1$ (21 points)	
Correlation	±10% Error	±20% Error	%	±10% Error	±20% Error	±10% Error	±20% Error	±5% Error	±7.5% Error
Bhagwat and Ghajar (2013)	59	96	**10.9**	19	67	56	100	62	81
Bonnecaze et al. (1971)	**73**	92	**11.2**	0	50	**84**	100	**100**	100
Cioncolini and Thome (2012)	54	63	54.4	0	0	53	68	48	91
Gomez et al. (2000)	54	95	**10.8**	25	69	49	100	62	81
Greskovic and Cooper (1975)	29	53	18.6	**56**	81	31	44	0	0
Guzhov et al. (1967)	**85**	94	**9.3**	19	63	**96**	100	81	100
Lockhart and Martinelli (1949)	37	70	16.4	0	63	27	62	**100**	100
Morooka et al. (1989)	45	69	18.2	0	0	43	75	14	48
Nicklin et al. (1962)	**73**	92	**11.2**	0	50	**85**	100	**100**	100
Rouhani and Axelsson (1970)	59	90	12.6	0	50	60	96	57	95
Smith (1969)	**89**	97	**7.3**	**56**	81	**94**	100	10	62
Sun et al. (1981)	64	78	14.8	0	0	69	91	76	100
Woldesemayat and Ghajar (2007)	64	83	16.4	0	19	68	93	24	91
Yashar et al. (2001)	50	77	17.2	44	69	35	72	**100**	100

Table 4.10 Void fraction correlation comparison for 122 data points for +20^{o}

Pipe Orientation: +20^{o}									
122 Data Points			RMS Error	$0 < \alpha \leq 0.25$ (26 points)		$0.25 < \alpha \leq 0.75$ (76 points)		$0.75 < \alpha < 1$ (20 points)	
Correlation	±10% Error	±20% Error	%	±10% Error	±20% Error	±10% Error	±20% Error	±5% Error	±7.5% Error
Bhagwat and Ghajar (2013)	**81**	99	**10.3**	**85**	96	75	100	55	85
Bonnecaze et al. (1971)	**89**	99	**8.6**	50	92	**100**	100	95	100
Cioncolini and Thome (2012)	49	57	104.9	0	0	53	67	40	90
Gomez et al. (2000)	78	98	**11.0**	**80**	96	71	100	55	75
Greskovic and Cooper (1975)	26	66	19.0	**73**	96	17	57	0	0
Guzhov et al. (1967)	**89**	98	**8.9**	**80**	96	**97**	100	85	95
Lockhart and Martinelli (1949)	47	84	19.3	54	92	30	73	**100**	100
Morooka et al. (1989)	47	89	14.3	4	69	**100**	100	15	45
Nicklin et al. (1962)	**89**	98	**8.6**	50	96	**100**	100	95	100
Rouhani and Axelsson (1970)	63	92	12.8	4	84	70	93	70	85
Smith (1969)	**87**	97	11.8	69	85	91	100	5	60
Sun et al. (1981)	70	95	10.9	16	80	82	99	85	95
Woldesemayat and Ghajar (2007)	65	75	40.8	4	8	74	91	15	100
Yashar et al. (2001)	44	71	39.5	27	39	37	75	**100**	100

Table 4.11 Void fraction correlation comparison for 350 data points for upward inclined pipe orientation

Upward Inclined Pipe Orientation (+5°, +10° and +20°)									
350 Data points			RMS Error	$0 < \alpha \leq 0.25$ (59 points)		$0.25 < \alpha \leq 0.75$ (223 points)		$0.75 < \alpha < 1$ (68 points)	
Correlation	±10% Error	±20% Error	%	±10% Error	±20% Error	±10% Error	±20% Error	±5% Error	±7.5% Error
Bhagwat and Ghajar (2013)	69	96	**10.6**	44	79	66	100	59	87
Bonnecaze et al. (1971)	79	93	**10.3**	22	62	**89**	100	96	100
Cioncolini and Thome (2012)	53	61	75.1	0	0	53	66	47	92
Gomez et al. (2000)	61	97	**10.8**	49	83	54	100	54	75
Greskovic and Cooper (1975)	27	56	19.1	**64**	88	25	47	0	0
Guzhov et al. (1967)	**86**	95	**9.1**	42	75	**96**	100	84	96
Lockhart and Martinelli (1949)	41	75	17.5	24	71	28	67	**100**	100
Morooka et al. (1989)	45	78	16.7	2	32	61	85	13	44
Nicklin et al. (1962)	79	93	10.3	22	64	**89**	100	96	100
Rouhani and Axelsson (1970)	58	91	12.7	2	61	58	96	60	91
Smith (1969)	**88**	98	**9**	**56**	87	**95**	100	9	63
Sun et al. (1981)	67	83	13.4	7	35	74	93	82	97
Woldesemayat and Ghajar (2007)	65	81	27.9	3	16	69	92	18	96
Yashar et al. (2001)	48	76	27.2	39	56	35	74	**100**	100

Performance of Correlations for $0 < \alpha \leq 0.25$

Low accuracy was observed for selected correlations in this region due to low values of measured void fraction. Slight difference between measured and predicted void fraction yields high percentage error of prediction. For example, measured void fraction of 0.07 and predicted void fraction of 0.1 gives difference of 0.03 and 43% percent error. Greskovic and Cooper (1975) predicted total data points in this region with highest accuracy of 59% and 56% within ±10% error bands for $+5^o$ and $+10^o$ as shown in Tables 4.8 and 4.9, column 4. However, accuracy of correlations improved as pipe orientation shifted to $+20^o$ (Table 4.10, column 4) as Bhagwat and Ghajar (2013) performed best by predicting 85% of data points within ±10% error bands. Gomez et al. (2000) and Guzhov et al. (1967) also predicted 80% of data in this region. This was followed by Greskovic and Cooper (1975) which predicted 73% of data points in $+20^o$ within ±10% error bands. For the total of 59 data points for this void fraction region in upward inclined pipe orientation, Greskovic and Cooper (1975) performed best by predicting 64% of data points in ±10% error bands (Table 4.11, column 4). Even though this value is relatively low, it is acceptable since most correlations perform below 50% accuracy in this region. The second top performing correlation is Smith (1969) which predicted 56% of data followed by Gomez et al. (2000) which predicted 51% of total data points. Accuracy of correlations improve in the ±20% error bands as Greskovic and Cooper (1975), Smith (1969) and Gomez et al. (2000) predicted 90%, 87% and 85% in this region respectively. Cioncolini and Thome (2012), Morooka et al. (1989), Rouhani and Axelsson (1970), Sun et al. (1981) and Woldesemayat and Ghajar (2007) all predicted less than 10% of data within ±10% error bands for this void fraction region.

Performance of Correlations for $0.25 < \alpha \leq 0.75$

Accuracy of void fraction correlations was observed to significantly increase in the $0.25 < \alpha \leq 0.75$ region as most of the correlations perform satisfactorily. Guzhov et al. (1967) performed

consistently accurate in the $+5^o$, $+10^o$ and $+20^o$ (Tables 4.8 to 4.10, column 6) by predicting 96%, 96% and 97% of data points within ±10% error bands in this void fraction region. Smith (1969) also predicted 99%, 94% and 91% for $+5^o$, $+10^o$ and $+20^o$ pipe orientation. Other correlations like Bonnecaze et al. (1971), Nicklin et al. (1962) and Morooka et al. (1989) all showed increased accuracy with inclination angle as they all predicted a little above 80% of data points in the $+5^o$ and $+10^o$, and 100% in ±10% error bands for $+20^o$. For the total of 223 data points in this void fraction region in upward inclined pipe orientation (Table 4.11, column 6), Guzhov et al. (1967) performed best by predicting 96% of data within ±10% error bands, followed closely by Smith (1969) which predicted 95% of data in this region. Bonnecaze et al. (1971) and Nicklin et al. (1962) also performed satisfactorily by predicting 89% of data in this region. Greskovic and Cooper (1975) performed least by predicting only 47% of 223 data points within ±10% error bands in this void fraction region. Hence the best performing void fraction correlation in present study for upward inclined pipe orientation in $0.25 < \alpha \leq 0.75$ region is Guzhov et al. correlation (1967).

Performance of Correlations for $0.75 < \alpha < 1$

As shown in the void fraction plot in Figures 4.19 to 4.24, the higher void fraction region has very low sensitivity to changes in superficial velocity or flow rate of gas phase. This effect makes the correlations predict void fraction with very high accuracy. In $+5^o$ (Table 4.8, column 8), Lockhart and Martinelli (1949) and Yashar et al. (2001) predicted 100% of data points within ±5% error bands for this void fraction region. Bonnecaze et al. (1971) and Nicklin et al. (1962) predicted 93% of data within ±5% error bands. However, Smith (1969) and Morooka et al. (1989) predicted only 11% of data points in this region within ±10% error bands. Greskovic and Cooper (1975) performed least by predicting none of the data points in this region. In $+10^o$ pipe orientation (Table 4.9, column 8), Bonnecaze et al. (1971), Nicklin et al. (1962), Yashar et al. (2001) and Lockhart and Martinelli (1949) all predicted 100% of data points within ±5% error

bands. However, Greskovic and Cooper (1975) performed least by predicting none of the data points in this region. In $+20^o$ pipe orientation (Table 4.10, column 8), Lockhart and Martinelli (1949) and Yashar et al. (2001) performed best by predicting 100% of data in this void fraction region within ±5% error bands. Bonnecaze et al. (1971) and Nicklin et al. (1962) predicted 95% of void fraction data in this region. For the total of 68 void fraction data points measured in this region, Lockhart and Martinelli (1949) and Yashar et al. (2001) predicted 100% of void fraction data within ±5% error bands for upward inclined pipe orientation while Greskovic and Cooper (1975) predicted none of the data points in this void fraction region as shown in Figure 4.11, column 8.

4.2.3 Best Performing Correlation for Upward Inclined Pipe Orientation

The top performing correlation based on percent RMS error was determined for each pipe orientation and for the entire upward inclined pipe orientation. As shown in Table 4.8 and column 3, the best performing correlation having lowest RMS error for $+5^o$ is Smith (1969) with 6.9% in RMS error. This was followed by Guzhov et al. (1967) having 9.1% RMS error and Bhagwat and Ghajar (2013) having 10.8% in RMS error. The highest percent RMS error was calculated for Cioncolini and Thome (2012) with 51.9% in RMS error.

The best performing correlation in $+10^o$ (Table 4.9, column 3) based on lowest percent RMS error was Smith (1969) with 7.3% followed by Guzhov et al. (1967) having 9.3% in RMS error. Gomez et al. (2000) had RMS error of 10.8% followed by Bhagwat and Ghajar (2013) with 10.9% in RMS error. Cioncolini and Thome (2012) had the highest percent RMS error of 54.4%.

In $+20^o$ pipe orientation, Nicklin et al. (1962) and Bonnecaze et al. (1971) gave lowest percent RMS error of 8.6%. Guzhov et al. (1967) gave 8.9% in RMS error followed by Bhagwat and Ghajar (2013) which gave 10.3% in RMS error as shown in Table 4.10, column 3. Complete performance analyses of the three upward inclined pipe orientations ($+5^o$, $+10^o$ & $+20^o$) is shown

in Table 4.11. A total of 350 void fraction data points were measured in these orientations (+5^o, +10^o, and +20^o), and the best performing correlation was selected. The lowest RMS error of 9% was calculated for Smith (1969) which was followed closely by Guzhov et al. (1967) having 9.1% in RMS error. Bonnecaze et al. (1971) and Nicklin et al. (1962) both gave RMS error of 10.3%, Bhagwat and Ghajar (2013) had 10.6% in RMS error followed by Gomez et al. (2000) with 10.8% of RMS error. The highest RMS error of 75.1% was calculated for Cioncolini & Thome (2012). Hence the best correlation for predicting void fraction in present study for upward inclined pipe orientation is Smith (1969) followed closely by Guzhov et al. (1969) having a difference of 0.1%.

In downward inclined pipe orientation (-5^o, -10^o, and -20^o), Greskovic & Cooper (1975) completely failed to predict the void fraction data and was removed from the list of selected correlations for comparison leaving 13 correlations. Regardless of void fraction model i.e., drift flux or slip ratio, it was observed that void fraction correlations under-predict the data points for stratified flow in the downward inclined pipe orientation. The high void fraction in stratified flow region was attributed to liquid phase acceleration downstream due to gravity thereby significantly increasing void fraction. The number of under-predicted void fraction data points was observed to increase with increase in pipe orientation in the downward direction. The effect of pipe orientation on Gomez et al. (2000) which was observed as the top performing correlation in the downward inclined pipe orientation is shown in Figures 4.28 to 4.30.

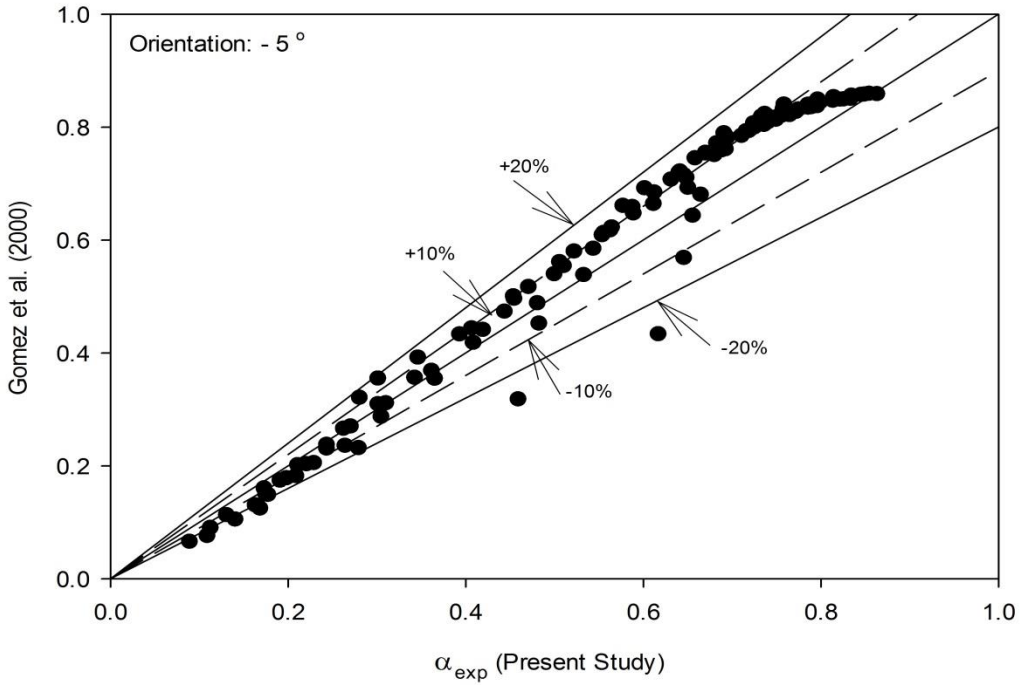

Figure 4.28 Gomez et al. (2000) predictions of 115 data points for -5^{o} pipe orientation

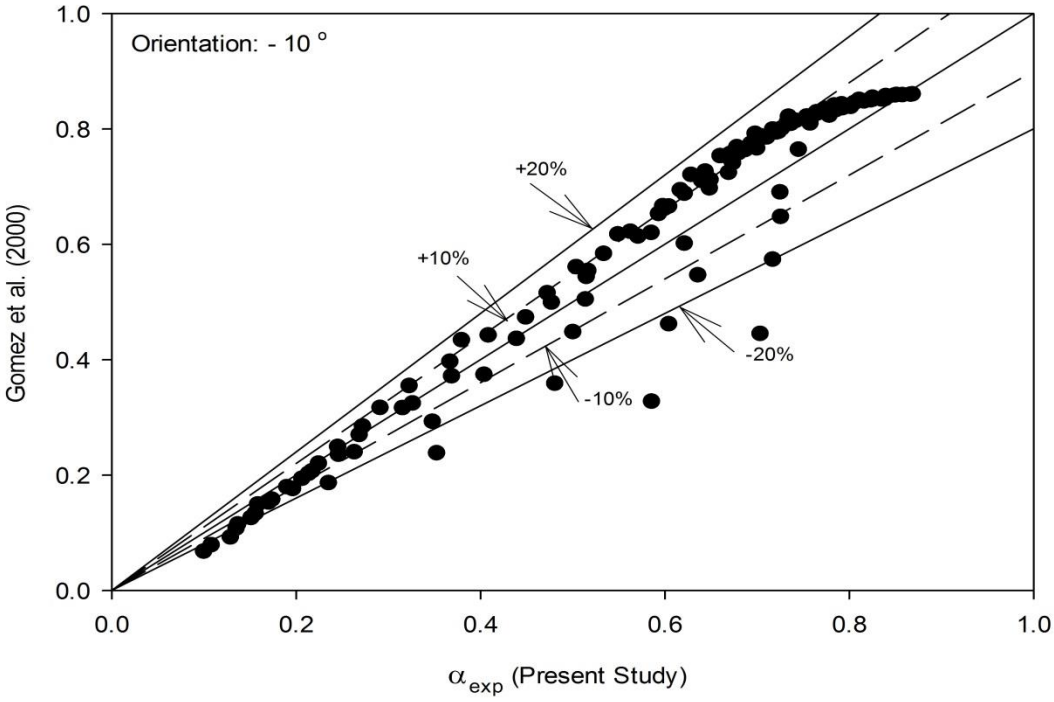

Figure 4.29 Gomez et al. (2000) predictions of 119 data points for -10^{o} pipe orientation

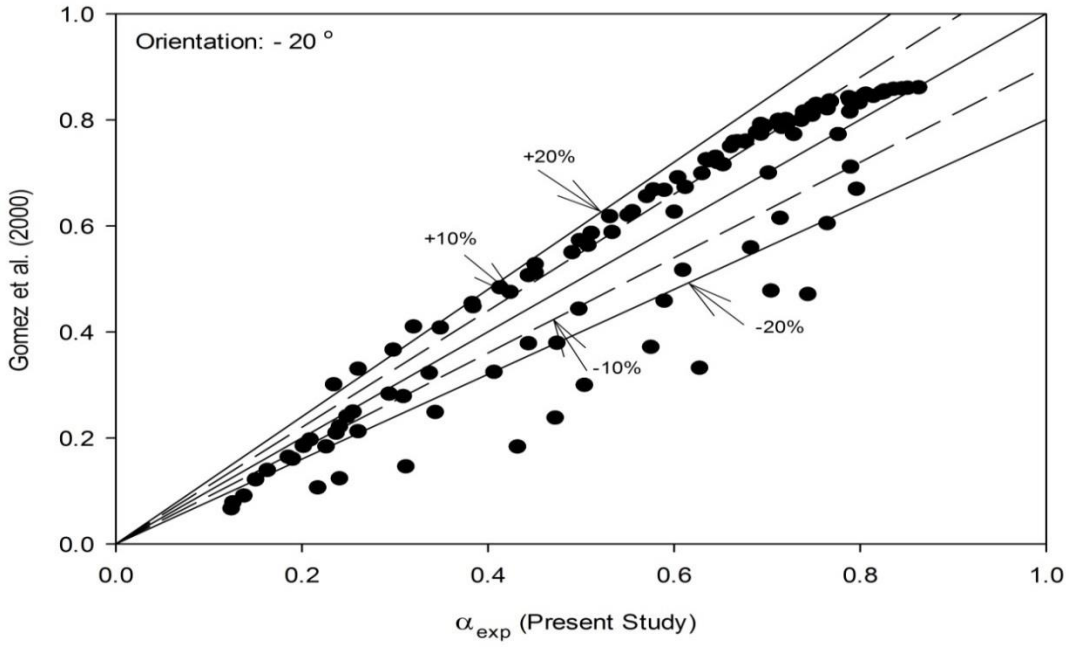

Figure 4.30 Gomez et al. (2000) predictions of 116 data points for -20^o pipe orientation

Only 2 data points were under-predicted (below the -20% error band) by the Gomez et al. (2000) for -5^o as shown in Figure 4.28. These under-predicted points were observed to increase to 5 points in -10^o and 15 points in -20^o pipe orientations (Figures 4.29 and 4.30). All other correlations were observed to under-predict more points than Gomez et al. (2000) as pipe inclination was increased from -5^o through -10^o to -20^o. Beggs and Brill (1973) conducted extensive study of inclined air-water two phase flow in 1 and 1.5 inch diameter pipes over the entire pipe orientation of -90^o to +90^o. The statistical average percent error of the liquid holdup correlation developed by Beggs and Brill (1973) showed for downhill inclinations of -5^o, -10^o, -15^o and -20^o are +0.13%, -0.84%, +1.16% and +0.29%, respectively. This indicates that highest value over-prediction of liquid holdup was observed at -15^o before reducing at -20^o. Since $\varepsilon = 1 - \alpha$, then the highest value for void fraction under-prediction for Beggs and Brill (1973) was observed at -15^o whereas in present study highest percentage of under-predicted data points was observed at -20^o. Detailed analyses of performance of the selected correlations in downward inclined pipe orientation are given in Tables 4.12 to 4.15.

Table 4.12 Void fraction correlation comparison for 115 data points for -5°

Pipe Orientation: -5°									
115 Data Points			RMS Error	0 < α ≤ 0.25 (18 points)		0.25 < α ≤ 0.75 (74 points)		0.75 < α < 1 (23 points)	
Correlation	±10% Error	±20% Error	%	±10% Error	±20% Error	±10% Error	±20% Error	±5% Error	±7.5% Error
Bhagwat and Ghajar (2013)	59	71	19.5	22	33	55	72	57	83
Bonnecaze et al. (1971)	69	85	14.4	0	44	76	91	**96**	100
Cioncolini and Thome (2012)	56	68	51.3	0	0	61	74	48	94
Gomez et al. (2000)	50	95	**11.4**	**44**	78	39	97	43	78
Guzhov et al. (1967)	**77**	89	**12.0**	6	50	**88**	95	83	100
Lockhart and Martinelli (1949)	40	62	19.2	6	33	28	57	**100**	100
Morooka et al. (1989)	44	70	20.9	0	6	43	77	17	44
Nicklin et al. (1962)	69	85	14.4	0	44	76	91	**96**	100
Rouhani and Axelsson (1970)	60	72	19.6	0	11	62	78	57	87
Smith (1969)	**82**	94	**9.7**	**44**	83	**87**	94	0	78
Sun et al. (1981)	62	76	17.9	11	39	72	85	83	100
Woldesemayat and Ghajar (2007)	70	76	20.3	6	6	72	87	9	96
Yashar et al. (2001)	49	75	19.8	**44**	72	33	68	**96**	100

Table 4.13 Void fraction correlation comparison for 119 data points for -10^{o}

Pipe Orientation: -10^{o}									
119 Data Points			RMS Error	$0 < \alpha \leq 0.25$ (19 points)		$0.25 < \alpha \leq 0.75$ (70 points)		$0.75 < \alpha < 1$ (30 points)	
Correlation	±10% Error	±20% Error	%	±10% Error	±20% Error	±10% Error	±20% Error	±5% Error	±7.5% Error
Bhagwat and Ghajar (2013)	63	81	**15.4**	16	42	60	84	73	100
Bonnecaze et al. (1971)	**69**	81	16.8	5	42	71	81	**93**	100
Cioncolini and Thome (2012)	60	71	49.3	0	0	59	71	20	100
Gomez et al. (2000)	59	92	**12.2**	**58**	79	41	93	43	77
Guzhov et al. (1967)	72	86	14.3	5	58	**79**	87	77	93
Lockhart and Martinelli (1949)	40	67	21.2	0	68	27	53	**97**	97
Morooka et al. (1989)	43	71	22.7	0	21	37	74	23	57
Nicklin et al. (1962)	**69**	81	16.8	5	42	71	81	**93**	100
Rouhani and Axelsson (1970)	60	73	21.6	0	26	60	74	53	67
Smith (1969)	**79**	88	**12.5**	**53**	79	**77**	86	10	90
Sun et al. (1981)	62	71	20.1	0	16	63	76	73	97
Woldesemayat and Ghajar (2007)	66	74	21.7	5	5	67	80	27	100
Yashar et al. (2001)	47	72	21.6	32	58	33	64	**93**	93

Table 4.14 Void fraction correlation comparison for 116 data points for -20^{o}

Pipe Orientation: -20^{o}									
116 Data Points			RMS Error	$0 < \alpha \leq 0.25$ (16 points)		$0.25 < \alpha \leq 0.75$ (75 points)		$0.75 < \alpha < 1$ (25 points)	
Correlation	±10% Error	±20% Error	%	±10% Error	±20% Error	±10% Error	±20% Error	±5% Error	±7.5% Error
Bhagwat and Ghajar (2013)	53	85	**16.0**	13	63	43	85	64	96
Bonnecaze et al. (1971)	**62**	72	24.0	0	25	67	75	**76**	84
Cioncolini and Thome (2012)	50	67	39.8	0	0	48	73	52	84
Gomez et al. (2000)	35	81	**19.4**	**25**	63	19	80	48	72
Guzhov et al. (1967)	37	72	22.0	0	38	**67**	75	**72**	84
Lockhart and Martinelli (1949)	39	65	26.8	6	38	32	64	**76**	76
Morooka et al. (1989)	41	66	28.8	0	6	39	72	24	44
Nicklin et al. (1962)	**62**	71	24.0	0	25	**67**	75	**76**	84
Rouhani and Axelsson (1970)	52	66	28.0	0	13	56	73	44	48
Smith (1969)	**63**	77	20.2	6	63	**67**	76	16	64
Sun et al. (1981)	**61**	66	26.7	6	6	**67**	71	56	76
Woldesemayat and Ghajar (2007)	52	68	22.8	6	13	52	73	12	72
Yashar et al. (2001)	42	72	25.0	**38**	75	67	75	**72**	76

Table 4.15 Void fraction correlation comparison for 350 data points for downward inclined orientation

Downward Inclined Pipe Orientation (-5°, -10°, and -20°)									
350 Data Points			RMS Error	$0 < \alpha \leq 0.25$ (53 points)		$0.25 < \alpha \leq 0.75$ (219 points)		$0.75 < \alpha < 1$ (78 points)	
Correlation	±10% Error	±20% Error	%	±10% Error	±20% Error	±10% Error	±20% Error	±5% Error	±7.5% Error
Bhagwat and Ghajar (2013)	58	79	17	17	45	52	80	65	94
Bonnecaze et al. (1971)	**67**	79	18.8	2	38	**71**	82	**88**	95
Cioncolini and Thome (2012)	55	69	47	0	0	56	73	39	93
Gomez et al. (2000)	48	89	**14.7**	**43**	74	33	90	45	76
Guzhov et al. (1967)	62	82	16.6	4	49	**78**	86	77	92
Lockhart and Martinelli (1949)	40	65	22.6	4	47	29	58	**91**	91
Morooka et al. (1989)	43	69	24.3	0	11	40	74	22	49
Nicklin et al. (1962)	**67**	79	18.8	2	38	**71**	82	**88**	95
Rouhani and Axelsson (1970)	57	70	23.3	0	17	59	75	51	67
Smith (1969)	**75**	86	**14.8**	36	76	**77**	85	9	78
Sun et al. (1981)	62	71	21.8	6	21	67	77	71	91
Woldesemayat and Ghajar (2007)	63	73	21.6	6	8	64	80	17	90
Yashar et al. (2001)	46	73	22.2	**38**	68	45	69	**87**	90

Performance of Correlations for $0 < \alpha \leq 0.25$

For -5^o void fraction data, all correlations perform unsatisfactorily as the highest prediction of void fraction data in this region was given by Gomez et al. (2000), Smith (1969) and Yashar et al. (2001) with only 44% accuracy in ±10% error bands as shown in Table 4.12, column 4. All other correlations predict 6% or less of data points except Bhagwat and Ghajar (2013) which predicted 22% and Sun et al. (1981) which predicted 11% of data. Similar poor performance was observed in -10^o and -20^o (Tables 4.13 and 4.14, column 4). Gomez et al. (2000) predicted with highest accuracy of 58% of the void fraction data in this region for -10^o and Yashar et al. (2001) having highest accuracy of 38% for -20^o. For the downward inclined pipe orientation and a total of 53 data points in this region, none of the correlations performed satisfactorily as Gomez et al. (2000) had the highest accuracy of only 43% of data within ±10% error bands.

Performance of Correlations for $0.25 < \alpha \leq 0.75$

Accuracy of correlations improved in this region as observed in upward inclined pipe orientation as Guzhov et al. (1967) predicted 88% of data within ±10% error bands for -5^o (Table 4.12, column 6), followed by Smith (1969) which predicted 87% in this region. They both gave the highest accuracy in -10^o and -20^o by predicting 79% and 77% for -10^o, and 67% each for -20^o pipe orientation. Bonnecaze et al. (1971), Nicklin et al. (1962) and Sun et al. (1981) all predicted 67% of data within ±10% error bands for -20^o. Lockhart and Martinelli (1949) and Cioncolini and Thome (2012) predicted only 32% of data in this region in -20^o. For a total of 219 void fraction data points in this region, Guzhov et al. (1967) performed best with accuracy of 78% followed closely by Smith (1969) which predicted 77% of data as shown in Table 4.15, column 6.

Performance of Correlations for $0.75 < \alpha < 1$

Lockhart and Martinelli (1949) predicted 100% of data for -5^o pipe orientation in this region within ±5% error bands. Bonnecaze et al. (1971), Nicklin et al. (1962) and Yashar et al. (2001)

predicted 96% of data in this region. Smith (1969) performed least by predicting none of the data points within the ±5% error bands as shown in Table 4.12, column 8. For -10^{o}, Lockhart and Martinelli (1949) predicted 97% of data within this region followed by Bonnecaze et al. (1971), Nicklin et al. (1962) and Yashar et al. (2001) all predicting 93% of data in this region as shown in Table 4.13, column 8. Accuracy of void fraction correlations decreased in the -20^{o} pipe orientation as shown in Table 4.14, column 8 as the highest accuracy was 76% for Lockhart and Martinelli (1949), Bonnecaze et al. (1971) and Nicklin et al. (1962). 72% of data was predicted by Guzhov et al. (1967) and Yashar et al. (2001) in this void fraction region. Woldesemayat and Ghajar (2007) performed least by predicting only 12% of data within the ±5% error bands. For the total of 78 void fraction data points measured in this region for downward inclined pipe orientation, Lockhart and Martinelli (1949) predicted the data with highest accuracy of 91% within ±5% error bands. Bonnecaze et al. (1971) and Nicklin et al. (1962) predicted 88% of data in this region followed closely by Yashar et al. (2001) which predicted 87% of data in this void fraction region within ±5% error bands. Lowest accuracy of prediction was observed for Smith (1969) having only 9% in this void fraction region.

4.2.4 Best Performing Correlation for Downward Inclined Pipe Orientation

For -5^{o} pipe orientation, Smith (1969) performed best with the lowest percent RMS error of 9.7% followed by Gomez et al. (2000) having RMS error of 11.4%. Guzhov et al. (1967) gave 12% in RMS error and Cioncolini and Thome (2012) had highest RMS error of 51.3% as shown in Table 4.12, column 3.

For -10^{o} pipe orientation, Gomez et al. (2000) performed best with 12.2% in RMS error followed by Smith (1969) having 12.5% in RMS error. Bhagwat and Ghajar (2013) came third with RMS

error of 15.4% while Cioncolini and Thome (2012) gave highest RMS error of 49.3% as shown in Table 4.13, column 3.

Bhagwat and Ghajar (2013) performed best in -20^{o} pipe orientation with lowest RMS error of 16% followed by Gomez et al. (2000) having 19.4% in RMS error. Once again, Cioncolini and Thome had highest RMS error of 39.8% as shown in Table 4.14, column 3.

Based on lowest value of RMS percent error calculated for each correlation as shown in Table 4.15, the best performing correlation in predicting void fraction data in downward inclined pipe orientation is the Gomez et al. (2000) with 14.7% RMS error. This was followed by Smith (1969) with RMS error of 14.8% and then Guzhov et al. (1967) having 16.6% RMS error while the least performing correlation was found to be Cioncolini and Thome (2012) with RMS error of 47%. Detailed analysis of measured void fraction for near horizontal pipe orientation ($+5^{o}$, $+10^{o}$, $+20^{o}$, -5^{o}, -10^{o} and -20^{o}) is given in Table 4.16.

Table 4.16 Void fraction correlation comparison for 700 data points for all six pipe orientations (near horizontal)

All Orientations									
700 Data Points			RMS Error	$0 < \alpha \leq 0.25$ (112 points)		$0.25 < \alpha \leq 0.75$ (442 points)		$0.75 < \alpha < 1$ (146 points)	
Correlation	±10% Error	±20% Error	%	±10% Error	±20% Error	±10% Error	±20% Error	±5% Error	±7.5% Error
Bhagwat and Ghajar (2013)	64	88	**14.2**	31	62	59	90	62	90
Bonnecaze et al. (1971)	73	86	15.1	12	50	**80**	91	**92**	97
Cioncolini and Thome (2012)	54	65	62.6	0	0	54	69	43	92
Gomez et al. (2000)	55	93	**12.9**	**46**	78	43	95	49	75
Guzhov et al. (1967)	**74**	89	**13.4**	23	62	**87**	93	80	94
Lockhart and Martinelli (1949)	40	70	20.2	14	59	29	63	**96**	96
Morooka et al. (1989)	44	74	20.9	1	22	50	80	17	47
Nicklin et al. (1962)	73	86	15.1	12	51	**80**	91	**92**	97
Rouhani and Axelsson (1970)	58	81	18.8	1	39	59	85	56	79
Smith (1969)	**81**	92	**12.2**	**46**	81	**86**	93	9	71
Sun et al. (1981)	65	77	18.1	6	28	71	85	76	94
Woldesemayat and Ghajar (2007)	64	77	24.9	5	12	66	86	17	93
Yashar et al. (2001)	47	74	24.8	38	62	40	72	**94**	95

4.2.5 Best Performing Correlation for Near Horizontal Pipe Orientation (six inclination angles) in Present Study

After conducting comprehensive analyses of selected void fraction correlations, the top performing correlations for 112 data points of void fraction in region of $0 < \alpha \leq 0.25$ was observed to be Gomez et al. (2000) and Smith (1969) which predicted 46% within ±10% error bands as shown in Table 4.16, column 4. This was followed by Yashar et al. (2001) which predicted 38% of data points in the ±10% error bands.

442 void fraction data points were measured in the $0.25 < \alpha \leq 0.75$ region and the correlation with most accurate prediction was found to be Guzhov et al. (1967) which predicted 87% of data points within ±10% error bands followed by Smith (1969) with 86% accuracy in predicting the 442 data points. Bonnecaze et al. (1971) and Nicklin et al. (1962) also performed satisfactorily by predicting 80% of data in this region as shown in Table 4.16, column 6.

146 experimental data points were measured in the region of $0.75 < \alpha < 1$, Lockhart and Martinelli (1949) had the highest accuracy by predicting 96% of void fraction data within ±5% error bands. This was followed by Yashar et al. (2001) which predicted 94% of data within ±5% error bands. Bonnecaze et al. (1971) and Nicklin et al. (1962) also performed satisfactorily by predicting 92% of data in this region. Smith (1969) performed least by predicting only 9% of data within this error band as shown in Table 4.16, column 8.

In sum, the best performing correlation in near horizontal pipe orientations based on percent RMS error in present study is Smith (1969) with 12.2% RMS error as shown in Table 4.16, column 3. This was followed by Gomez et al. (2000) with RMS error of 12.9% and then Guzhov et al. (1967) with RMS error of 13.4%. High RMS error was observed for Yashar et al. (2001) having 24.8% and Woldesemayat and Ghajar (2007) having 24.9%. The least performing correlation for near horizontal orientations was observed to be Cioncolini and Thome (2012) with RMS error of

62.6%. The poor performance of Cioncolini and Thome (2012) confirms that the correlation was developed exclusively for annular flow with $\alpha > 0.7$. For measured void fraction data above this α value, the correlation predicted 92% of data within ±10% error bands for near horizontal pipe orientation.

4.3 Effect of Pipe Orientation on Void Fraction

To determine the effect of pipe orientation on void fraction, specific flow rates combination which cover all flow patterns were selected for void fraction measurement and repeated for each pipe orientation. At low flow rates of liquid and gas phase, void fraction in the upward inclined pipe orientation was observed to decrease with inclination angle while in the downward inclined pipe orientation, void fraction was observed to increase with inclination angle. However at high flow rates combination of liquid and gas phase, void fraction was independent of pipe orientation as there were no unique trends observed in either upward or downward inclined orientation. Variation of void fraction with pipe orientation at low flow rate combination of liquid and gas phase is shown in Figure 4.31.

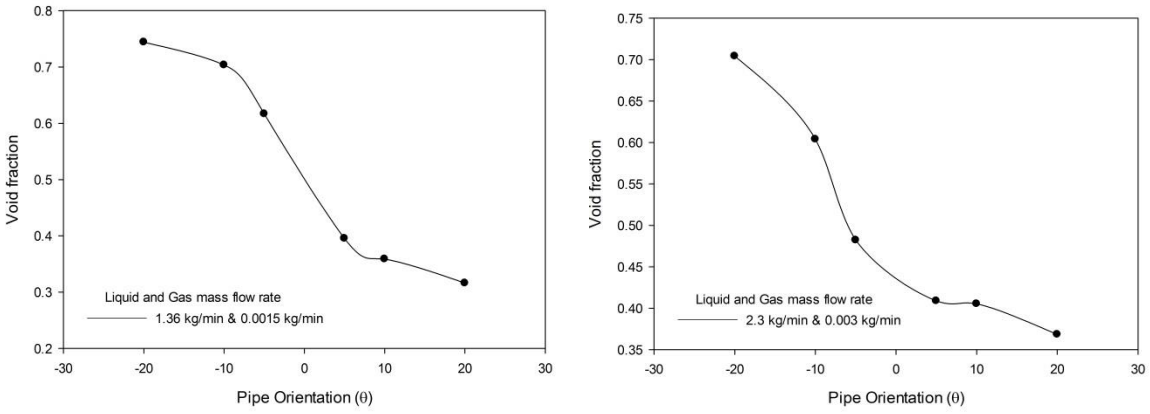

Figure 4.31 Effect of pipe orientation on void fraction (low mass flow rate combination)

Effect of pipe orientation can be observed for the lowest flow combination selected for void fraction measurement in present study (1.36 kg/min & 0.0015 kg/min of liquid and gas phase).

Void fraction increases as pipe orientation shifts in the negative direction and decreases as pipe orientation shifts in positive direction. Effect of pipe orientation on void fraction was observed to be significant in the negative pipe orientation while only a slight constant decrease was observed in the positive orientation. Kokal and Stanislav (1989b) conducted experimental two phase flow studies in inclined pipe for -9^o to +9^o and reported that higher liquid holdup was observed in uphill flow due to effect of gravity and the reverse was observed in downhill flow. Slight effect of pipe orientation was observed in liquid holdup which they attributed to bubble rise velocity which only changes slightly with inclination angle. A similar trend in upward inclined orientation was observed by Wongwises and Pipathattakul (2006). Beggs and Brill (1973) also reported that as inclination angle shifted downwards from horizontal, gravitational force reduced liquid phase velocity and increased slippage and liquid holdup, and as angle increased further the liquid fills the entire pipe cross section thereby reducing slippage and liquid holdup. They also observed that the degree of liquid holdup changes with inclination angle was different for different flow rates. Effect of pipe orientation on liquid holdup developed by Breggs and Brill (1973) is shown in Figure 4.32. λ in Figure 4.32 represent input liquid content.

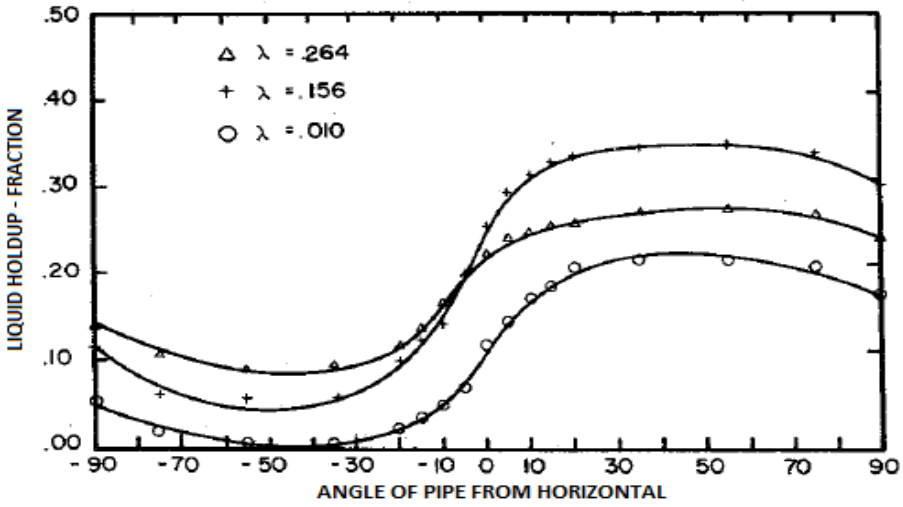

Figure 4.32 Liquid holdup vs pipe orientation by Beggs & Brill (1973)

By definition, $\varepsilon = 1 - \alpha$, where ε is liquid holdup and α is void fraction. This indicates that the void fraction vs pipe orientation plot would be an inverted plot of liquid holdup vs angles shown in Figure 4.32. The effect of pipe orientation on void fraction at high flow rate combinations is given as Figure 4.33.

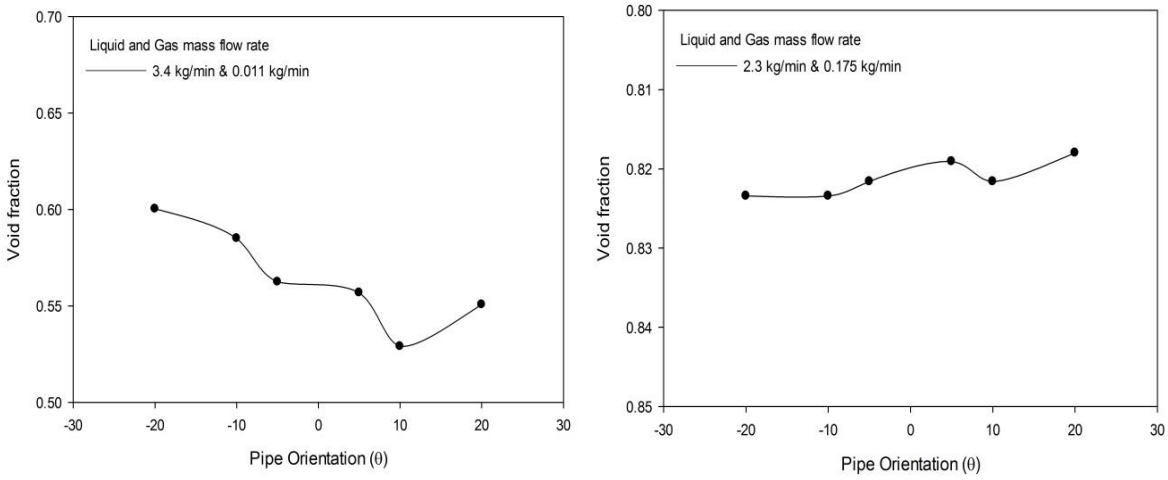

Figure 4.33 Effect of pipe orientation on void fraction (high flow rate combination)

By comparing Figures 4.31 and 4.33, the difference in void fraction for each orientation was eliminated as void fraction vs pipe orientation was observed to flatten out as gas phase flow rate increased. Hence, due to mixing and presence of high frequency disturbance waves in two phase flow, void fraction is independent of pipe orientation for high flow rate combinations. Similar observation was made by Perez (2008) who reported that slight increase in liquid holdup (decrease in void fraction) was detected for low superficial velocities of liquid phase for upward inclined pipe which increased with increase in pipe orientation.

4.4 Flow Reversal

Flow reversal also known as backward flow is a unique phenomenon often encountered in co-current upward two phase flow where the liquid phase is observed to flow backwards due to effects of gravity. Investigators have conducted research over decades on flooding in counter-current two phase flow in vertical pipes where the liquid phase is injected either from the top or mid pipe level while gas phase is injected from the bottom of the pipe. Consequently, the liquid phase flows downwards due to gravity as the gas phase flows upwards. The liquid phase flow rate is kept constant while gas flow rate is gradually increased until the gas phase inertial force is sufficient to overcome the gravitational pull on the liquid phase. Thus, the gas phase lifts the liquid phase and both phases move in the upward direction. The transition point from counter-current two phase flow to co-current two phase flow is identified as the onset of flooding. Flooding is observed at very high gas flow rates, therefore flow is always in the annular region. Based on the flow pattern at which flooding occurs (annular flow), mathematical models have been developed to predict flooding by accounting for interfacial shear, friction factor, liquid film thickness and other two phase parameters required for accurate modeling. Thus, based on the flow configuration used by these researchers (counter-current flow), flooding is the inverse of flow reversal and the models developed to predict flooding suitably predict flow reversal in vertical upward annular two phase flow.

Taitel et al. (1982) described flow reversal in vertical upward pipes as inverse of flooding which is observed as gas phase is changed from high flow rate to low flow rates which leads to partial down flow of liquid phase, hence the term downward counter-current two phase flow. Stability analysis based on dimensionless interfacial shear and relative film thickness were used to develop a model to further analyze the relation developed by Bharathan et al. (1979) to predict flooding and flow reversal in vertical upward pipes given as Equation (4.7).

$$\tau'_i = [A + B(\delta')^n] \frac{(U_{sg}')^2}{2(1-2\delta')^4} \quad (4.7)$$

And as developed by Bharathan et al. (1979),

$$U'_{sg} = \left\{ \frac{2(1-2\delta')^4}{A+B\delta'^n} \left[\frac{U'_{sl}}{2\delta'^2} + \frac{2}{3}\delta' \right] \right\}^{0.5} \quad (4.8)$$

Where A, B and n are constants and are pipe diameter dependent. For 2.5 cm pipe, A = 0.005, B = 280 and n = 2.13. For 5.1 cm pipe, A = 0.005, B = 406 and n = 2.04.

McQuillan et al. (1985) conducted experimental studies on flooding in vertical two phase flow and were able to observe flooding by altering various flow parameters like system pressure, gas flow rate and amplitude of injected artificial wave to stimulate flooding. A model was developed to predict flooding based on dimensionless superficial velocity given as Equation (4.9).

$$U^*_{sg} = U_{sg}\rho_g^{0.5}\left[gD\left(\rho_l - \rho_g\right)\right]^{-0.5} \quad (4.9)$$

Zabaras and Dukler (1988) conducted extensive studies on the mean film thickness at transition point from backward flow to flooding which they described that waves become unstable and grow explosively to force the liquid phase upwards, hence flooding is the onset of instability. Wall shear stress was measured by electro chemical probes and interfacial friction factor was calculated and analyzed with mean film thickness to plot the flooding curve and locate the transition points.

Various correlations exist in literature to predict flooding as discussed above and the most popular correlation for predicting flooding and flow reversal in vertical pipes was developed by Hewitt and Wallis (1963) and given as Equation (4.10).

$$\left(\left(\frac{U_{sg}\rho_g^{0.5}}{[gD(\rho_l-\rho_g)]^{0.5}} \right)^{0.5} + \left(\frac{U_{sl}\rho_l^{0.5}}{[gD(\rho_l-\rho_g)]^{0.5}} \right)^{0.5} \right)^{0.5} = Constant \quad (4.10)$$

The nature of flow reversal in present study can be described as gas phase interfacial acceleration of liquid phase due to high velocity and low density. The high gas phase velocity forces a portion of the low velocity liquid phase up the inclined pipe, but this portion of liquid phase falls back under gravity due to high density. And in a continuous process the liquid phase rises and falls at constant flow rates of liquid and gas phase. This sequential process describes the term flow reversal in co-current two phase flow in upward inclined pipes. In present study, flow reversal was observed in non-separated flow regimes (slug, slug/wavy and wavy flows). Models to calculate interfacial shear for these flow patterns do not exist due to very complex geometry resulting from discontinuities in the liquid and gas phase in the two phase flow. Simmons and Hanratty (2001) also observed reversed flow for liquid slug during their two phase flow experimental studies in small angle upflow. Since there exist no model to analyze these flow patterns, alternate mode of analysis was adopted in present study. The alternate mode of analysis is divided into two methods. The first method being Bernoulli's equation using actual liquid and gas phase velocities for analysis and the second method being dimensionless numbers using superficial velocities to analyze and predict flow reversal in inclined two phase flow system.

Method 1, Bernoulli's equation

After careful observation of the flow reversal points during experimentation, it was noted that flow reversal has very small dependence on system pressure, i.e., pressure of the liquid and gas phase for specified flow rates in a smooth pipe. For example, at the lowest liquid and gas flow rates of 1.36 kg/min and 0.0015 kg/min having the lowest system pressure of 103.5 kPa, flow reversal was not observed for $+5^{o}$. However, by increasing the gas flow rate to 0.003 kg/min and keeping the liquid flow rate constant, system pressure increased to 104.7 kPa and flow reversal was observed. The system pressure stays relatively constant over the flow reversal points for each pipe orientation and no notable trend was observed. Instinctively, it is expected that flow reversal occurs below a certain system pressure for each pipe orientation in a smooth pipe. However, the

results of measured system pressure were counter intuitive because flow reversal was observed within a certain range of system pressure. This range of system pressure was observed to be different for each pipe orientation. Thus, leaving room to explore how the individual phase actual velocity changes in the flow reversal region by using the Bernoulli equation.

Bernoulli's equation for single phase fluid is given by

$\frac{1}{2}\rho U^2 + \rho g z + P = Constant$, where $\frac{1}{2}\rho v^2$ is termed the dynamic pressure of the system and U is actual velocity of individual phase.

For two phase flow,

$$P_{dy(l)} = \frac{1}{2}\rho_l (U_{sl}(1-\alpha))^2 \; and \; P_{dy(g)} = \frac{1}{2}\rho_g (U_{sg}\alpha)^2$$

$$P_{dy(sys)} = \frac{1}{2}\left[\rho_l (U_{sl}(1-\alpha))^2 + \rho_g (U_{sg}\alpha)^2\right]$$

U_{sl} and U_{sg} are superficial velocities of liquid and gas phase, ρ_l and ρ_g are densities of liquid and gas phase.

The actual velocities of the liquid and gas phases were used for calculating the system dynamic pressure because no trend in dynamic pressure plot was noticed by using superficial velocities in calculations. This was due to the constant values of liquid phase flow rates over which flow reversal was observed. In the $+5^o$ pipe orientation, flow reversal was observed over a certain range of gas flow rates for a fixed liquid flow rate (1.36 kg/min) and the resulting dynamic pressure vs gas flow rate was plotted and shown as Figure 4.34.

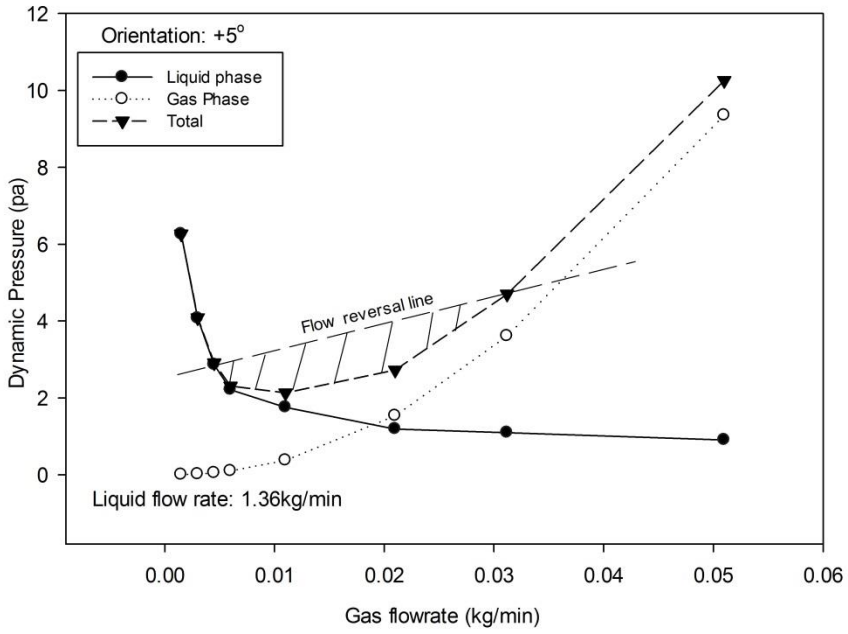

Figure 4.34 Dynamic pressure plot showing flow reversal points for +5^{o}

Dynamic pressure for the liquid phase was observed to decay exponentially with gas flow rate because increase in gas flow rate at constant liquid flow rate increases void fraction and the dynamic pressure of the liquid phase is a function of 1 – α, hence it decays. Likewise, the gas phase dynamic pressure grows exponentially with increase in void fraction since void fraction increases with increase in gas flow rate at constant liquid flow rate as shown in Figure 4.34. Flow reversal was observed to occupy the shaded portion of the plot for +5^{o} pipe orientation. Increase in pipe inclination increased the area occupied by flow reversal on the dynamic pressure plot as gravity becomes more significant and liquid phase falls further downwards in the pipe under gravity. The dynamic pressure plot for +10^{o} is shown as Figures 4.35.

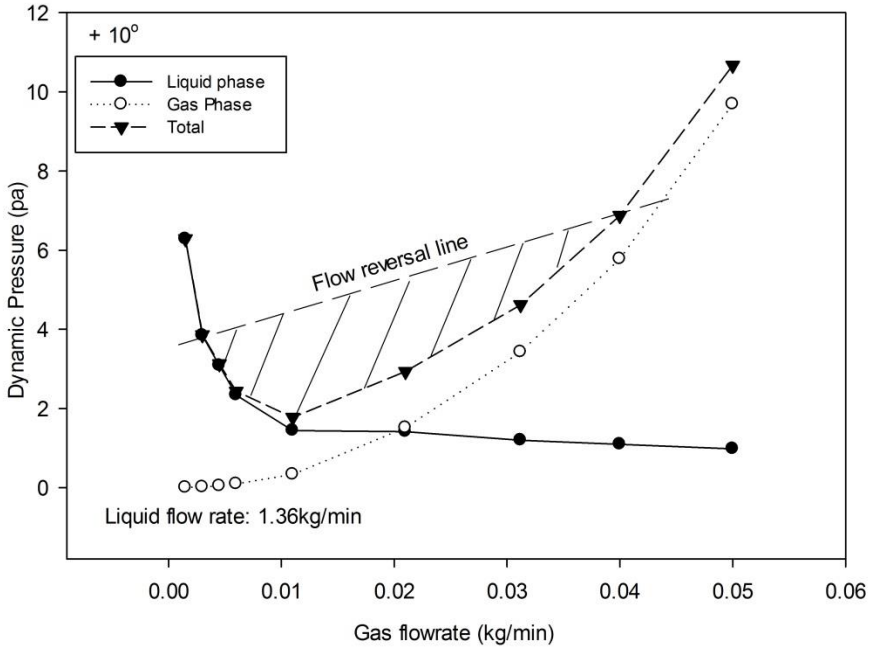

Figure 4.35 Dynamic pressure plot showing flow reversal points for +10^{o}

By comparing Figures 4.34 and 4.35, the effect of pipe orientation can easily by observed as the flow reversal curve goes deeper and wider in +10^{o}. As a result, flow reversal points occupy a larger area on the dynamic pressure plot for +10^{o} than +5^{o} pipe orientation. It should be noted that flow reversal was observed at constant liquid flow rate of 1.36 kg/min in +5^{o} and +10^{o} as shown in Figures 4.34 and 4.35. More back flow points were observed in +20^{o} pipe orientation and the representative dynamic pressure vs gas flow rate plot for +20^{o} is shown as Figure 4.36.

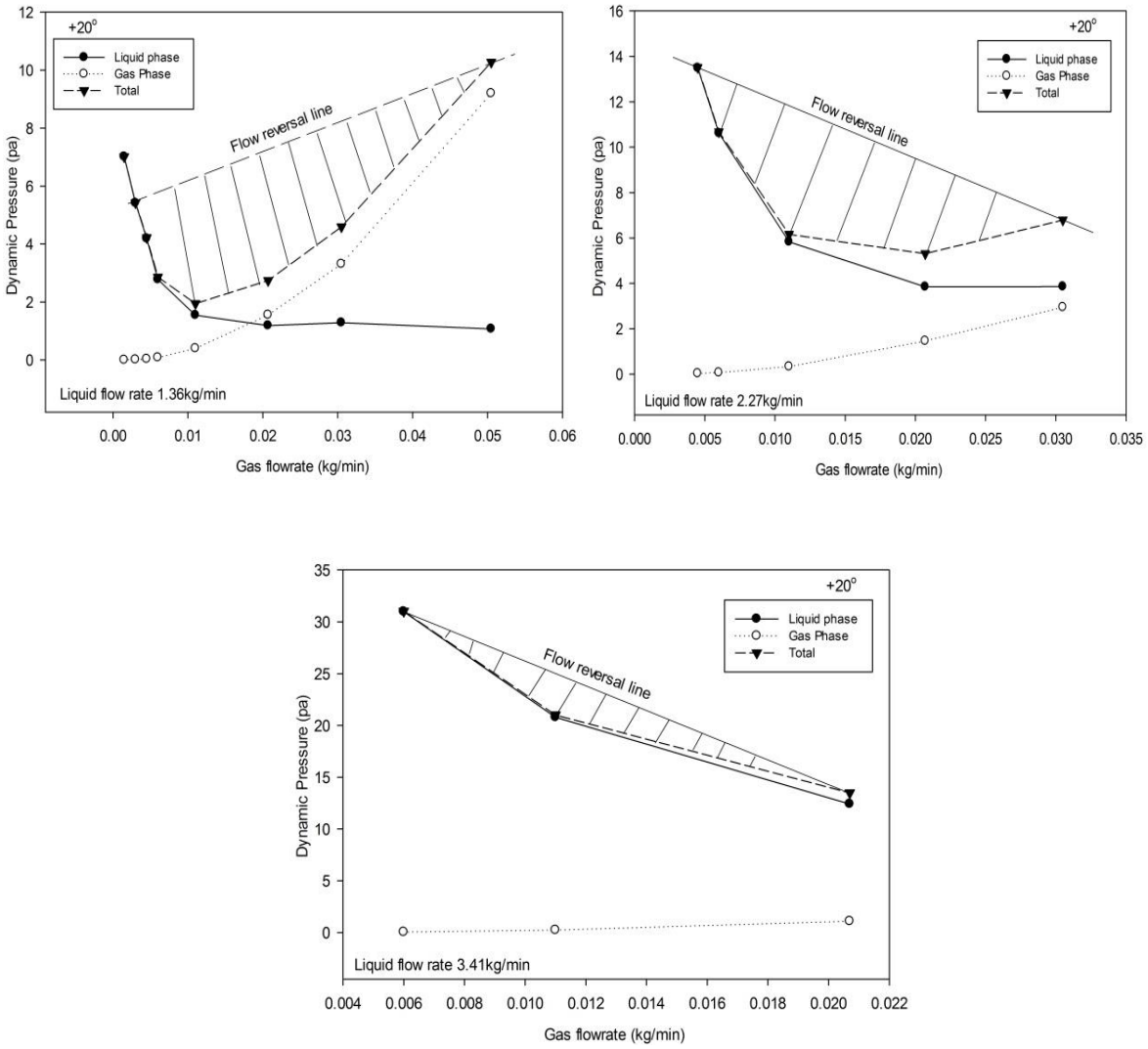

Figure 4.36 Dynamic pressure plot showing flow reversal points for +20^{o}

As pipe orientation shifted to +20^{o}, the dynamic pressure plot for constant liquid flow rate of 1.36 kg/min showed further increase in area from +10^{o} as shown in Figure 4.36. However, flow reversal was also observed at higher liquid phase flow rates of 2.27 kg/min and 3.41 kg/min in +20^{o} which was not the case for +5^{o} and +10^{o}. It was noted that at constant liquid phase flow rate, flow reversal curve goes deeper and increases in area over the range of gas phase flow rates which it is observed. Whereas for +20^{o} pipe orientation, flow reversal curve at higher liquid phase flow rates of 2.27 kg/min and 3.41 kg/min was observed to decrease in area and flatten out over

the range of gas flow rates. Flow reversal was further investigated for +45^{o} and this phenomenon was observed at higher void fraction, liquid phase flow rates and predominantly over the wavy flow pattern. Dynamic pressure plot for flow reversal points in +45^{o} are shown in Figure 4.37.

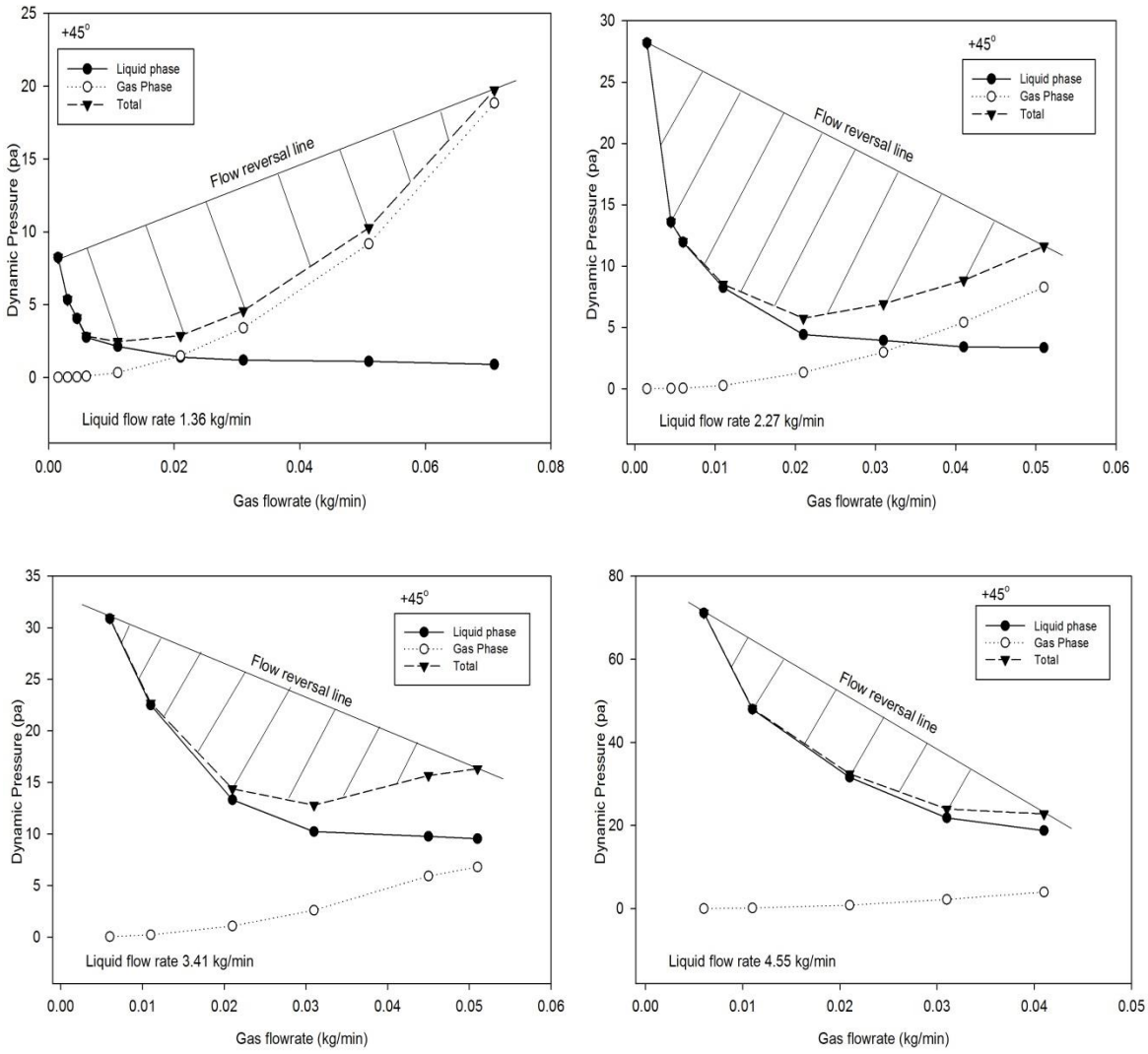

Figure 4.37 Dynamic pressure plot showing flow reversal points for +45^{o}

From Figure 4.37, flow reversal plot for +45^{o} at constant liquid flow rate of 1.36 kg/min follow similar trend as that shown for +5^{o}, +10^{o} and +20^{o}. At higher liquid flow rates of 2.27 kg/min, 3.41 kg/min and 4.55 kg/min observed for +20^{o} and +45^{o}, similar trends were observed as shown in Figures 4.36 and 4.37. It should be noted that as pipe orientation increases from +5^{o} to +45^{o},

the dynamic pressure below which flow reversal is observed for the specified gas flow rate increases. Since dynamic pressure is a function of gas flow rate and pipe orientation increases the required flow rate to overcome flow reversal, increase in pipe orientation increases the range of void fraction over which flow reversal occurs. Thus, increase in pipe orientation shifts flow reversal points from slug flow to wavy flow in present study. And it is expected that as pipe orientation increases beyond $+45^{o}$, flow reversal will progress into the annular flow region as reported by investigators who conducted research on flooding and flow reversal for counter current two phase flow in vertical pipes. Void fraction measured for flow reversal points in each pipe orientation was plotted against the gas flow rate and is shown as Figure 4.38.

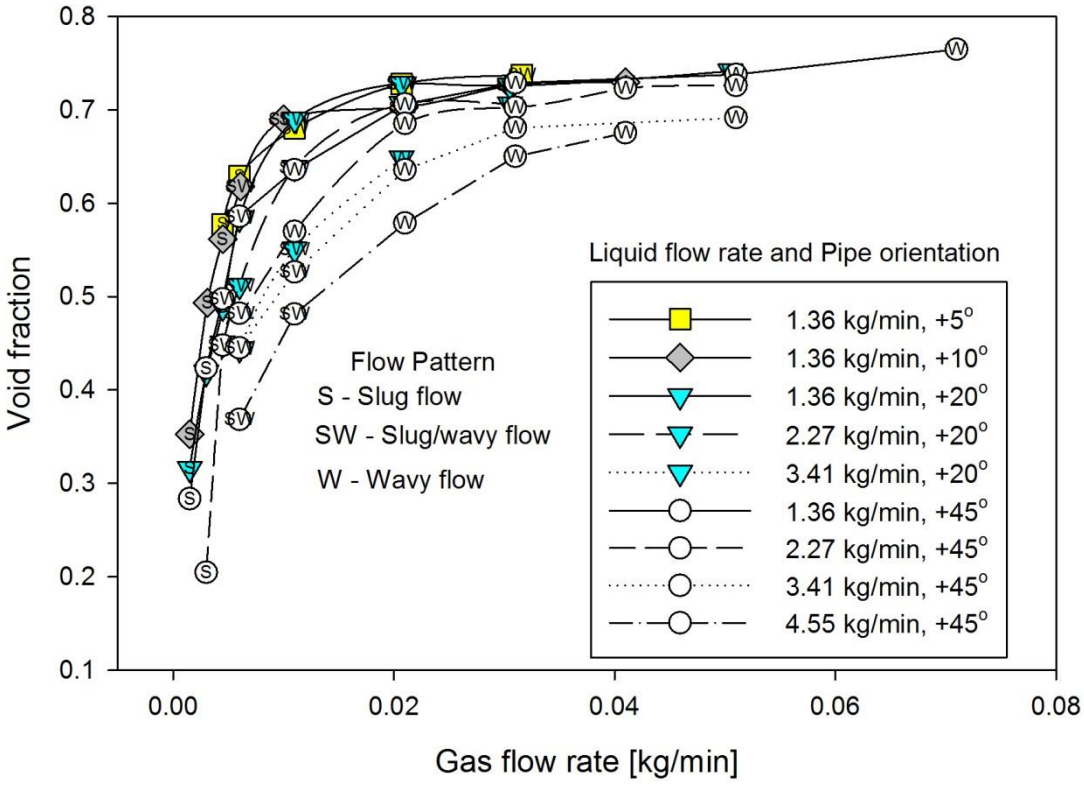

Figure 4.38 Void fraction vs gas flow rate at different pipe orientations in flow reversal region

A specific shape is assigned to each pipe orientation as shown in Figure 4.38, square represents $+5^o$, diamond represents $+10^o$, inverted triangle represents $+20^o$ and circle represents $+45^o$. The solid lines represent constant liquid flow rate of 1.36 kg/min, broken lines represent 2.27 kg/min, dotted lines represent 3.41 kg/min and center line represents 4.55 kg/min. Figure 4.38 shows the void fraction at given gas phase flow rate for each pipe orientation and the corresponding flow pattern observed. It can be observed that increase in pipe orientation increases the range of void fraction over which flow reversal occurs. More flow reversal points were observed with increase in pipe inclination due to increased effects of gravity on the liquid phase and higher gas flow rate is required to overcome it. The range of void fraction and number of flow reversal points analyzed for each pipe orientation is shown in Table 4.17.

Table 4.17 Range of measured void fraction for flow reversal region

Pipe orientation	Liquid flow rate (kg/min)	Number of data points	Range of void fraction
$+5^o$	1.36	5	0.58-0.74
$+10^o$	1.36	8	0.35-0.73
$+20^o$	1.36	8	0.32-0.74
	2.27	5	0.45-0.71
	3.41	3	0.44-0.65
$+45^o$	1.36	9	0.28-0.77
	2.27	8	0.21-0.73
	3.41	6	0.39-0.69
	4.55	5	0.37-0.68

A total of 57 void fraction data points were measured in the flow reversal region. 5 points for $+5^o$, 8 points for $+10^o$, 16 points for $+20^o$ and 28 points for $+45^o$ as shown in Table 4.17. The range of void fraction (difference between high and low limits) at constant liquid flow rate of 1.36 kg/min increases as pipe orientation shifts from $+5^o$ to $+45^o$. Similar observations were made for higher liquid flow rates of 2.27 kg/min and 3.41 kg/min. Therefore, increase in pipe orientation increases

both the number of flow reversal points and range of void fraction at constant liquid flow rate as shown in Table 4.17.

Method 2, Dimensionless numbers

Three dimensionless numbers were used for analyzing flow reversal and they are Froude number, Reynolds number and Weber number.

Froude number gives the relationship between inertial force and gravitational force in a flowing fluid system. Froude number based on superficial gas velocity and superficial liquid velocity can both be calculated in two phase flow depending on the standpoint chosen by investigator for analysis. Since flow reversal in present study was observed at constant liquid phase flow rate while increasing the gas flow rate, superficial gas velocity was used for calculating Froude number. Thus, by interpretation Froude number in present study gives the critical relationship between the gas phase inertial force and the gravitational force acting on the liquid at different pipe orientations. Froude number for an inclined system is given as Equation (4.11)

$$Fr_{sg} = \sqrt{\frac{\rho_g}{\rho_l - \rho_g}} \frac{U_{sg}}{(gDsin\theta)^{0.5}} \tag{4.11}$$

It should be noted that the Hewitt and Wallis (1963) correlation and McQuillan et al. (1985) relation shown in Equations (4.9) and (4.10) for predicting flooding and flow reversal in vertical pipe are in the form of Froude number, therefore *sin* θ was incorporated in Equation (4.11) to account for pipe inclination. The plots showing the effect of gas flow rate on Froude number is shown as Figure 4.39.

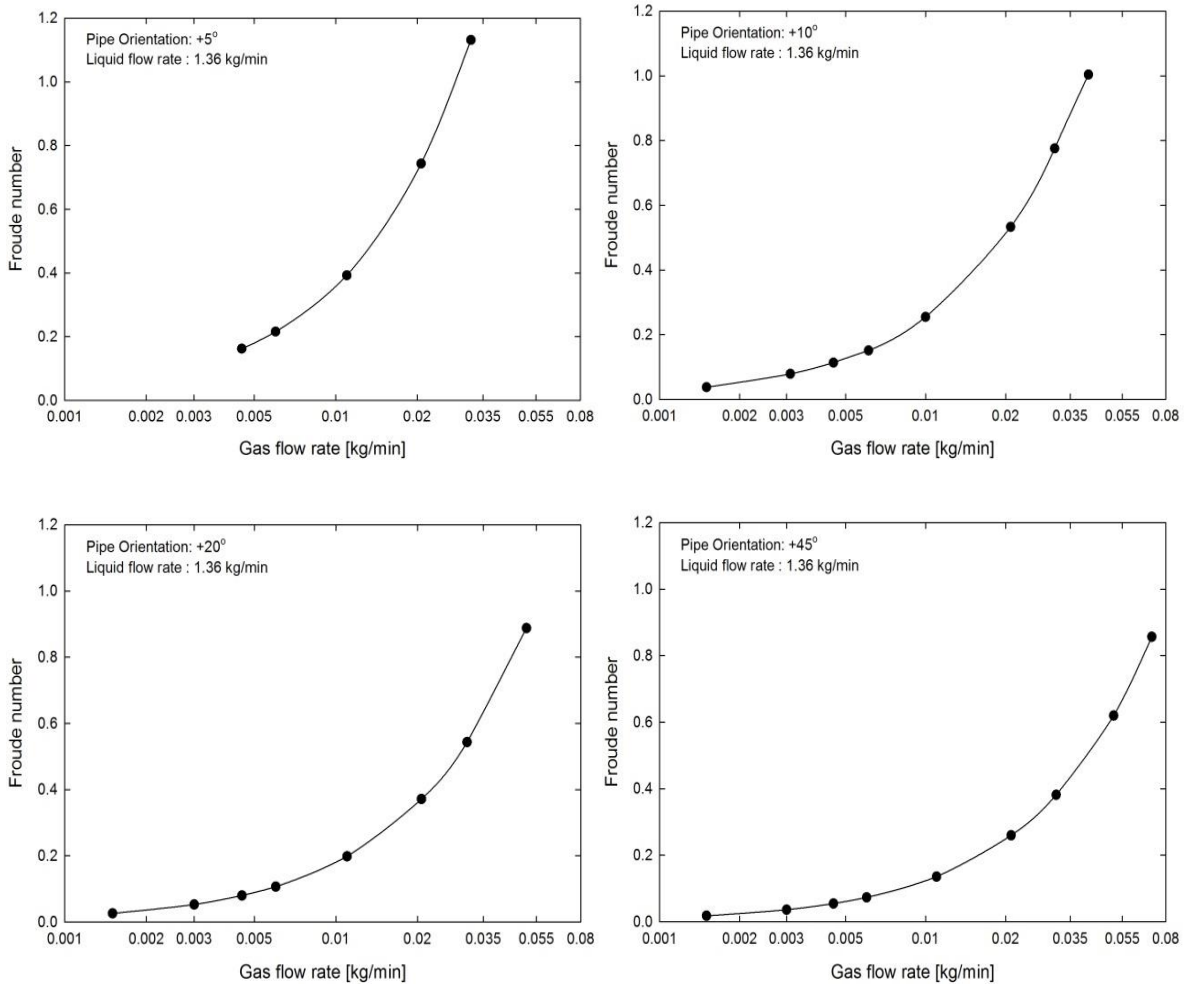

Figure 4.39 Froude number vs gas flow rate in flow reversal region

The plots in Figure 4.39 show an exponential growth in Froude number with increase in gas flow rate. The steeper curve in $+5^{o}$ was observed to stretch out in length and decrease in values as pipe orientation changed to $+10^{o}$ all the way to $+45^{o}$. This indicates that the dominance of gravitational force over inertial force at constant liquid flow rate increases with increase in pipe orientation. Froude number was observed to be $\leq 1$for the flow reversal region at constant liquid flow rate of 1.36 kg/min over pipe orientations from $+5^{o}$ through $+45^{o}$. This shows that gravitational force is always $\geq$ inertial force in order for flow reversal to occur. At higher liquid flow rates of 2.27 kg/min and 3.41 kg/min in $+20^{o}$, and 2.27 kg/min, 3.41 kg/min and 4.55 kg/min in $+45^{o}$, the Froude number was observed to be < 1 in both pipe orientations. This also confirms that the

gravitational force acting on the liquid phase increases with pipe orientation even at higher liquid phase flow rates. Details of flow reversal for each pipe orientation based on maximum Froude number at constant liquid flow rates is given as Table 4.18.

Table 4.18 Maximum Froude number at constant liquid flow rates for each pipe orientation

Pipe orientation	Liquid flow rate (kg/min)	Gas flow rate (kg/min)	Froude number (Max)
$+5^o$	1.36	0.03	1.13
$+10^o$	1.36	0.04	1.01
$+20^o$	1.36	0.05	0.89
	2.27	0.03	0.53
	3.41	0.02	0.35
$+45^o$	1.36	0.07	0.86
	2.27	0.05	0.59
	3.41	0.05	0.56
	4.55	0.04	0.45

From Table 4.18, simultaneous effect of pipe orientation and liquid flow rate can be seen on the maximum Froude number below which flow reversal occurs. For example, the maximum Froude number constantly decreases from 1.13 to 0.86 at liquid flow rate of 1.36 kg/min as pipe orientation shifted from $+5^o$ to $+45^o$. Similarly, at $+20^o$ and 3.41 kg/min of liquid flow rate, the maximum Froude number is 0.35. Based on earlier discussion that increase in pipe orientation increases gravitational force on the liquid phase and Froude number becomes smaller, it is expected that at $+45^o$ and 3.41 kg/min the maximum Froude number should be less than 0.35 for $+20^o$. However, increase in pipe inclination also increases the required gas flow rate needed to lift the reversing liquid phase. Hence, the maximum Froude number in $+45^o$ is higher than $+20^o$ because of higher gas flow rate of 0.05 kg/min needed to overcome gravitational force as shown in Table 4.18.

Reynolds number gives the relationship between the inertial forces of a flowing fluid with respect to its viscous force. Analysis with Reynolds number basically determines if flow is laminar, turbulent or simply in transition from laminar to turbulent flow. The superficial Reynolds number of the flow reversal region was recorded to come up with another dimensionless parameter to analyze flow reversal over the different pipe orientations in present study. The range of superficial Reynolds number for liquid and gas phase over the flow reversal region for each pipe orientation is given as Table 4.19.

Table 4.19 Range of gas phase superficial Reynolds number for each pipe orientation

Pipe orientation	Liquid flow rate (kg/min)	Re_{sl}	Range of Re_{sg}
$+5^o$	1.36	2600	300 - 2900
$+10^o$	1.36	2400	140 - 4800
$+20^o$	1.36	2400	140 - 4700
	2.27	3700	400 - 2800
	3.41	5700	600 - 1900
$+45^o$	1.36	2300	140 - 6500
	2.27	3900	140 - 4700
	3.41	5900	400 - 4700
	4.55	7800	600 - 3800

The superficial Reynolds number for liquid and gas phase was rounded to the nearest hundred as shown in Table 4.19. It should be noted that the lower limit of superficial gas Reynolds number was rounded to the nearest ten because of the low values observed and also to minimize errors of approximation. Effect of pipe orientation can be seen on liquid phase superficial Reynolds number shown in Table 4.19. At constant liquid flow rate of 1.36 kg/min, superficial liquid Reynolds number was observed to decrease from 2600 to 2300 as pipe orientation shifted from $+5^o$ to $+45^o$ due to increased slippage of liquid phase. Decrease in liquid phase superficial Reynolds number with pipe orientation subsequently increases the necessary superficial gas Reynolds number required to overcome liquid back flow in the pipe. And as pipe orientation

shifted from $+5^{o}$ to $+45^{o}$, the higher limit of superficial gas Reynolds number increased from 2900 to 6500. It should also be noted that at higher constant liquid flow rates of 2.27 kg/min, 3.41 kg/min and 4.55 kg/min, there was a corresponding decrease in superficial gas Reynolds number required to overcome flow reversal. This explains that elimination of flow reversal is not a function of gas phase flow rate alone but liquid and gas phase as they both play an important role to overcome flow reversal. In sum, analysis by superficial Reynolds number of the liquid and gas phase gave the range over which flow reversal was observed and the effect of pipe orientation on liquid and gas superficial Reynolds number as shown in Table 4.19.

Weber number gives the relationship between the inertial force acting on a fluid and the surface tension of the fluid. Weber number is generally used in multiphase flow to analyze fluid conditions having curved surfaces and often used to predict transition to bubbly flow. By definition, surface tension of a fluid is the contractive tendency of that fluid which enables it to resist external force. Thus, analysis using Weber number in present study was believed to give more information on the physics of flow reversal. The ratio of inertial force imposed by the gas phase to liquid phase surface resistance over the flow reversal region for the each pipe orientation was calculated and interpreted for increasing gas flow rate. Weber number relation and the representative plot for Weber number vs gas flow rate is given as Equation (4.12) and Figure 4.40.

$$We = \rho_g U_{sg}^2 D/\sigma \qquad (4.12)$$

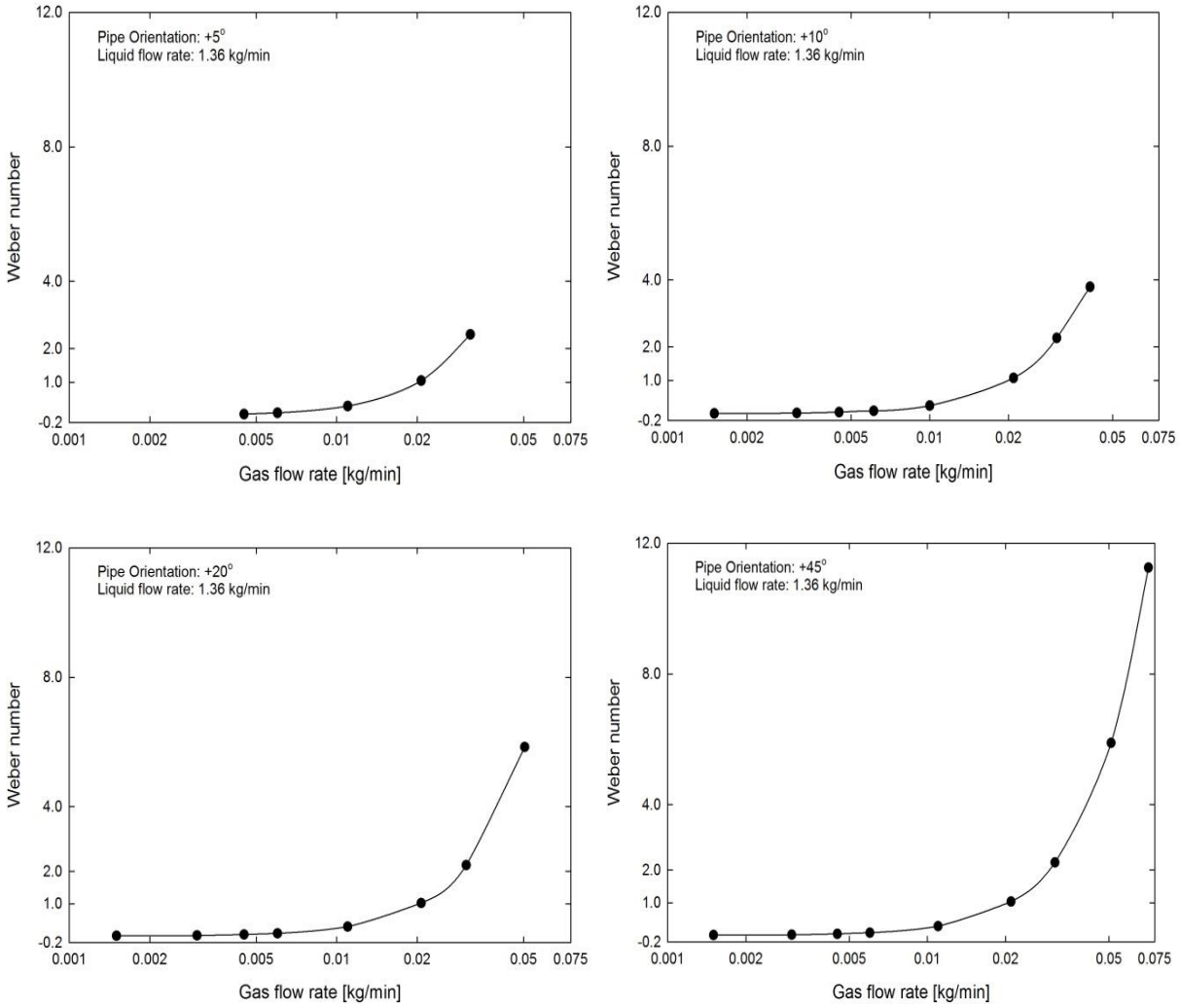

Figure 4.40 Weber number vs gas flow rate in flow reversal region

As shown in Figure 4.40, Weber number can be observed to increase exponentially with increase in gas flow rate. At the onset of flow reversal for each pipe orientation at constant liquid flow rate of 1.36 kg/min, surface tension of liquid phase was observed to dominate the inertial force of the gas phase and Weber number was observed to be << 1. Weber number stays relatively constant in the low gas flow rate region and grows exponentially at high gas flow rates. Hence, the inertial force of gas phase dominates the surface tension as flow reversal is eliminated and Weber number is > 1. Weber number curve shown in Figure 4.40 can be observed to stretch over the *x*-axis of the plots (gas flow rate) as pipe orientation shifted from $+5^{o}$ all the way to $+45^{o}$. This specifies that

increase in pipe orientation increases the inertial force needed to overcome the surface tension in the flow reversal region. At higher liquid flow rates of 2.27 kg/min, 3.41 kg/min and 4.55 kg/min, similar curves were observed for Weber number vs gas flow rate. The plot of Weber number vs gas flow rate shown as Figure 4.40 follows the same trend as Froude number vs gas flow rate plot shown as Figure 4.39, but subtle distinctions still exist between the two plots. A critical look at both plots will reveal that the maximum Froude number for each pipe orientation at constant liquid flow rate decreases with increase in pipe orientation while the maximum Weber number for each pipe orientation increases with increase in pipe orientation in the flow reversal region. Details of the maximum Weber number below which flow reversal occurs for each pipe orientation is shown as Table 4.20.

Table 4.20 Maximum Weber number at constant liquid flow rate for each pipe orientation

Pipe orientation	Liquid flow rate (kg/min)	Gas flow rate (kg/min)	Weber number (Max)
$+5^o$	1.36	0.03	2.42
$+10^o$	1.36	0.04	3.79
$+20^o$	1.36	0.05	5.85
	2.27	0.03	2.06
	3.41	0.02	0.9
$+45^o$	1.36	0.07	11.25
	2.27	0.05	5.48
	3.41	0.05	4.96
	4.55	0.04	3.06

As shown in Table 4.20, it can be observed that at constant liquid flow rate, the maximum Weber number above which flow reversal ceases to occur increases with pipe orientation.

In sum, analysis using Bernoulli's equation and dimensionless numbers gave thorough investigation in present study and can be used to effectively predict flow reversal in smooth inclined pipes. It should be noted that observation of flow reversal points were based on visual

identification and are somewhat subjective but the comprehensive analysis discussed above provides consistency in observation. Improved flow reversal identification should be carried out by measuring pressure drop in the inclined two phase system where negative pressure drop signifies back flow. Also, present study on flow reversal is pipe surface (smooth) and diameter dependent, hence analysis can be integrated over rough and larger diameter pipes to develop a correlation to predict flow reversal.

CHAPTER V

CONCLUSIONS AND RECOMMENDATIONS

A comprehensive study on flow patterns and void fraction was conducted in near horizontal pipe orientation. The work done in present study is divided into three areas: flow patterns and flow maps, void fraction and flow reversal. Studies were conducted in six pipe orientations: $+5^{o}$, $+10^{o}$, $+20^{o}$, -5^{o}, -10^{o} and -20^{o}. Experiments were conducted using air-water as working fluid in a 12.7 mm diameter pipe and 700 void fraction data points were measured. Analysis in present study was divided into two: upward inclined pipe orientation and downward inclined pipe orientation. Similar major flow patterns were observed in the three upward inclined pipe orientation and they are slug flow, bubbly flow, wavy flow and annular flow. Flow pattern maps plotted for the three pipe orientations in the upward direction show similar trends in transition boundaries. However, change in pipe orientation shifted the transition boundaries accordingly and these shifts were illustrated by superposition of the flow maps developed for each pipe orientation. Similar analysis was done for the downward inclined pipe orientation. Flow patterns in the upward and downward inclined pipe orientations were compared, flow maps developed were also compared and the effect of pipe orientation was observed. Measured void fraction was validated with data from other sources and by prediction with the top correlations in present study. Void fraction correlation comparison was also carried out to determine the best performing correlation in present study for near horizontal pipe orientation and within specific regions of void fraction. The conclusions and recommendations for the three main areas in present study are discussed below.

5.1 Conclusions of Flow Patterns and Flow Maps

Stratified flow observed in the downward inclined pipe orientation was not observed in the upward pipe orientation due to the role played by gravitational force on the liquid phase. In the case where gravitational force acts in opposite direction of flow (upward inclined pipe), slippage occurs at low liquid flow rates as the liquid phase fills the pipe cross section leading to discontinuity of the gas phase and hence, stratified flow is eliminated. However, in the downward inclined pipe orientation, gravity acts in same direction as flow and complete separation of liquid and gas phase was observed in the pipe known as stratified flow. Similar observations were made by Oddie et al. (2003), Wongwises and Pipathattkul (2006), Ghajar and Tang (2007) and Tzotzi et al. (2011).

The physical structure of slug flow was observed to be different in the downward inclined pipe orientation due to the simultaneous effects of gravitational and buoyant forces acting in the two phase flow. In the upward inclined pipe orientation, gravity opposes the flow while buoyant force acts in flow direction while in the downward inclined orientation, gravity acts in the flow direction while buoyant force tries to oppose it. The slug flow observed in the upward inclined pipe orientation has its nose pointing in the flow direction while a laterally inverted slug flow which has a nose pointing in opposite flow direction was observed in the downward inclined pipe orientation due to buoyant force.

The flow maps developed for the upward and downward inclined pipe orientations were compared and it was observed that for the upward inclined pipe orientation, the flow map contracted as transition boundaries shifted to lower flow rate of liquid and gas phase as pipe orientation progressed from $+5^{o}$ to $+20^{o}$ while in the downward inclined pipe orientation, the flow map expanded as transition boundaries shifted to higher flow rate of liquid and gas phase. Similar observations were made by Barnea (1987) and Tzotzi et al. (2011). In sum, observations on flow

patterns and flow maps in present study are consistent with the observation reported by different investigators over the years.

5.2 Conclusions of Void Fraction Measurement and Analysis

Void fraction measurement was carried out using air-water as working fluids in a 12.7 mm diameter pipe with the aid of quick closing valves. 700 void fraction data points were measured in six pipe orientations and experimental uncertainty was calculated. Maximum uncertainty of ±42% was calculated in $+20^{o}$ pipe orientation for very low void fraction of 0.03, however for void fraction values above 0.08 the maximum uncertainty was in the range of ±10% to ±16%. The minimum uncertainty calculated for all pipe orientations in present study was found to be ±1.3%. Variation of void fraction with flow patterns was observed at different pipe orientations as the range of measured void fraction for individual flow pattern was observed to either increase or decrease with respect to change in pipe orientation.

Effect of pipe orientation on void fraction was also observed for low liquid and gas flow rate region at different pipe orientations in present study and this effect disappeared at high liquid and gas flow rates. Hence, it was concluded that void fraction reduces as pipe orientation shifted upwards due to increased slippage of the liquid phase while in the downward inclined pipe orientation, void fraction increases with increase in pipe orientation. However, void fraction was independent of pipe orientation at high liquid and gas flow rates. Similar observations were reported by Beggs and Brill (1973) and Wongwises and Pipathattakul (2006).

Validation of measured void fraction data was done by comparison with inclined void fraction data obtained from Beggs (1972) and Mukherjee (1979) for upward and downward inclined pipe orientation. For the upward pipe orientation, compared data was found to be within ±10% error with present study and ±7.5% error in downward pipe orientation. Further comparison was done

by predictions of the top performing correlations. Validation was divided into two void fraction regions which are $0 < \alpha < 0.5$ and $0.5 \leq \alpha < 1$. The selected correlations predicted measured void fraction in the region of $0 < \alpha < 0.5$ within ±15% error and $0.5 \leq \alpha < 1$ within ±7.5% error.

Prediction performance of fourteen void fraction correlations was done to come up with the top performing void fraction correlation for the upward inclined pipe orientation, downward inclined pipe orientation and near horizontal pipe orientation. Based on the least RMS error in present study, the most successful void fraction correlation in upward inclined pipe orientation is Smith (1969), the most successful void fraction correlation in the downward inclined pipe orientation is Gomez et al. (2000) and for near horizontal pipe orientation, the top performing correlation in present study is Smith (1969).

5.3 Conclusions on Flow Reversal

Flow reversal in co-current two phase flow in upward inclined pipes was observed, investigated and thoroughly analyzed in present study. Since flow reversal was observed in slug, slug/wavy and wavy flows, modeling of interfacial shear was impossible due to non-uniform two phase geometry in pipe cross section. Hence, Bernoulli's equation and dimensionless numbers were adopted for analysis of flow reversal. The dynamic pressure from the Bernoulli's equation was used to indicate the trend of flow reversal with the corresponding gas flow rates for each pipe orientation and the effect of pipe orientation on dynamic pressure plots were observed. Froude number, Reynolds number and Weber number are the dimensionless numbers selected for analysis of flow reversal. Each dimensionless number gave the range over which flow reversal was observed for each pipe orientation and this comprehensive analysis can be used to effectively predict flow reversal in smooth pipe for $+5^{o}$, $+10^{o}$, $+20^{o}$ and $+45^{o}$.

5.4 Recommendations for Void Fraction Correlations Analysis

Based on the prediction performance of void fraction correlations selected for comparison in present study, the following void fraction correlations are recommended for upward inclined pipe orientation, downward inclined pipe orientation and near horizontal pipe orientation for $0 < \alpha \leq 0.25$, $0.25 < \alpha \leq 0.75$ and $0.75 < \alpha < 1$ regions. The recommendations are given in Tables 5.1 to 5.3.

Table 5.1 Recommendation of the best performing correlation for specific void fraction regions for upward inclined pipe orientation.

Void Fraction Region	Correlation
0 – 0.25	Greskovic and Cooper (1975)
0.25 – 0.75	Guzhov et al. (1967)
0.75 – 1	Lockhart and Martinelli (1949) & Yashar et al. (2001)

Table 5.2 Recommendation of the best performing correlation for specific void fraction regions for downward inclined pipe orientation.

Void Fraction Region	Correlation
0 – 0.25	Gomez et al. (2000)
0.25 – 0.75	Guzhov et al. (1967)
0.75 – 1	Lockhart and Martinelli (1949)

Table 5.3 Recommendation of the best performing correlation for specific void fraction regions for near horizontal pipe orientation.

Void Fraction Region	Correlation
0 – 0.25	Gomez et al. (2000) & Smith (1969)
0.25 – 0.75	Guzhov et al. (1967)
0.75 – 1	Lockhart and Martinelli (1949)

It should be noted that the selected correlations in Tables 5.1 to 5.3 predicted measured void fraction with the highest accuracy within ±10% error bands for void fraction regions of $0 < \alpha \leq 0.25$ and $0.25 < \alpha \leq 0.75$, and ±5% error for void fraction region of $0.75 < \alpha < 1$.

5.5 Recommendations for Flow Reversal

Flow reversal in co-current two phase flow should be further investigated at pipe inclinations above $+45^{o}$ to verify the major flow pattern over which flow reversal occurs above $+45^{o}$. Flow reversal should be investigated in rough and larger diameter pipes in order to have sufficient data needed to develop a correlation to predict flow reversal in inclined pipes.

REFERENCES

Asante, B., (2002). Accounting for Liquids in Gas Pipeline Simulations. PSIG Annual Meeting, Portland, Oregon, October 23-25.

Baker, D., (1954). Simultaneous Flow of Oil and Gas. Oil and Gas Journal. 53, 183-195.

Bankoff, S.G., (1960). A Variable Density Single Fluid Model for Two Phase Flow with Particular Reference to Steam Water Flow. Trans, ASME, Journal of Heat Transfer. 82, 265-272.

Barnea, D., Shoham, O., Taitel, Y., (1982). Flow Pattern Transition for Downward Inclined Two Phase flow: Horizontal to Vertical. Chemical Engineering Science. 37, 5, 735-740.

Barnea, D., Shoham, O., Taitel, Y., (1985). Gas-Liquid Flow in Inclined Tubes: Flow Pattern Transition for Upward Flow. Chemical Engineering Science. 40, 1, 131-136.

Barnea, D., (1987). A Unified Model for Predicting Flow-Pattern Transitions for the Whole Range of Pipe Inclinations. International Journal of Multiphase Flow. 13, 1, 1–12.

Beggs, H.D., (1972). An Experimental Study of Two Phase Flow in Inclined Pipes. PhD Dissertation. The University of Tulsa, Tulsa, OK. Department of Petroleum Engineering.

Beggs H.D., Brill, J.P., (1973). A Study of Two-Phase Flow in Inclined Pipes. Journal of Petroleum Technology. 25, 5, 607–617.

Bhagwat, S.M., (2011). Study of Flow Patterns and Void Fraction in Vertical Downward Two-Phase Flow. MS Dissertation, Department of Mechanical and Aerospace Engineering, Oklahoma State University, Stillwater, Oklahoma, USA.

Bhagwat, S.M., Ghajar, A.J., (2013). A Flow Pattern Independent Drift Flux Model Based Void Fraction Correlation for a Wide Range of Gas-Liquid Two Phase Flow. International Journal of Multiphase Flow (In Press).

Bharathan, D., Wallis, G.B., Richter, H.J., (1979). Air-Water Counter-current Annular Flow in Vertical Tubes. Electric Power Research Institute Rep. EPRI NP-786.

Bonnecaze, R.H., Erskine, W., Greskovic, E.J., (1971). Holdup and Pressure Drop for Two Phase Slug Flow in Inclined Pipes. AIChE Journal. 17, 1109-1113.

Brennan, C.E., (2005). Fundamentals of Multiphase Flow. Chapter 7: Flow Patterns. Cambridge University Press.

Cioncolini, A., Thome, J.R., (2012). Void Fraction Prediction in Annular Two Phase Flow. International Journal of Multiphase Flow. 43, 72–84.

Cook, W., (2008). An Experimental Apparatus for Measuremet of Pressure Drop and Void Fraction and Non-Boiling Two Phase Heat Transfer and Flow Visulization in Pipes for all Inclinations. Mechanical Engineering. Stillwater, Oklahoma State University. MS Thesis.

Czop, V., Barbier, D., Dong, S., (1994). Pressure Drop, Void Fraction and Shear Stress Measurements in Adiabatic Two Phase Flow in Coiled Tube. Nucl. Eng. Design. 149, 323-333.

Dezhang, L., Ning, O., (1992). Flow Pattern and Heat Transfer behavior of Boiling Two Phase Flow in Inclined Pipes. Journal of Thermal Science. 1, 3.

Dix, G.E., (1971). Vapor Void Fractions for Forced Convection with Subcooled Boiling at Low Flow Rates. Berkeley, University of California. PhD thesis.

Dukler, A.E., Wicks III, M., Cleveland, R.G., (1964). Frictional Pressure Drop in Two Phase Flow: A Comparison of Existing Correlations for Pressure Loss and Holdup. AIChe Journal. 10, 38–43.

Ghajar, A.J., Bhagwat, S.M., (2013). Flow Patterns, Void Fraction and Pressure Drop in Gas-Liquid Two Phase Flow at Different Pipe Orientations. Book Chapter in Frontiers and Progress in Multiphase Flow (In Press).

Ghajar, A.J., Tang, C.T., (2007). Heat Transfer Measurements, Flow Pattern Maps and Flow Visualization for Non-Boiling Two-Phase Flow in Horizontal and Slightly Inclined Pipe. Heat Transfer Engineering. 28, 6, 525–540.

Godbole, P.V., (2009). Study of Flow Patterns and Void Fraction in Vertical Upward Two-Phase Flow. MS Dissertation, Department of Mechanical and Aerospace Engineering, Oklahoma State University, Stillwater, Oklahoma, USA.

Godbole, P.V., Tang, C.C., Ghajar, A.J., (2011). Comparison of Void Fraction Correlations for Different Flow Patterns in Upward Vertical Two-Phase Flow. Heat Transfer Engineering. 32, 10, 843–860.

Gomez, L.E., Shoham, O., Taitel, Y., (2000). Prediction of Slug Holdup: Horizontal and Upward vertical. International Journal of Multiphase flow. 26, 517-521.

Greskovic, E.J., Cooper, W.T., (1975). Correlation and Prediction of Gas Liquid Holdup in Inclined Flow. AIChE Journal. 21, 1189-1192.

Guzhov, A.L., Mamayev, V.A., Odishariya, G.E., (1967). A Study of Transportation in Gas Liquid Systems. In: 10th International Gas Union Conference, Hamburg, Germany, June 6-10.

Hamersma, P.J., Hart, J., (1987). A Pressure Drop Correlation for Gas/Liquid Pipe Flow with a Small Liquid Holdup. Chemical Engineering Science. 42, 5, 1187-1196.

Hart, J., Hamersma, P.J., Fortuin, J.M.H., (1989). Correlations Predicting Frictional Pressure Drop and Liquid Holdup during Horizontal Gas Liquid Pipe Flow with a Small Liquid Holdup. International Journal of Multiphase Flow. 15, 947-964.

Hewitt, G.F., Wallis, G.B., (1963). Flooding and Associated Phenomenon in Falling Film in a Tube. AERE-R 4614.

Hugmark, G.A., (1962). Holdup in Gas Liquid Flow. Chem. Eng. Progr. 58, 62-65.

Kawaji, M., Anoda, Y., Nakamura, H., Tasaka, T., (1987). Phase and Velocity Distribution and Holdup in High Pressure Steam/Water Stratified Flow in a Large Diameter Horizontal Pipe. International Journal of Multiphase Flow. 13, 145-159.

Kawanishi, K.., Hirao, Y., Tsuge, A., (1990). An Experimental Study on Drift Flux Parameters for Two Phase Flow in Vertical Round Tubes. Nuclear Engineering and Design. 120, 447-458.

Kokal, S.L., Stanislav, J.F., (1989a). An Experimental Study of Two Phase Flow in Slightly Inclined Pipes - I. Flow Patterns. Chemical Engineering Science. 44, 3, 665–679.

Kokal, S.L., Stanislav, J.F., (1989b). An Experimental Study of Two Phase Flow in Slightly Inclined Pipes - II. Liquid Holdup and Pressure Drop. Chemical Engineering Science. 44, 3, 681–693.

Lin, P.Y., Hanratty, T.J., (1987). Effect of Pipe Diameter on Flow Patterns for Air-Water Flow in Horizontal Pipes. International Journal of Multiphase Flow. 13, 4, 549-563.

Lockhart, R.W., Martinelli, R.C., (1949). Proposed Correlation of Data for Isothermal Two Phase, Two Component in Pipes. Chemical Engineering Progress. 45, 39–48.

Mandhane, J.M., Gregory, G.A., Aziz, K., (1974). A Flow Pattern Map for Gas--Liquid Flow in Horizontal Pipes. International Journal of Multiphase Flow. 1, 4, 537-553.

McQuillan, K.W., Whalley, P.B., Hewitt, G.F., (1985). Flooding in Vertical Two Phase Flow. International Journal of Multiphase Flow. 11, 741-760.

Minami, K., Brill, J.P., (1987). Liquid Holdup in Wet Gas Pipelines. SPE Prod. Eng. 5, 36-44.

Morooka, S., Ishizuka, T., Zuka, M., Yoshimura, K., (1989). Experimental Study on Void Fraction in a Simulated BWR Fuel Assembly (Evaluation of Cross-Sectional Averaged Void Fraction). Nuclear Engineering and Design. 114, 91-98.

Mukherjee, H., (1979). An Experimental Study of Inclined Two Phase Flow. PhD Dissertation. The University of Tulsa, Tulsa, OK. Department of Petroleum Engineering.

Mukherjee, H., Brill, J.P., (1985). Empirical Equations to Predict Flow Patterns in Two Phase Inclined Flow. International Journal of Multiphase Flow. 11, 3, 299-314.

Nicklin, D,J., Wilkes, J.O., Davidson, J.F., (1962). Two Phase Flow in Vertical Tubes. Institute of Chemical Engineers. 40, 61-68.

Oddie, G., Shi, H., Durlofsky, L.J., Aziz, K., Pfeffer, B., Holmes, J.A., (2003). Experimental Studies of Two and Three Phase Flows in Large Diameter Inclined Pipes. International Journal of Multiphase Flow. 29, 527–558.

Oshinowo, O., (1971). Two Phase Flow in a Vertical Tube Coil. Department of Chemical Engineering and Applied Chemistry. Toronto, University of Toronto. PhD Thesis.

Palmer, C.M., (1975). Evaluation of Inclined Two Phase Flow Liquid Holdup Correlations using Experimental Data, MS Thesis, The University of Tulsa, Tulsa, OK, Department of Petroleum Engineering.

Perez, V.H., (2008). Gas-Liquid two Phase Flow in Inclined Pipes. School of Chemical, Environmental and Mining Engineering, University of Nottingham, United Kingdom. PhD Thesis.

Rouhani, S.Z., Axelsson, E., (1970).Calculations of Void Fraction in the Subcooled and Quality Boiling Regions. International Journal of Heat and Mass Transfer. 13, 383-393.

Schicht, H.H., (1969). PhD Thesis. ETH, Zurich.

Simmons, J.H., Harantty, T.J., (2001). Transition from Stratified to Intermittent Flows in Small Angle Upflows. International Journal of Multiphase Flow. 27, 599-616.

Smith, S.L., (1969). Void Fraction in Two Phase Flow: A Correlation Based upon an Equal Velocity Head Model. Proc. Inst. Mech. Engrs, London. 184, 647-657

Spedding, P.L., Ferguson, M.E.G., Watterson, J.K., (1999). A Study of Two-Phase Co-current Flow in Inclined Pipe. Dev. Chem. Eng. Mineral Process. 7, 147-177.

Spedding, P.L., Nguyen, V.T., (1980). Regime Maps for Air Water Two Phase Flow. Chemical Engineering Science. 35, 779-793.

Spedding, P.L., Spence, D.R., (1993). Flow Regimes in Two-Phase Gas-Liquid Flow. International Journal of Multiphase Flow. 19, 2, 245-280.

Sun, K., Duffey, R., Peng, C., (1981). Prediction of Two Phase Mixture Level and Hydrodynamically Controlled Dryout under Flow Conditions. International Journal of Multiphase Flow. 7, 521–543.

Taitel, Y., Barnea, D., Dukler, A. E., (1982). A Film Model For The Prediction of Flooding and Flow Reversal for Gas-Liquid Flow in Vertical Tubes. International Journal of Multiphase Flow. 8, 1-10.

Taitel, Y., Dukler, A.E., (1976). A Model For Predicting Flow Regime Transitions in Horizontal and Near Horizontal Gas-Liquid Flow. American Institute of Chemical Engineers Journal. 22, 1, 47–55.

Thome, J.R., (2006). Engineering Data Book III, Chapter 17: Void Fractions in Two Phase Flows. Wolverine Tube Inc.

Troniewski, L., Ulbrich, R.., (1984). The Analysis of Flow Regime Maps of Two-Phase Gas-Liquid Flow in Pipes. Chemical Engineering Science. 39, 7-8, 1213-1224.

Tshuva, M., Barnea, D., Taitel, Y., (1999). Two Phase Flow in Inclined Parallel Pipes. International Journal of Multiphase Flow. 25, 1491-1503.

Tzotzi, C., Bontozoglou, V., Andritsos, N., (2011). Effect of fluid properties on Flow Patterns in Two-Phase Gas-Liquid Flow in Horizontal and Downward Pipes. Industrial and Engineering Chemistry Research. 50, 645–655.

Wallis, G.B., (1969). One Dimensional Two Phase Flow. McGraw-Hill Inc. New York.

Weisman, J., Duncan, D., Gibson, J., Crawford, T., (1979). Effects of Fluid Properties and Pipe Diameter on Two-Phase Flow Patterns in Horizontal Lines. International Journal of Multiphase Flow. 5, 6, 437-462.

Weisman, J., Kang, S.Y., (1981). Flow Pattern Transition in Vertical and Upwardly Inclined Pipes. International Journal of Multiphase Flow. 7, 3, 271-291.

Woldesemayat, M.A., Ghajar, A.J., (2007). Comparison of void fraction correlations for different flow patterns in horizontal and upward inclined pipes. International Journal of Multiphase Flow. 33, 347-370.

Wongwises, S., Pipathattakul, M., (2006). Flow Pattern and Void Fraction of Two-Phase Gas-Liquid Flow in an Inclined Narrow Annular Channel. Experimental Thermal and Fluid Science. 30, 345–354.

Yashar, D.A., Wilson, M.K., Kopke, H.R., Graham, D.M., Chato, J.C., Newell, T.A., (2001). An Investigation of Refrigerant Void Fraction in Horizontal, MicroFin Tubes. HVAC&R Research. 7, 67–82.

Yijun, J., Rezkallah, K., (1993). A Study on Void Fraction in Vertical Co-current Upward and Downward Two-Phase Gas-Liquid Flow - I: Experimental Results. Chemical Engineering Communication. 126, 221-243.

Zabaras, G.J., Dukler, A.E., (1988). Countercurrent Gas-Liquid Annular Flow, Including the Flooding State. AIChe Journal. 34, 389-396.

Zubar, N., Findlay, J.A., (1965). Average Volumetric Concentration in Two Phase Flow Systems. Journal of Heat Transfer. 87, 435-468.

VITA

ADEKUNLE LUKMAN OYEWOLE

Candidate for the Degree of

Master of Science

Thesis: STUDY OF FLOW PATTERNS AND VOID FRACTION IN INCLINED TWO PHASE FLOW

Major Field: Mechanical Engineering

Biographical:

Born in Nigeria, son of Mr. & Mrs. Oyewole.

Education:

Received Bachelor of Science in Mechanical Engineering at University of Ilorin, Ilorin Nigeria, July 2009.

Completed the requirements for the Master of Science in Mechanical Engineering at Oklahoma State University, Stillwater Oklahoma, December 2013.

Experience:

Teaching Assistant, Oklahoma State University (2012-2013)

Professional Memberships:

National Society of Black Engineers, Oklahoma State University Student Branch.